

Electronic Thesis and Dissertation Repository

9-25-2013 12:00 AM

Impact Craters as Habitats for Life: Endolithic Colonization of Shocked Gneiss from the Houghton Impact Structure, Devon Island, Canada

Alexandra Janine Pontefract
The University of Western Ontario

Supervisor
Dr. Gordon Osinski
The University of Western Ontario

Graduate Program in Geology
A thesis submitted in partial fulfillment of the requirements for the degree in Doctor of Philosophy
© Alexandra Janine Pontefract 2013

Follow this and additional works at: <https://ir.lib.uwo.ca/etd>



Part of the [Biogeochemistry Commons](#)

Recommended Citation

Pontefract, Alexandra Janine, "Impact Craters as Habitats for Life: Endolithic Colonization of Shocked Gneiss from the Houghton Impact Structure, Devon Island, Canada" (2013). *Electronic Thesis and Dissertation Repository*. 1668.
<https://ir.lib.uwo.ca/etd/1668>

This Dissertation/Thesis is brought to you for free and open access by Scholarship@Western. It has been accepted for inclusion in Electronic Thesis and Dissertation Repository by an authorized administrator of Scholarship@Western. For more information, please contact wlsadmin@uwo.ca.

IMPACT CRATERS AS HABITATS FOR LIFE: ENDOLITHIC COLONIZATION OF
SHOCKED GNEISSES FROM THE HAUGHTON IMPACT STRUCTURE, DEVON
ISLAND, CANADA

(Thesis format: Integrated Article)

by

Alexandra Pontefract

Graduate Program in Earth Science, Specialization in Planetary Science

A thesis submitted in partial fulfillment
of the requirements for the degree of
Doctor of Philosophy

The School of Graduate and Postdoctoral Studies
The University of Western Ontario
London, Ontario, Canada

© Alexandra Pontefract 2013

Abstract

Meteorite impacts are ubiquitous throughout our solar system and are a fundamental geological process on rocky and icy planetary bodies. Though initially detrimental to biology, an impact event can favourably change the availability and habitability of a substrate for endolithic organisms, which are then able to (re)colonize micro-fractures and pore spaces created during the impact. The colonization of rocks by endolithic communities is an advantageous trait, especially in environments such as hot or cold deserts, where temperature shifts, low water availability and high UV indices pose a significant problem. On Mars, similar conditions – albeit, more extreme – prevail. In these instances, impact structures could provide refuge to endolithic organisms. Previous work has shown the increase of microbial biomass with shock level in sedimentary rocks, related to increases in porosity. However, sedimentary rocks experience a collapse of pore spaces at pressures over ~35 GPa and, thus, do not support endolithic colonization at pressures higher than this. In contrast, the porosity of crystalline rocks such as gneisses increases proportionally until vapourization. This study considers shocked gneisses from the 39 Ma, 23 km diameter Haughton impact structure, Devon Island, Canada, and investigates the relationship between shock metamorphism and microbial colonization. Utilizing a variety of microscopy techniques, the subsurface community was visualized and the biomass levels calculated with increasing shock metamorphism. Average cell abundance was found to increase with shock level, with a maximum of 10^8 cells/g. It was found that microbial biomass did increase with increasing porosity, and was not affected by reductions in trace element concentrations of the rock, likely being more dependent on exogenous nutrients within meteoric waters or supplied aurally. It can be concluded that crystalline substrates can become habitats for endolithic organisms through the process of impact metamorphism, providing an excellent refuge in extreme environments. On Mars where the substrate is largely basaltic, it is suggested that impact craters would be an excellent target for life detection due to extensive deposits of shocked basalt. These more mafic rocks, coupled with the presence of hydrothermal activity, would have potentially provided significant colonization potential on early Mars and may continue to provide refuge today.

Keywords

Impact Crater, Endolith, Origins, Analogue, Mars, Gneiss, Life.

Co-Authorship Statement

Chapter 2: Samples and XRF data for the sedimentary rocks in this study were collected by John Parnell, and initial analyses performed by John Parnell, Gordon Osinski and Charles Cockell. TOC data was collected and analysed by Paula Lindgren. Sample collection, identification of shock and ICP analyses for the shocked crystalline gneisses were done by Alexandra Pontefract. Manuscript was written by Alexandra Pontefract along with synthesis of all data sets and reinterpretation of the sedimentary and TOC data, with comments and editing by John Parnell, Gordon Osinski, Charles Cockell, Paula Lindgren and Gordon Southam.

Chapter 3: All sample collection, preparation, analysis and interpretation were conducted by Alexandra Pontefract. Charles Cockell assisted with statistical analyses, and all contributing authors provided comments and editing for the manuscript which was written by Alexandra Pontefract.

Chapter 4: As in previous chapters, all sample collection, preparation and analyses were performed by Alexandra Pontefract. Charles Cockell assisted in DNA extraction methodology and in statistical analysis. Manuscript was written by Alexandra Pontefract. Gordon Southam, Charles Cockell and Gordon Osinski provided comments, suggestions and editing on the finished manuscript.

Chapter 5: Experiment concepts and experiment runs were designed and performed by Alexandra Pontefract, with suggestions for modification provided by Gordon Southam. Charles Cockell and Gordon Southam assisted with the determination of what sequencing should be completed. Anion/cation analyses from Iceland springs were done by Sophie Nixon. Manuscript was written by Alexandra Pontefract, with comments and edits by Charles Cockell, Gordon Osinski and Gordon Southam.

Acknowledgments

First and foremost, I would like to extend my deepest thanks to Gordon Osinski, Gordon Southam and Charles Cockell for their guidance, insight and inspiration during this project. I am grateful to have been given the opportunity to work with them and have enjoyed the many science talks over the years. I have also been incredibly grateful to have been able to continue to perform research in the Arctic. Thank you as well to Charles for giving me the opportunity to work in your lab and for the wonderful experience of working in Iceland.

There are many technicians and operators who have provided invaluable assistance to me along the way: many thanks must go to Karen Nygard for going above and beyond the call of duty, as well as Richard Gardener and Carrie Hay of the Biotron. Thank you to Todd Simpson and Tim Goldhawk at Nanofab, Robert Gordon at APS, Monique Durr and Charlie Wu at Biotron Analytical Services, Ivan Barker and the Zap Lab, Mike Hall and Steven Wood. Thank you also to Jason Hanson at Research and Testing.

Many thanks to my colleagues over the years who have provided field support, insight into analysis and commentary: Louisa Preston, Christopher Omelon, Phil McCausland, Robbie Flemming, Zoe Lindo, Jay Nadeau, Jeremiah Shuster, Jenine McCutcheon, Alaura Singleton, Haley Sapers, Cassandra Marion Beauchamp, Mike Craig, Matthew Ward, Radu Capitan, Sophie Nixon, Casey Bryce, Livio Tornabene, Rebecca Greenberger, Melissa Battler and Bhairavi Shankar. I would like to thank the various funding bodies that have assisted me in completing my thesis and provided support for conferences and courses: The University of Western Ontario, the National Sciences and Engineering Research Council, the Canadian Astrobiology Training Program, the Northern Scientific Training Program, Canadian Institute for Advanced Research, ASTRO-CPSX funding program and the Polar Continental Shelf Project for providing logistical support in the Arctic.

Thank you to the wonderful admin people of Earth Sciences for solving many a logistical issue – Marie Schell, Claire Mortera, Katherine Johnston, Margaret Moulton and Kevin Jordon, and thank you to my office mates in 1031 for providing much needed laughter, support and science chats over the years. Thanks to Lindsay Baxter, Marie Burford, Alaura Singleton, Louisa Preston, Sol Pound, Jeff Pound and Yani Sarquis Adamson for keeping me going and keeping me sane. Thank you to my partner Gastón Keller for all of your love and support.

Finally, I would like to thank those people who were there at the beginning: to Lynn Rothschild for setting the path, Jon Stone and Ralph Pudritz for making it possible, and Warwick Vincent for introducing me to the Arctic and fuelling a passion for this research that has lasted all these years. Thank you to my parents Keith and Lynette Pontefract for their constant love, encouragement and unfailing support.

Table of Contents

Abstract	ii
Co-Authorship Statement	iii
Acknowledgments	iv
List of Tables	ix
List of Figures	x
List of Appendices	xii
List of Abbreviations	xiv
Chapter 1 : Introduction	1
1.1 Meteorite Impacts on Terrestrial Bodies.....	1
1.2 Haughton as an Analogue for Mars	2
1.3 The Macro and Microscale Effects of an Impact.....	3
1.3.1 Macroscale Lithological Changes.....	3
1.3.2 Microscale Lithological Changes	5
1.3.3 Chemistry and Porosity.....	5
1.4 Meteorite Impacts and Biology.....	7
1.4.1 Microbial Endolithy	7
1.4.2 Hydrothermal Phase of Impact Biology	8
1.5 Thesis Outline	9
1.6 References.....	12
Chapter 2 : The Effects of Meteorite Impacts on the Availability of Bioessential Elements for Endolithic Organisms	17
2.1 Introduction.....	17
2.2 Methods.....	19
2.2.1 Field Site	19
2.2.2 Sample Collection and Processing.....	21

2.2.3	Shock Classification.....	22
2.2.4	Total Organic Carbon	22
2.2.5	XRF.....	24
2.2.6	ICP-AES	24
2.2.7	SEM-BSE and EDS Analysis	24
2.3	Results.....	25
2.3.1	TOC in Houghton CMR.....	25
2.3.2	Sedimentary Samples.....	25
2.3.3	Crystalline Samples	28
2.3.4	SEM-BSE and EDS	28
2.4	Discussion.....	32
2.5	Biological Implications.....	35
2.6	Concluding Remarks.....	35
2.7	References.....	36
Chapter 3 : Impact-generated endolithic habitats within crystalline rocks of the Houghton impact structure, Canada.....		40
3.1	Introduction.....	40
3.2	Methods.....	42
3.2.1	Field Site	42
3.2.2	Sample Collection and Processing.....	42
3.2.3	Bulk Cell Counts.....	44
3.2.4	Confocal Scanning Laser Microscopy	47
3.2.5	CSLM Image Acquisition and Processing.....	47
3.2.6	Scanning Electron Microscopy	48
3.3	Results.....	49
3.3.1	Bulk Cell Counts.....	49

3.3.2	CSLM.....	49
3.3.3	SEM	54
3.4	Discussion.....	54
3.4.1	Microbial Biomass and Shock Metamorphism.....	57
3.4.2	Subsurface Morphology.....	58
3.5	Concluding Remarks.....	59
3.6	References.....	59
Chapter 4 : Microbial community composition within impact-generated endolithic habitats in crystalline rocks		63
4.1	Introduction.....	63
4.2	Methods.....	65
4.2.1	Field Site	65
4.2.2	DNA Extraction, Sequencing and Statistical Analysis	66
4.2.3	Culturing.....	66
4.3	Results.....	68
4.3.1	Culturing	68
4.3.2	16S Analysis and Diversity Calculations.....	68
4.3.3	N ₂ Fixation.....	74
4.4	Discussion.....	74
4.5	Concluding Remarks.....	77
4.6	References.....	77
Chapter 5 : The habitability of shocked gneisses within a post-impact hydrothermal system.....		85
5.1	Introduction.....	85
5.2	Methods.....	87
5.2.1	Field Experimental Method	87
5.2.2	Krýsuvík (Seltún).....	88

5.2.3	Geysir	90
5.2.4	Simulated Haughton Hydrothermal System	90
5.3	Results	94
5.3.1	Field Experiments – Seltún	94
5.3.2	Field Experiments – Geysir	94
5.3.3	Simulated Haughton Hydrothermal System	95
5.4	Discussion	98
5.5	Concluding Remarks	102
5.6	References	103
Chapter 6	Discussion	107
6.1	Meteorite Impacts and Endolithy	107
6.1.1	Microbial Biomass as a Function of Shock Metamorphism	107
6.1.2	Prevalence of Bioessential Elements in Shocked Lithologies	109
6.1.3	Community Composition	110
6.1.4	Shocked Lithologies in Hydrothermal Systems	111
6.2	Meteorite Impacts and the Origins of Life	112
6.3	Future Work	115
6.4	Epilogue	116
6.5	References	117
Appendix A	120
Appendix B	129
Appendix C	135
Appendix D	140
Curriculum Vitae	146

List of Tables

Chapter 2:

Table 2-1. Calculation of TOC contents. The numbers within the parentheses represent the number of different samples that were analysed..... 26

Chapter 3:

Table 3-1. Classification of shock level in gneisses 45

Chapter 4:

Table 4-1. List of diversity statistics and phylum abundances for unshocked, moderate shock and high shock populations..... 72

Chapter 5:

Table 5-1. ICP/IC data collected from Seltún and Geysir. 89

Table 5-2. Metagenomic analysis from Seltun and Geysir using *454* pyrosequencing. Alpha diversity indices have been calculated for Bacteria only..... 97

List of Figures

Chapter 2:

- Figure 2-1. (a) Map showing location of the Haughton impact structure on Devon Island ... 20
- Figure 2-2. Photomicrographs and backscattered electron images of crystalline gneiss..... 23
- Figure 2-3. Graphs showing XRF data of sedimentary lithologies for some biologically relevant elements. 27
- Figure 2-4. Graphs showing combined XRF and ICP data for crystalline rocks of various elements plotted against the ratio of Al_2O_3/SiO_2 29
- Figure 2-5. Graphs showing the means of several different elements, compiled from XRF and ICP data (see Appendix A5a) 30
- Figure 2-6. SEM-BSE micrographs of shocked gneiss 31

Chapter 3:

- Figure 3-1. (a) Landsat image of the Haughton Crater, Devon Island, Canada, courtesy of G.R. Osinski..... 43
- Figure 3-2. SEM-BSE micrographs showing (a) unshocked crystalline gneiss, (b) moderately shocked gneiss 45
- Figure 3-3. Average # cells/g and porosity plotted versus shock level. Porosity data adapted from Singleton et al. (2011) 50
- Figure 3-4. (a) and (b) show CSLM micrograph with live/dead stain and reveal epilithic and endolithic colonization of fractures and vesicles within the rock..... 51
- Figure 3-5. Average # cells/g plotted versus shock level (a) and depth within the substrate (b) through *in situ* analysis 52
- Figure 3-6. Plot of bulk cell counts vs. *in situ* counts 53
- Figure 3-7. SEM-BSE micrographs of endolithic organisms within shocked gneiss. (a) Zoom out of lithic substrate shocked to ~50 GPa 55
- Figure 3-8. (a) CSLM micrograph with *in situ* LIVE/DEAD BacLight stain..... 56

Chapter 4:

- Figure 4-1. Micrographs of cultured isolates from shocked gneisses (left side) and SEM micrographs of *in situ* colonization..... 67

Figure 4-2. (a) Percentage abundances of 16S DNA for the bacterial communities from unshocked, moderate shock and highly shocked gneisses..... 69

Figure 4-3. Percentage abundance of the phototrophic bacterial communities from the unshocked, moderately shocked and highly shocked gneisses, presented at the class level .. 70

Figure 4-4. Nonmetric multidimensional scaling plot (NMDS) for bacterial 16S DNA from unshocked, moderately shocked and highly shocked populations..... 73

Chapter 5:

Figure 5-1. (a) Mudpots at Seltun, with a maar in the background. (b) Hydrothermal pool used for experiment 50m downstream from source. (c) Black filamentous streamers upstream of experiment 91

Figure 5-2. (a) Hydrothermal pool above Geysir showing outflow down the hill. Source is in foreground 92

Figure 5-3. (a) SE2 micrograph showing iron sulfide/sulphate deposits from Seltún, unknown mineral; scale bar is 2µm..... 96

Figure 5-4. (a) pH measurements for weeks 3 through 6 of the experiment 99

Figure 5-5. (a) SE2 micrograph of sulfur reducing bacteria on an unshocked coarse rock sample. Fine coating on rock is EPS and FeS; scale is 500µm 100

List of Appendices

Appendix A:

A1. Shock level categories based on petrographic analysis of gneiss	120
A2. Sample coordinates shown in UTM as well as sample descriptions for all three suites of rocks utilized in this study.	121
A3. The total amount of organic carbon (% TOC) in Haughton target rocks and clast-rich melt rocks.....	124
A4. Table shows XRF results depicting major oxide composition of sedimentary rocks from the Haughton Crater.....	125
A5. Table shows XRF and ICP results depicting major oxide composition of crystalline rocks from the Haughton Crater	126
A6. Table shows ICP results depicting trace element composition of crystalline rocks from the Haughton Crater.....	127
A7. Calculated Z-values for select major oxide data for the crystalline samples using a non-parametric Mann-Whitney U-test	128

Appendix B:

B1. Site locations for samples used in bulk cell counts and CSLM counts.....	129
B2. Bulk cell count raw data using Zeiss Z1 compound microscope in bright field.....	130
B3. <i>In situ</i> cell counts (live and dead) per 150,000 μm^2 area bin using the CSLM.	131

Appendix C:

C1. BG-11 Media.....	135
C2. A5 Metal Mix.....	135
C3. Raw DNA data for the Bacterial classes for unshocked gneisses	136
C4. Raw 16S rDNA data for the Bacterial classes for moderately shocked (3-4) gneisses.	137
C5. Raw DNA data for the Bacterial classes for highly shocked (6-7) gneisses.....	138
C6. Raw DNA data for eukaryal and fungal classes for two samples.	139

Appendix D:

D1. Modified Barr's Medium for sulfate reducing bacteria. 140

D2. Haughton Minimal Media Recipe..... 140

D3. ICP-AES/IC and ICP-MS data for Haughton hydrothermal experiment..... 141

List of Abbreviations

AIC	Akaike Information Criterion
ANOSIM	Analysis of Similarity
BG-11	Blue-Green Algae 11 Media
BSE	Back-Scattered Electrons
CMR	Clast Rich Melt-rock
CSLM	Confocal Scanning Laser Microscopy
DNA	Deoxyribonucleic Acid
EDX	Electron Dispersive X-ray (Detector)
EDS	Electron Dispersive Spectroscopy
EPS	Exopolysaccharide
Ga	Billion years
GPa	Gigapascals
ICP-AES	Inductively Coupled Plasma Emission Spectroscopy
LHB	Late Heavy Bombardment
LUCA	Last Universal Common Ancestor
Ma	Million years
NMDS	Nonmetric Multi-Dimensional Scaling
OGT	Optimal Growth Temperature
PAR	Photosynthetically Active Radiation
RNA	Ribonucleic Acid
rRNA/DNA	Ribosomal RNA/DNA
SEM	Scanning Electron Microscopy
SRB	Sulfate Reducing Bacterium
TOC	Total Organic Carbon
XRD	X-Ray Diffraction
XRF	X-Ray Fluorescence

“Somewhere, something incredible is waiting to be known.”
– Carl Sagan

Chapter 1 : Introduction

1.1 Meteorite Impacts on Terrestrial Bodies

Since the origin of our solar system, meteorite impacts have been an active and, at times, dominant geological process, having the ability to drastically change the surface of any planetary body and contribute to its geologic history. Prior to the 1960's, meteorite impacts on the Earth were not considered to be a significant event, and it was not until the advent of the space program that their importance was recognized (French 1998). To date, 184 impact structures have been identified on Earth (Earth Impact Database 2013) ranging from small circular bowls to complex structures such as those in Sudbury, Canada, or Vredefort, South Africa. From an economic perspective, several impact structures have proven to be viable sources for rock and mineral deposits as well as a source of hydrocarbons (French 1998). Far from the economic advantages, however, meteorite impacts were also shown to have a significant effect on terrestrial life, producing the major extinction event of 65 Ma ago, marking the end of the Cretaceous (Alvarez et al., 1980).

Exploration of our solar system has revealed an abundance of impact craters on every terrestrial planet in our solar system, including the icy moons of Jupiter and Saturn. This has made it possible to determine relative geologic ages of solar system bodies, assuming a steady state influx of cratering. It has also been suggested that large impact events may have affected nearly grown planets and may account for the unexplained occurrences in planetary motions, compositions and atmospheres (French 1998). An important observation, however, is that the influx of materials producing craters has not stayed the same over time and that at some point in the history of the solar system the influx was much greater (Sleep et al., 1989). Separately from this, a spike in the cratering record has been observed between 3.8 and 4.0 Ga – a period that has since been termed the Late Heavy Bombardment (LHB). Constrained to a period of time shortly after the formation of the solar system, the LHB is thought to have lasted from approximately 4.2 Ga – 3.8 Ga (e.g., Tera et al., 1974; Sleep et al., 1989; Kring and Cohen 2002), potentially delivering as much as 2.0×10^{20} kg of material to the Earth alone (Abramov and Mojzsis

2009). Given that the earliest incidence of life occurs at 3.8 Ga on the Earth (Fedo and Whitehouse 2002) and that the habitable period of Mars has been proposed to have lasted from between 4.0 to 3.0 Ga (Fairén et al., 2010), an important question to be asked is: how might the LHB have influenced the origins of life here on Earth and the possibility of life occurring on other planets within our solar system? Are impact events solely a frustration in the occurrence and evolution of Life, or can they be a catalyst? This thesis aims to explore these questions through an analysis of the differences in the response of the substrate to impact events, and through that, the effects of lithology on microbial growth, with specific emphasis on the impact shocked gneisses of the Haughton impact structure, Devon Island, Canada.

1.2 Haughton as an Analogue for Mars

The Haughton structure is a 39 Ma complex impact structure found on the north-western portion of Devon Island, Nunavut, in the Canadian high-Arctic archipelago at 75°N (Osinski et al., 2005a). The geology of this island has been well documented, with studies going back as far as the 1960s. The target rocks under the Haughton structure are almost entirely sedimentary in origin and represent lower Paleozoic rocks of the Arctic Platform. This ~1880 m sequence (pre-impact thickness) is comprised almost entirely of limestone and dolostone, and overlays gneisses of the Precambrian basement of the Canadian Shield. These sequences are near-horizontal, but do have a dip of 5° to the west. Thus, older sequences are visible as one moves west to east across the island (Osinski et al., 2005a). Haughton has an apparent diameter of ~23 km, with a final crater rim estimate of 16 km in diameter, where final crater rim estimate indicates the diameter of the topographic rim that rises above the outermost slump blocks not covered by ejecta (Osinski and Pierazzo 2013).

The most identifiable feature of the impact structure is the pale-grey crater-fill deposits, which form a discontinuous layer throughout the centre of the structure. These deposits are clast-rich impact melt rocks within which clasts of shocked gneiss may be found. Another salient feature of the structure is its hydrothermal deposits, seen in the form of several alteration products, such as selenite and marcasite, as well as the presence of hydrothermal vugs (areas where hydrothermal fluids have infiltrated rock and left

behind mineralized cavities); (Osinski et al., 2005b). These deposits follow the listric and concentric faults that are characteristic of the gravitational collapse of a transient crater, indicating that the location of hydrothermal deposits is heavily controlled by faulting (Osinski et al. 2005b). Finally, lacustrine deposits (comprising the Haughton Formation) are present in and around the centre of the crater, revealing the transient presence of a lake during the Neogene (Osinski et al. 2005a). These sediments contain fossilized pollen grains, plants and vertebrate skeletons, and represent a late stage in the biological succession of the crater. The Haughton impact structure presents itself as an ideal analogue to impact craters on Mars due to its situation within the Canadian High Arctic, and is currently the only impact crater possessing crystalline rocks residing within a polar desert. Though the conditions within the Arctic are much less severe than those of the Antarctic, low levels of available liquid water, high seasonal UV indices as well as large variations in temperature swing make the Haughton structure a suitable analogue for investigating the efficacy of an impact structure as a habitable environment within the harsh conditions found on Mars.

1.3 The Macro and Microscale Effects of an Impact

1.3.1 Macroscale Lithological Changes

An impact event involves the release of an immense amount of energy over a very short period of time. Meteorite impacts occur at speeds upwards of 11 m/s, contacting the Earth with little-to-no reduction in cosmic velocity, and are generally large, being over 50 m for a stony meteorite and >20 m for an iron bearing projectile (French 1998). The entire event consists of three main stages (Gault et al., 1968): 1) Contact and Compression, 2) Excavation and 3) Modification. During the contact and compression stage, which lasts on the order of milliseconds to seconds, the projectile immediately begins to cause the formation of a crater through the generation of a hypervelocity shock wave that radiates out through the target rock and back through the projectile itself (see Chapter 2). This rebounding, or rarefaction wave, causes unloading in the projectile, resulting in vapourization and melting of the projectile (Gault et al., 1968). Some of the target rock nearest to the point of impact is also vapourized, followed by a zone of generated melt. A zone of shock metamorphism is created out to where pressures drop below 5 GPa, after

which fracturing and brecciation occur. The vapourization of the projectile and arrival of the rarefaction wave back to the target is generally accepted as the end of the contact and compression stage (Gault et al., 1968). Grading into the “excavation” stage, the crater is opened up due to a complex interaction of the outwards-directed rarefaction wave and shock wave. This process causes the rock to be driven outward, resulting in a symmetric excavation of the target rock (Osinski et al., 2013). Further outwards, rock is generally driven further downward and outward, the entire process taking anywhere from 5 to 90 seconds. Once the excavation has ended, and the transient crater has reached its maximum diameter, modification occurs due to gravity (Melosh and Ivanov 1999), generally causing the formation of radial and listric faults as well as a central uplift in the case of complex craters. In the case of very large impacts, a multi-ring basin may form, e.g., Orientale on the Moon, though the mechanics of this process are poorly understood and highly contested. On Earth, no multi-ring basin has been conclusively discovered as basins of this size require impactors on the order of hundreds of kilometres in diameter, and such large craters are highly eroded (Morgan and Warner 1999).

This entire process results in rocks outside the crater being covered in an ejecta blanket, with crater-fill deposits (breccias and melt rocks) within the crater. These breccias contain clasts that are often significantly reduced in density and in some cases are so metamorphosed that they resemble pumice and have the ability to float in water. A final important factor to consider in the macro-scale effects of impact cratering, something important to both Earth and Mars, is that of an impact into a water-bearing substrate. If the impactor strikes a target that contains an active groundwater system, the initial water table will likely be completely vaporized. This elimination, however, will create a void space that will be filled by waters rising from depth (Osinski et al., 2005b), which will result in a hydrothermal system within the crater. Impact-related hydrothermal systems have been documented at over 70 terrestrial craters (Naumov 2005), however, most of these craters have been severely eroded. The deposits at the Haughton impact structure, Canada, are some of the best preserved in the world and thus provide a unique opportunity to study impact-generated hydrothermal activity and any associated biological regime.

Initial temperatures at Haughton were thought to be well over 2000°C, eventually cooling to a main stage of hydrothermal activity between 200°C and 80°C (Osinski et al., 2005b). These waters would have been kept warm by slowly cooling impact melt rocks over upwards of several thousand years and it is likely that a convection system developed. It is important to note that the location of hydrothermal deposits within the craters is constrained by crater geology, and is confined along the areas of listric and concentric faults along the crater rim (Osinski et al., 2005b).

1.3.2 *Microscale Lithological Changes*

Although the macroscale effects of an impact event are initially quite obvious, over the scale of geologic time these signals erode, which can occur through burial, successive tectonic events or weathering. Due to this loss of large-scale identifiers for an impact event, an alternate method of detection was developed in order to validate the existence of a putative impact structure (French and Koeberl 2010). In addition to the changes occurring to the lithology on a macroscale, the extreme temperatures and pressures cause alterations to minerals on the micron scale, a process termed “shock metamorphism”. Some minerals, such as quartz, plagioclase, K-feldspar and biotite respond in highly predictable ways to shock and can be used to indicate the level of pressure that the rock was exposed to, or “shock level”. Seminal work by Chao (1968), Stöffler (1966, 1971) and von Engelhardt (1969) provided the first attempt at correlating these effects with a quantifiable shock level, and has been best described within nonporous crystalline rocks (Stöffler 1971). Still the determination of shock level based on petrographic work, and even by other means such as crystal strain and peak broadening in XRD analyses (Burt et al., 2005), is quite subjective and there is not yet a widely accepted demarcation for these shock levels. One of the most up-to-date reviews of the classification system was published by Singleton et al. (2011), and provides the most defined demarcation of shock level in crystalline rocks for the Haughton impact structure to date.

1.3.3 *Chemistry and Porosity*

Given the imprecision inherent in classifying shock levels, very little work has been completed in an attempt to correlate chemical changes of the substrate with increasing shock metamorphism. More specifically, there are very little data regarding the changes

in biologically-relevant trace elements (Wackett et al., 2004) with shock level. Work by Osinski et al. (2010) sought to understand the changes in the major oxides as well as trace elements through XRF analysis in carbonates. Surprisingly, no correlation was found between shock level and changes in elemental composition, matching a similar study by Lindgren et al. (2007). In a paper by Fike et al. (2003), attempted to elucidate whether there were changes in both the major oxide and trace element composition in unshocked versus shocked samples using ICP analysis. The data did show a lowering in elemental concentration within the shocked species, however, the sample set was too small to reveal whether they were discrete changes in shocked samples, or rather indicative of original rock chemistry.

In contrast, porosity in shocked samples has received more attention in the literature. The best datasets currently presenting porosity as it scales with shock level come from analysis of carbonate-bearing sandstones from the Houghton structure (Cockell and Osinski 2007; Osinski 2007). Pioneering work in this topic can be found in extensive papers by Keiffer (1971, 1976) on the Coconino sandstones of Meteor Crater, Arizona. These works show an increase in porosity from approximately 10 GPa to 30 GPa after which the grains of the sample begin to experience flow, and porosity is reduced to below 5% (Cockell et al., 2005). Significantly less work has been completed depicting porosity changes in crystalline rocks. In a comparative study by Cockell et al. (2002), low-shocked gneiss samples (< 10 GPa) were found to have a density of 2.61 g/cm³, and a pore surface area of 0.004 m²/g, whereas high shock (> 20 GPa) had a density of 1.17 g/cm³ and a pore surface area of 0.10 m²/g. Singleton et al. (2011) takes this analysis a step further, by presenting porosity data from 30 samples of shocked gneiss from the Houghton impact structure, and correlating that with a much more comprehensive classification system based on Stöffler (1971). These data show that porosity in the crystalline samples begins at 0 and theoretically increases until the rock is vaporized. No collapse of pore spaces was seen at higher shock levels (Singleton et al., 2011).

1.4 Meteorite Impacts and Biology

1.4.1 *Microbial Endolithy*

The increase in porosity experienced by shocked rocks, and most especially, within shocked gneisses poses interesting opportunities when thinking about microbial growth within rocks – termed microbial endolithy. Microbial endolithy (specifically cryptoendolithy, which refers to colonization of a rock interior with no obvious access point) has been well documented (Cockell 2004; Cockell et al., 2005; Cockell et al., 2002; Cockell et al., 2003; de los Ríos et al., 2005; Friedmann and Ocampo, 1976; Nienow et al., 1988; Omelon 2008; Wierzchos and Ascaso 2001) and significant work has been completed studying microbe-mineral interactions (Barker et al., 1997; Douglas and Beveridge 1998; Hirsch et al., 1995; Konhauser et al., 2008; Vestal 1988). Interest in cryptoendolithic environments first began to gain momentum after their discovery in the Antarctic dry deserts, a place thought to be too hostile for the existence of life (Friedmann and Ocampo 1976). The ability to inhabit the interior of rocks is a significant advantage to microorganisms residing in harsh environments such as hot or cold deserts. These rocks provide protection from wind ablation, UV radiation, maintain a more regulated thermal regime, and provide micro-environments for the collection of sediments and water allowing for metabolically relevant redox reactions to occur (Cockell et al., 2005). Most commonly, these cryptoendolithic communities are photosynthetically-based, and can be visualized as a coherent band of growth several millimetres beneath the rock's surface.

Most of the microbial colonization that has been documented to date has been within sandstones, but has also been demonstrated to occur in evaporitic lithologies as well as limestones and within granites as chasmoendoliths (Omelon 2008). These types of rocks are highly translucent and allow for photosynthetically active radiation (PAR) to penetrate several millimetres into the substrate, allowing for the development of a photosynthetic microbial community. Microbial growth within impact-shocked sandstones was first documented by Cockell and Osinski (2007; 2004; 2002), showing a direct relationship between growth and increased shock level, as the pore spaces within the rock opened. However, comparatively, little work has been done on the shocked gneisses of the Haughton structure. This is of little surprise given the fact that crystalline

rocks generally make fairly poor endolithic habitats due to their low porosity and translucence. What is interesting is the idea of taking a substrate that was previously incapable of supporting life, and creating habitat through an impact event.

To date, three studies have looked at the shocked gneisses of the structure: Cockell et al. (2003; 2002) and Fike et al. (2003). The studies by Cockell et al. (2003, 2002), characterised the ability of PAR to penetrate into the gneiss subsurface, as well as variations experienced in temperature. The endolithic community was found to be predominantly within the genus *Chroococciopsis* and the epilithic (or surface-dwelling) community included species from *Aphanothese*, and *Gloeocapsa*. Furthermore, in relation to the epilithic communities, cryptoendoliths contained lower levels of UV screening pigments, such as scytonemin (Cockell et al., 2002). The work conducted by Fike et al. (2003), focused on characterising the associated heterotrophic community within the shocked gneisses through 16S rRNA sequencing of cultured isolates. Work on induced microbial endolithic habitats in shocked rocks has important astrobiological implications – both in the search for life on other planets, such as Mars, and in the idea of life being transported through space via meteorites (Panspermia hypothesis). Since impact cratering is an ubiquitous process throughout our system, it is plausible that if life did arise on Mars, shocked lithology could have provided shelter for these organisms under harsh conditions.

1.4.2 *Hydrothermal Phase of Impact Biology*

The documentation of microbial life associated with hydrothermal systems is quite large (Martin et al., 2008; Konhauser 2007; Karl 1995). On Earth, hydrothermal systems can develop anywhere where fluids come in contact with a heat source, which is typically endogenic. These areas have long been proposed as locations for the origins of life (Holm 1992), though some believe that these vents would not provide enough of a concentrating mechanism for putative organic molecules and informational-molecular precursors (Miller and Lazcano 1995). On Mars, which has been predicted to have had large initial levels of H₂O (frozen and solid), hydrothermal activity would have been associated with the large-scale tectonic events leading to the formation of Tharsis, for example (Osinski et al., 2013). Mars and the Earth have also enjoyed an extensive period of impact cratering

that would have provided an exogenous heat source in the form of a melt sheet to drive a hydrothermal system (Kirismaä and Osinski 2013). The promotion of rock/water interactions within a concentrated bowl may have proved ideal for the origins of life. To date, however, no microbial colonization has been discovered syngenetic to an impact-induced hydrothermal system. Given that the hydrothermal phase of the Haughton impact structure would likely have been quite extensive, it is conceivable that microbial communities could have developed. Thermophilic organisms capable of metabolising sulfur and iron, for example, could have existed alongside surface phototrophic communities. A study by Parnell et al. (2010) revealed significant sulfur isotope fractionation of the sulfide minerals at Haughton, providing a strong case for the presence of thermophilic sulfate reducing bacteria during the formation of these hydrothermal deposits. At modern-day hydrothermal systems, there is a very wide range of both aerobic and anaerobic metabolic reactions occurring, feeding off of dissolved metals and gasses created both through the interaction of magma with oxygenated seawater and through serpentinization (Martin et al., 2008). Though serpentinization is also a possibility in impact-induced hydrothermal systems, it is unlikely that it occurred at Haughton impact structure due to the primarily sedimentary target. The types of microbial community that might be seen at Haughton would be entirely dependent on the temperature and geochemistry of the fluid.

1.5 Thesis Outline

The purpose of this thesis is to determine the suitability of a crystalline impact lithology to support life under Arctic conditions. The impact process can mobilize biologically-relevant elements within the substrate, and for endolithic organisms, this process has important implications for life that is forced to seek refuge within the interior of rocks. Chapter 2 discusses bulk chemical ICP and XRF analyses for both shocked gneisses and sandstones to analyse the effect of an impact event on rock chemistry and to identify if impoverishment of bioessential elements occurred. It was found that unshocked target rocks and rocks that have experienced pressures up to ~80 GPa from the Haughton impact structure, Devon Island, Canada, show a discernible change in the major oxides, as well as changes in the distribution of elements with increasing shock level for both the

sedimentary and crystalline targets. The crystalline target rocks contain significant amounts of glass at higher shock levels (up to ~95% by volume), which improves the availability of bioessential elements to microbial endoliths as glasses are more easily dissolved by organic acids than crystalline substrates.

Though the bulk chemical analysis did reveal some impoverishment of the substrate, it did not seem to have a deleterious effect on colonization, as distinct endolithic bands could be seen within highly shocked samples. As such, Chapter 3 deals with the relationship between microbial biomass and shock level, as a function of porosity. A total of 27 samples, targeting the top 1 cm of rock, were examined using CSLM, SEM and bright field microscopy to investigate the relationship of biomass to shock level, which was found to correlate with increases in porosity. We found that crystalline gneisses that experienced pressures between 35 and 60 GPa provide the most ideal habitat for cryptoendolithic organisms, indicating that the slight reduction in available bioessential elements was not a deterrent, also suggesting perhaps an exogenous food source for these communities.

Within microbiology it is a generally accepted fact that only ~ 1% of the biota present in a given system is cultivable. In Chapter 4 we sought to elucidate the “community ecology” of impact shocked gneisses, and in so doing, also provide the first detailed 16S rDNA analysis of a cryptoendolithic community in a crystalline lithology from the Arctic. Using 454 pyrosequencing the 16S rDNA for Bacteria from 22 different samples spanning three shock populations (unshocked, moderate and highly shocked) was sequenced, as well as for Fungi and Algae from two samples. In contrast to Antarctic communities, these shocked gneisses are not dominated by cyanobacteria, but rather by common soil bacteria such as the Actinobacteria. Primary production is largely carried out by species from the Chloroflexi, with Cyanobacteria such as *Oscillatoria* sp. only occurring in small amounts among the shocked samples. It is clear from this study that the less stringent environmental pressures experienced in the Arctic likely result in this more-varied community, where less specialized organisms are able to survive.

The final research chapter of this thesis departs from the present-day colonizers of the Haughton structure and instead focuses on the post-impact hydrothermal regime and the unknown effects that hydrothermal fluids may have had on the impact shocked

gneisses in terms of chemical dissolution as well as colonization potential. To explore this idea, two sets of experiments were conducted: 1) Placement of a range of shocked gneisses in two hot springs in Iceland (Krýsuvík and Geysir); 2) Reproduction in the lab of the putative post-impact Haughton fluid geochemistry containing a thermophilic sulfate reducing bacteria (SRB). In the first of the Iceland experiments, the spring used at Krýsuvík was at a pH of 2 with a temperature of 38°C. Extensive colonization of the rocks was seen at the higher shock levels, with a shock level 3 rock showing extensive epilithic colonization by a filamentous organism. The second spring at Geysir had a pH of 8.1 and a temperature of 94°C at the location of immersion of samples. In such a high temperature environment, the number of species was significantly reduced, however, colonization of the highly shocked samples was observed, though this was strictly epilithic. In experiment #2, we again used three populations of shock (unshocked, moderate and highly shocked) under anaerobic conditions and two substrate types (coarse and fine) – exploring colonization potential and dissolution of the substrate under more controlled conditions. Cations such as Mg, K and Ca were observed to quickly dissolve into solution, a process that was more apparent in the biotic and higher shocked samples, and in the abiotic fine grained samples. There was a very distinct phenotypic change among the biotic vials, wherein among coarse substrates, suspended bacterial counts decreased with increasing shock. The highly shocked samples became entirely black and using SEM, were seen to be coated in a thick layer of FeS and extracellular polymeric substances and many vesicles were in-filled. In some instances, a weathered zone was visible around these in-filled vesicles. At the micron scale, the moderately shocked samples were also similarly colonized, sometimes quite extensively, even though macroscopically they appeared to have been relatively less influenced by SRB activity. Precipitation of unidentified tetrahedral and disk shaped carbonate minerals were also observed within the FeS-EPS surface layers demonstrating that the Haughton impact shocked gneisses can provide a substrate for planktonic bacteria in hydrothermal fluids, producing biomarkers comparable to, that observed within hydrothermal vugs at Haughton.

1.6 References

- Abramov, O. and Mojzsis, S. J. 2009. Microbial habitability of the Hadean Earth during the late heavy bombardment. *Nature* **459**:419–422.
- Alvarez, L. W., Alvarez, W., Asaro, F. and Michel, H. V. 1980. Extraterrestrial Cause for the Cretaceous-Tertiary Extinction. *Science* **208**:1095–1108.
- Barker, W. W., Welch, S. A. and Banfield, J. 1997. Biogeochemical weathering of silicate minerals. In J. Banfield and K. H. Nealson, editors. *Geomicrobiology: Interactions Between Microbes and Minerals*. Mineralogical Society of America, Atlanta. pp. 391–428.
- Burt, J. B., Pope, M. C. and Watkinson, A. J. 2005. Petrographic, X-ray diffraction, and electron spin resonance analysis of deformed calcite: Meteor Crater, Arizona. *Meteoritics & Planetary Science* **40**:297–306.
- Chao, E. C. T. 1968. Pressure and temperature histories of impact metamorphosed rocks - Based on petrographic observations. *Neues Jahrbuch für Mineralogie, Abhandlungen*. **108**:209–246.
- Cockell, C. S. 2004. Impact-shocked rocks - Insights into archean and extraterrestrial microbial habitats (and sites for prebiotic chemistry?). *Advances in Space Research* **33**:1231–1123.
- Cockell, C. S. and Lee, P. 2002. The biology of impact craters - a review. *Biological Reviews* **77**:279–310.
- Cockell, C. S., Lee, P., Broady, P., Lim, D. S. S., Osinski, G. R., Parnell, J., Koeberl, C., L. Pesonen, and J. Salminen. 2005. Effects of asteroid and comet impacts on habitats for lithophytic organisms - a synthesis. *Meteoritics & Planetary Science* **40**:1901–1914.
- Cockell, C. S., Lee, P., Osinski, G. R., Horneck, G., and Broady, P.. 2002. Impact-induced microbial endolithic habitats. *Meteoritics & Planetary Science* **37**:1287–1298.
- Cockell, C. S., McKay, C. P., and Omelon, C. R.. 2003. Polar endoliths - an anti-correlation of climatic extremes and microbial diversity. *International Journal of Astrobiology* **1**:305–310.
- Cockell, C. S. and Osinski, G. R.. 2007. Impact-induced impoverishment and transformation of a sandstone habitat for lithophytic microorganisms. *Meteoritics & Planetary Science* **42**:1985–1993.
- de los Ríos, A., Wierzchos, J., Sancho, L. G., Green, T. G. A. and Ascaso, C. 2005. Ecology of endolithic lichens colonizing granite in continental Antarctica. *The Lichenologist* **37**:383–395.

Douglas, S. and Beveridge, T. J. 1998. Mineral formation by bacteria in natural microbial communities. *FEMS Microbiology Ecology* **26**:79–88.

Earth Impact Database. Spray, J. G. and Elliot, B. 2013. Planetary and Space Science Centre, Fredericton. URL: <http://www.passc.net/EarthImpactDatabase/index.html>.

Fairén, A. G., Davila, A. F., Lim, D. S. S., Bramall, N., Bonaccorsi, R., Zavaleta, J., Uceda, E. R., Stoker, C., Wierzchos, J., and Dohm, J. M. 2010. Astrobiology through the ages of Mars: the study of terrestrial analogues to understand the habitability of Mars. *Astrobiology* **10**:821–843.

Fedo, C. M. and Whitehouse, M. J. 2002. Earth's Earliest Life. *Science* **296**:1448–1452.

Fike, D. A., Cockell, C. S., D. Pearce, and Lee, P. 2003. Heterotrophic microbial colonization of the interior of impact-shocked rocks from Houghton impact structure, Devon Island, Nunavut, Canadian high Arctic. *International Journal of Astrobiology* **1**:311–323.

French, B. 1998. *Traces of Catastrophe: A Handbook of Shock-Metamorphic Effects in Terrestrial Meteorite Impact Structures*. Lunar and Planetary Institute, Houston. pp. 17–30.

French, B. and Koeberl, C. 2010. The convincing identification of terrestrial meteorite impact structures: What works, what doesn't, and why. *Earth-Science Reviews* **98**:123–170.

Friedmann, E. I. and Ocampo, R. 1976. Endolithic Blue-Green Algae in the Dry Valleys: Primary Producers in the Antarctic Desert Ecosystem. *Science* **193**:1247–1249.

Gault, D. E., Oberbeck, V. R. and Quaide, W. L. 1968. Impact cratering mechanics and structures. In B. French and N. M. Short, editors. *Shock Metamorphism of Natural Materials*. Mono Book Corporation, Baltimore. pp. 87–99.

Hirsch, P., Eckhardt, F. E. W. and Palmer Jr., R. J. 1995. Methods for the study of rock-inhabiting microorganisms - a review. *Journal of Microbiological Methods* **23**:143–167.

Holm, N. G. 1992. Why are hydrothermal systems proposed as plausible environments for the origin of life? *Origins of life and evolution of the biosphere* **22**: 5–14.

Karl, D. M., editor. 1995. *The Microbiology of Deep-sea Hydrothermal Vents*. CRC Press, Boca Raton. pp. 35-124.

Kieffer, S. W. 1971. Shock Metamorphism of the Coconino Sandstone at Meteor Crater, Arizona. *Journal of Geophysical Research* **76**:5449–5473.

Kieffer, S. W., Phakey, P. P. and Christie, J. M. 1976. Shock Processes in Porous Quartzite: Transmission Electron Microscope Observations and Theory. *Contributions to Mineralogy and Petrology* **59**:41–93.

- Kirismaä, K. and Osinski, G. R. 2013. Impact-induced hydrothermal activity. In *Impact Cratering: Processes and Products*, Osinski, G.R. and E. Pierazzo eds. Wiley-Blackwell: Hoboken, NJ. pp. 76-87.
- Konhauser, K. O. 2007. *Introduction to Geomicrobiology*. Blackwell Publishing, Malden, MA. pp. 1–35, 192–292.
- Konhauser, K. O., Lalonde, S. V. and Phoenix, V. R. 2008. Bacterial biomineralization: Where to from here? *Geobiology* **6**:298–302.
- Kring, D. A. and Cohen, B. A. 2002. Cataclysmic bombardment throughout the inner solar system 3.9-4.0 Ga. *Journal of Geophysical Research* **107**(E2): 5009, 1–6.
- Lindgren, P., Parnell, J., Bowden, S., Taylor, C., Osinski, G. R. and Lee, P. 2007. Preservation of organic carbon in impact melt breccia, Haughton impact structure. *Lunar and Planetary Science XXXVIII*.
- Martin, W., Baross, J., Kelley, D. and Russell, M. J. 2008. Hydrothermal vents and the origin of life. *Nature Reviews Microbiology* **6**:805–814.
- Melosh, H. J. and Ivanov, B. A. 1999. Impact Crater Collapse. *Annual Review of Earth and Planetary Science* **27**:385–415.
- Miller, S. L. and Lazcano, A. 1995. The Origin of Life – Did it Occur at High Temperatures? *Journal of Molecular Evolution* **41**: 689–692.
- Morgan, J. and Warner, M. 1999. Chicxulub: The third dimension of a multi-ring impact basin. *Geology* **27**:407–410.
- Naumov, M. V. 2005. Principle features of impact-generated hydrothermal circulation systems: mineralogical and geological evidence. *Geofluids* **5**:165–184.
- Nienow, J. A., McKay, C. and Friedmann, E. I. 1988. The Cryptoendolithic Microbial Environment in the Ross Desert of Antarctica: Light in the Photosynthetically Active Region. *Microbial Ecology* **16**:271–289.
- Omelson, C. R. 2008. Endolithic Microbial Communities in Polar Desert Habitats. *Geomicrobiology Journal* **25**:404–414.
- Osinski, G. R. 2007. Impact metamorphism of CaCO₃-bearing sandstones at the Haughton structure, Canada. *Meteoritics & Planetary Science* **42**:1945–1960.
- Osinski, G. R., Cockell, C. S., Lindgren, P. and Parnell, J. 2010. The Effect of Meteorite Impacts on the Elements Essential for Life. Page Abstract #5252 *Astrobiology Science Conference 2010: Evolution and Life: Surviving Catastrophes and Extremes on Earth and Beyond*. Lunar and Planetary Institute, Houston.

- Osinski, G. R., Grieve, R. A. F., Tornabene, L. T. 2013. Excavation and impact ejecta emplacement. In *Impact Cratering: Processes and Products*, Osinski, G.R. and E. Pierazzo eds. Wiley-Blackwell: Hoboken, NJ. pp. 43–57.
- Osinski, G. R., Lee, P., Spray, J. G., Parnell, J., Lim, D. S. S., Bunch, T. E., Cockell, C.S., and Glass, B. 2005a. Geological overview and cratering model for the Houghton impact structure, Devon Island, Canadian high Arctic. *Meteoritics & Planetary Science* **40**:1759–1776.
- Osinski, G. R., Lee, P., Parnell, J., Spray, J. G., and Baron, M. 2005b. A case study of impact-induced hydrothermal activity: the Houghton impact structure, Devon Island, Canadian High Arctic. *Meteoritics & Planetary Science* **40**:1859–1877.
- Osinski, G. R., Tornabene L. L., Banerjee, N. R., Cockell, C. S., Flemming, R., Izawa, M. R. M McCutcheon, J., Parnell, J., Pickersgill, A. E., Pontefract, A., Preston, L., Sapers, H. M. and Southam, G. 2013. Impact-generated hydrothermal systems on Earth and Mars. *Icarus* **224**: 347–363.
- Parnell, J., Boyce, A., Thackrey, S., Muirhead, D., Lindgren, P., Mason, C., Taylor, C., Still, J., Bowden, S., Osinski, G. R., and Lee, P. 2010. Sulfur isotope signatures for rapid colonization of an impact crater by thermophilic microbes. *Geology* **38**:271–274.
- Singleton, A. C., Osinski, G. R., McCausland, P. J. A., and Moser, D. E. 2011. Shock-induced changes in density and porosity in shock-metamorphosed crystalline rocks, Houghton impact structure, Canada. *Meteoritics & Planetary Science* **46**:1774–1786.
- Sleep, N. H., Zahnle, K. J., Kasting, J. F. and Morowitz, H. J. 1989. Annihilation of ecosystems by large asteroid impacts on the early Earth. *Nature* **342**:139–142.
- Stöffler, D. 1966. Zones of Impact Metamorphism in the Crystalline Rocks of the Nördlinger Ries Crater. *Contributions to Mineralogy and Petrology* **12**:15–24.
- Stöffler, D. 1971. Progressive Metamorphism and Classification of Shocked and Brecciated Crystalline Rocks at Impact Craters. *Journal of Geophysical Research* **76**:5541–5551.
- Tera, F., Papanastassiou, D.A., Wasserburg, G.J. 1974. Isotopic evidence for a terminal lunar cataclysm. *Earth and Planetary Science Letters* **22**:1–21.
- Vestal, R. J. 1988. Biomass of the cryptoendolithic microbiota from the Antarctic desert. *Applied and Environmental Microbiology* **54**:957–959.
- von Engelhardt, W. and Beetsch, W. 1969. Shock Induced Planar Deformation Structures in Quartz from the Ries Crater, Germany. *Contributions to Mineralogy and Petrology* **20**.
- Wackett, L. P., Dodge, A. G. and Ellis, L. B. M. 2004. Microbial genomics and the periodic table. *Applied and Environmental Microbiology* **70**:647–655.

Wierzchos, J. and Ascaso, C. 2001. Life, decay and fossilisation of endolithic microorganisms from the Ross Desert, Antarctica. *Polar Biology* **24**:863–868.

Chapter 2 : The Effects of Meteorite Impacts on the Availability of Bioessential Elements for Endolithic Organisms¹

Alexandra Pontefract, Gordon R. Osinski, Paula Lindgren, John Parnell, Charles S. Cockell and Gordon Southam.

2.1 Introduction

Meteorite impact events are capable of generating extreme temperatures and pressures, causing the target substrate to undergo deformation, vaporization, melting and shock metamorphism. Although initially destructive in nature, these processes can favourably change the habitability of the target substrate for rock-dwelling (endolithic) organisms, which are able to (re)colonize fractures and pore spaces created by the impact (Cockell et al., 2005). Of further interest are the generation of post-impact hydrothermal systems and the role they play in hosting microbial life. Previous work has revealed the creation of hydrothermal systems immediately following an impact into a H₂O-bearing substrate (e.g., Naumov 1996; Osinski et al., 2012). These systems, depending on the size of the impactor, are capable of being active for up to several million years in large (100 km-scale) impact craters (e.g., Ames et al. 1998). When considering the current view that the origins of life are rooted in high temperature systems (Martin et al. 2008), as well as the continuity of impact events throughout the lifetime of a planetary body, it is plausible that such impact-generated systems could have played host to the origins of life on Earth, as well as on other bodies in the solar system (e.g., Cockell et al., 2002a; Osinski et al., 2001, 2005; Versh et al., 2006; Parnell et al., 2010).

The formation of communities in the interior of rocks (hereafter referred to as cryptoendolithic) has long been recognized as an advantageous response to harsh environmental conditions, especially in relation to cold, arid environments such as polar deserts (Friedmann et al., 1976; Friedmann 1980; Vestal 1988). These habitats can be created through a variety of processes: physical, chemical and biological. Organisms

¹This chapter was previously published: Pontefract, A., G. R. Osinski, P. Lindgren, J. Parnell, C. S. Cockell, and Southam, G.. 2012. The role of meteorite impacts on the availability of bioessential elements for Endolithic organisms. *Meteoritics & Planetary Science* **47**:1681-1691.

residing in, upon, or beneath these lithic habitats generally enjoy increased UV protection, shelter from wind ablation and temperature shifts, as well as benefitting from the build-up of wind-blown debris which often serves as a source of nutrients (Friedmann 1980). Finally, endolithic communities (both phototrophic and heterotrophic) are capable of acquiring their nutrients directly from the substrate itself (Konhauser 2007). Redox reactions occurring at the rock-water interface can provide fuel for microbial metabolism. Microbes themselves can also alter the chemistry of the environment through the production of organic acids, which aid in weathering the substrate (Konhauser 1998).

Given the benefits of an endolithic way of life in response to extreme environmental conditions, it has been posited that endolithic organisms could exist (or have existed) within impact craters on planets such as Mars (Cockell et al., 2002a) and/or within the deep Martian sub-surface (Boston et al., 1992). Studies by Cockell et al. (2002b, 2005) and Cockell and Osinski (2007) have shown that growth of endoliths within impact metamorphosed substrates correlates with shock level in both sedimentary and crystalline targets; however, the specifics of this relationship are still unclear. Increased porosity and translucence of the substrate may be major contributors to this relationship, but what is still unknown is the scaling of available nutrients with an increase in shock level. In particular, upon exposure to temperatures up to, and exceeding 2000°C, the target may experience redistribution or loss of elements essential for microbial metabolism. Importantly, there are six major elements that are necessary for life, C, H, N, O, P and S; as well as several that play key roles in DNA synthesis (mechanistic or enzyme function), cell membrane stability, pH balance, ion transport and enzymatic digestion such as Cl, K, Na, Mg, Mn, Fe, Cu, Co, Ni, Zn, and Se (Wackett et al., 2004). Many of these are present as hydrated oxides within rocks and, as such, are subject to volatilization during an impact event.

The purpose of this study is to determine whether element redistribution or element loss occurs within the target as the result of a meteorite impact, in order to elucidate the capability of a shocked target to provide sufficient major and trace elements to support microbial colonization (with the exception of N, which was not studied here since it can be 'easily' fixed by bacteria in endolithic habitats (Boison et al., 2004). Preliminary work by Fike et al. (2003) showed a potential loss in bioessential elements in a study of

crystalline rocks; however, later work by Lindgren et al. (2007) and Osinski et al. (2010), presented only in abstract form, suggested that there was no significant loss of bioessential elements in carbonaceous samples. We present new data on crystalline rocks and a synthesis of previous published and unpublished geochemical work completed on extensive data sets of both crystalline and sedimentary samples. To this end, the study of a relatively young and unaltered impact structure was necessary, and was satisfied by the Haughton impact structure in the Canadian High Arctic.

2.2 Methods

2.2.1 Field Site

The Haughton impact structure is located on the northwestern region of Devon Island, Nunavut, in the Canadian High Arctic archipelago at 75°08'N, 87°51'W (Osinski et al., 2005a). This 39 Ma complex impact structure has been well documented, with studies going back to the 1970s (e.g., Frisch and Thorsteinsson 1978; Grieve and Robertson 1979). The target rocks are almost entirely sedimentary and represent lower Paleozoic rocks of the Arctic Platform. This ~1880 m sequence (pre-impact thickness) is comprised of carbonates, with lesser amounts of evaporites, sandstone and shale, overlaying gneisses of the Precambrian basement of the Canadian Shield (Figure 2-1). Haughton has an apparent diameter of ~23 km, with a final crater rim estimate of 16 km in diameter (Osinski et al., 2005a). The most identifiable feature of the impact structure is the pale-grey crater-fill (clast-rich impact melt rocks) deposits, which form a discontinuous layer throughout the centre of the structure. Another salient feature of the structure is its hydrothermal deposits, seen in the form of several alteration products, such as selenite and marcasite, as well as the presence of hydrothermal vugs (Osinski et al., 2001, 2005b). Finally, lacustrine deposits comprising the Haughton Formation are present in and around the centre of the crater, which represent the transient presence of a lake during the Neogene several Myr after the crater formed. These sediments contain fossilized pollen grains, plants and vertebrate skeletons, and represent a late stage in the biological succession of the crater (Cockell et al., 2002a).

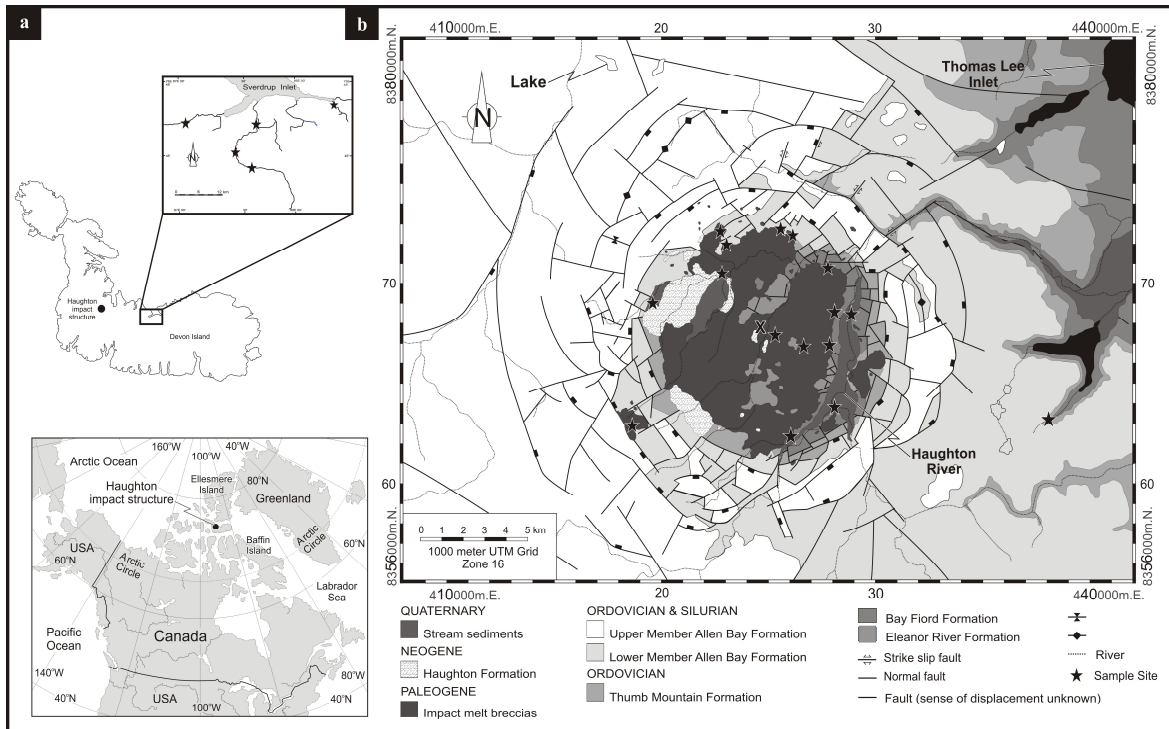


Figure 2-1. (a) Map showing location of the Haughton impact structure on Devon Island, as well as the location of Sverdrup Inlet (top). (b) Target stratigraphy in and around the Haughton structure. Modified after Osinski et al. (2005a). Sample sites for all data sets are shown as black stars both within and outside of the crater (a, b). Note that in some cases, multiple sites are represented by one marker due to their proximity. For detailed coordinates of each site, see Appendix A2.

2.2.2 *Sample Collection and Processing*

Samples for this study were collected during various field seasons from 1999 until 2010 from many different locations within and exterior to the crater, and consist of three separate suites (Figure 2-1).

Suite 1: Total Organic Carbon (TOC) Analysis: The samples of target bedrock that were analysed for TOC came from a wide range of pre-impact depths in the sedimentary target succession and include material from different formations: Allen Bay Formation, Thumb Mountain Formation, Bay Fiord Formation, Eleanor River Formation and Blanley Bay Formation (Figure 2-1). This corresponds to 10 samples of target carbonate, 2 samples of target sulfate, 4 samples of target sandstone and 4 samples of target shale. From the impact products, 5 samples of whole clast-rich melt rock from 4 different localities, and 6 lithic carbonate clasts in the clast-rich melt rock, from 6 different localities, were analysed. In addition to measuring the total organic carbon in the whole clast-rich melt rock, lithic carbonate clasts, with sizes of a few cm in diameter were analysed, to investigate the amount of organic carbon preserved after the carbonate clasts had been affected by a high temperature impact melt.

Suite 2: Sedimentary Target Analysis: Sedimentary samples corresponding to (1) unshocked (2) low shock (3) clast-rich melt rock (CMR) (4) CMR clasts and (5) post-impact sediments, were collected from several different units both within and outside of the crater. These samples were powdered using a pulveriser, and analysed using X-Ray Fluorescence Spectroscopy (XRF) (see below).

Suite 3: Crystalline Target Analysis: Crystalline (gneiss) samples representing the unshocked basement were collected from in-and-around Sverdrup Inlet (see Figure 2-1a). It is important to note here that we have assumed that the composition of the basement under the crater and the basement at Sverdrup Inlet is the same, but it is possible that significant heterogeneity is present. Shocked samples were collected within the crater from a wide number of locations on several of the breccia hills located both near the crater rim and towards the central uplift. These samples were thin-sectioned. Shocked samples were powdered using an alumina mortar and pestle (CoorsTek, Colorado, USA #60370). Samples from the unshocked crystalline basement were crushed using a Bico Chipmunk Crusher, and powdered using a T.M. Vibratory Ring Pulverizer. These

samples were then analysed using Inductively Coupled Plasma emission spectroscopy (ICP) (see below).

2.2.3 *Shock Classification*

Shock classification of crystalline rocks was done through the use of petrographic analysis (Figure 2-2). This process was necessary so as to determine the extent of alteration experienced by each sample, allowing for a correlation between the extent of heat and pressure that the substrate was exposed to and any corresponding changes in bulk chemistry. In this paper, we have used the classification system created by Singleton et al. (2011) for rocks at the Houghton structure, which expands on work by Stöffler (1966), Chao (1968), Metzler (1988), Bunch et al. (1997) and French (1998) (see Appendix A1). This new classification system refines the earlier shock level demarcations, dividing them into a much finer scale classification and allowing for a more in-depth correlative analysis. The classification system used in this paper for the crystalline strata cannot currently be applied to the sedimentary strata due to significant differences in the response of the lithology to shock. For a comparison of shock between carbonate and crystalline targets, see Osinski (2007). Shock classification schemes for carbonate rocks do not currently exist. It should be noted that in this paper broad terms referring to shock are sometimes used, i.e. “unshocked” refers to shock level 0 samples, “low shock” to shock levels 1–4, and “high shock” to shock levels 5–7.

2.2.4 *Total Organic Carbon*

Samples were analysed either through acquiring a powder by drilling out the components of interest, or crushing them to a fine powder using a TEMA mill after trimming the edges of the samples with a diamond saw blade to remove surface weathering and contamination. Before analysis the carbonate-bearing samples were treated with warm 25% hydrochloric acid (HCl) for removal of inorganic carbon (Gross 1971). The acid residues were analysed with a Carbon-Sulfur analyser (LECO CS225) at the University of Aberdeen for their total organic carbon content. Pre-impact target rocks from outside the crater were sampled and compared to the clast-rich melt rock. The composition of the CMR was assumed to be ~74% carbonates, ~10% evaporates, ~8% sandstone and ~8% shale, based on the pre-impact stratigraphy between 500 m and 2000 m.

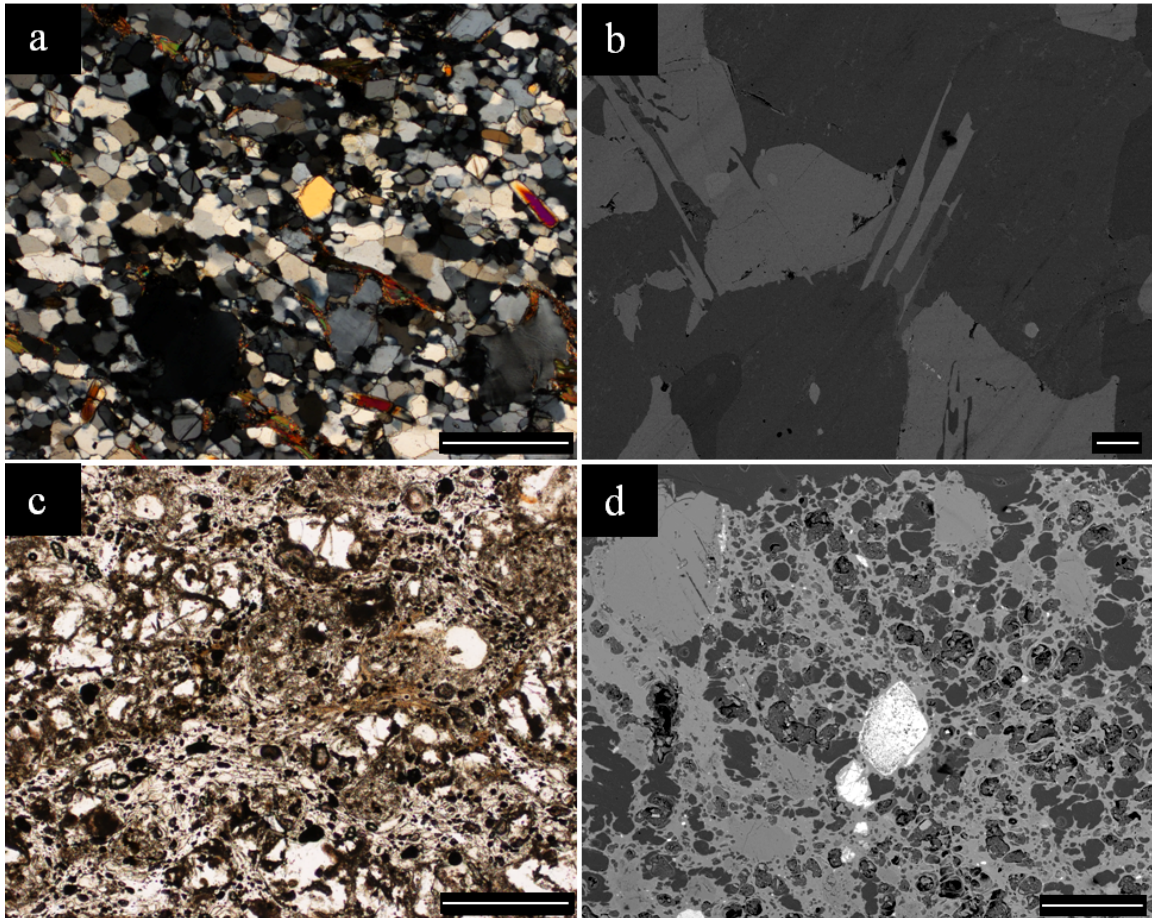


Figure 2-2. Photomicrographs and backscattered electron images of crystalline gneiss. (a) cross-polarized micrograph and (b) SEM-BSE micrograph of the unshocked basement gneiss from Sverdrup Inlet. The sample is largely comprised of quartz, plus sillmanite and biotite. (c) Plane-polarized micrograph and (d) SEM-BSE micrograph show a sample of gneiss of shock level 6 shocked at pressures exceeding 60 GPa. Note the extensive frothy texture and presence of glass phases. Scale bars for light micrographs (a,c) are 500 μm , scale bars for SEM-BSE micrographs (b,d) are 100 μm .

2.2.5 XRF

Analyses were carried out on a PHILIPS PW2440 4kW automated XRF spectrometer system by Geochemical Laboratories, McGill University, Montréal, Canada. This system uses a rhodium 60 kV end window X-ray tube, five X-ray detectors, four primary beam filters, eight analysing crystals, two fixed channels for simultaneous measurement of Na and F, and a PW2540 168 sample x-y autochanger. The major elements were analysed using 32 mm diameter fused beads prepared from a 1:5 sample: lithium tetraborate mixture. Minor element analyses were performed on 40 mm diameter pressed pellets prepared from a mixture of 10 g sample powder with 2 g Hoechst Wax C Micropowder. Data sets were analysed for statistical significance using a non-parametric Mann-Whitney U-test, which is similar to the t-test for determining whether two populations are statistically separate; however, it does not assume any specific distribution of the data, unlike the t-test which requires a normal distribution (Mann et al., 1947; McKnight et al., 2010).

2.2.6 ICP-AES

Analyses of major oxides and trace elements were done using a Perkin Elmer Elan ICP-MS by Acme Labs, Vancouver, Canada. Powdered samples were prepared in a lithium metaborate/tetraborate infusion, and then dissolved using ACS grade nitric acid. Loss on ignition (LOI) was determined by igniting a sample split, then measuring the weight loss. Total carbon and sulfur were determined using a Leco Carbon-Sulfur Analyser; samples were ignited in an induction furnace and adsorption of Carbon/Sulfur was measured by an infrared spectrometric cell. Detection limits for all of the major oxides were at 0.01%, with Cr_2O_3 at 0.002%. The dataset for trace element composition is limited to ICP data, as the XRF study did not include this analysis. Datasets were analysed using a non-parametric Mann-Whitney U-test, for non-normally distributed populations.

2.2.7 SEM-BSE and EDS Analysis

Polished thin sections of gneiss from each of the shock levels were analysed to identify any trends in the redistribution of major element composition with increasing shock. Areas of interest (regions containing vesicles and/or melt) were first identified using a

petrographic microscope. Samples were carbon coated using an Edwards Auto 306 and imaged on a Hitachi SU6600 Analytical FEG-SEM (Scanning Electron Micrograph), using a 5 segment back-scatter (BSE) detector. Semi-quantitative chemical information was collected using an Oxford 80 mm² XMax EDX (Electron Dispersive X-ray) detector, and analysed using Inca Microanalysis Suite, v. 4.11.

2.3 Results

2.3.1 TOC in Haughton CMR

The total organic carbon in the various target lithologies and impact products at Haughton are presented in Table 2-1 (see also Appendix A3). Both the carbonate clast fraction of the melt rock and the whole rock samples of melt rock contain low levels of organic carbon; 0.10 to 0.17% TOC, with an average value of 0.14%. This is substantially lower than the contribution of organic carbon measured as an input from the pre-impact target rocks, i.e., 0.66%; however, we found that the pre-impact sandstone target has a total organic carbon content that varies between 0.03 and 0.06%, which is lower than the melt rock values. The two samples of sulfate analysed here have values of 0.13 and 0.03% TOC respectively. We also found that organic carbon input to the CMR from the target was highly dependent on the shale (see Appendix A3), which has a pre-impact TOC of up to 11.43%, although samples of CMR only preserved 20% TOC on average (Table 2-1).

2.3.2 Sedimentary Samples

A total of 57 samples were analysed through XRF analysis (Appendix A4). For all of the major oxides analysed, none of these 'bulk' samples showed any relationship with shock level, with P actually showing higher concentrations in post-impact sediments (~ 0.07%) and impact melt breccia, than in the unshocked/low shock samples (~0.03%) (Figure 2-3). Many of the major oxides were close to, or at, the detection limits. In Figures 2-3b and 2-3c, there is an excellent correlation of Fe₂O₃:Al₂O₃ and P₂O₅:Al₂O₃ (irrespective of shock level, with the exception of the post-impact sediments, some of which fall off the line), with R² values of 0.9707 and 0.9742 respectively, and $p < 0.01$ for both. Figure 2-3a shows no correlation with shock level, a lack that is largely representative of the bulk of the data collected.

Table 2-1. Calculation of TOC contents. The numbers within the parentheses represent the number of different samples that were analysed. Italicized numbers located adjacent to % TOC values represent the standard deviation of the sample. See Appendix A3 for full data set.

Target bedrock	% TOC	Lithology contribution to clast-rich melt rock (%)	% TOC input from the target bedrock	
Carbonate (10)	0.12 (<i>0.07</i>)	74	0.09	
Sulphate (2)	0.08 <i>n/a</i>	10	0.01	
Sandstone (4)	0.05 (<i>0.01</i>)	8	0.004	
Shale (4)	7.01 (<i>5.26</i>)	8	0.56	
			Sum: 0.66	
% TOC target input	% TOC melt rock (5)	% TOC preserved in CMR	% TOC target carbonate (10)	% TOC carbonate clasts (6)
0.66	0.14	~20	0.12	0.14

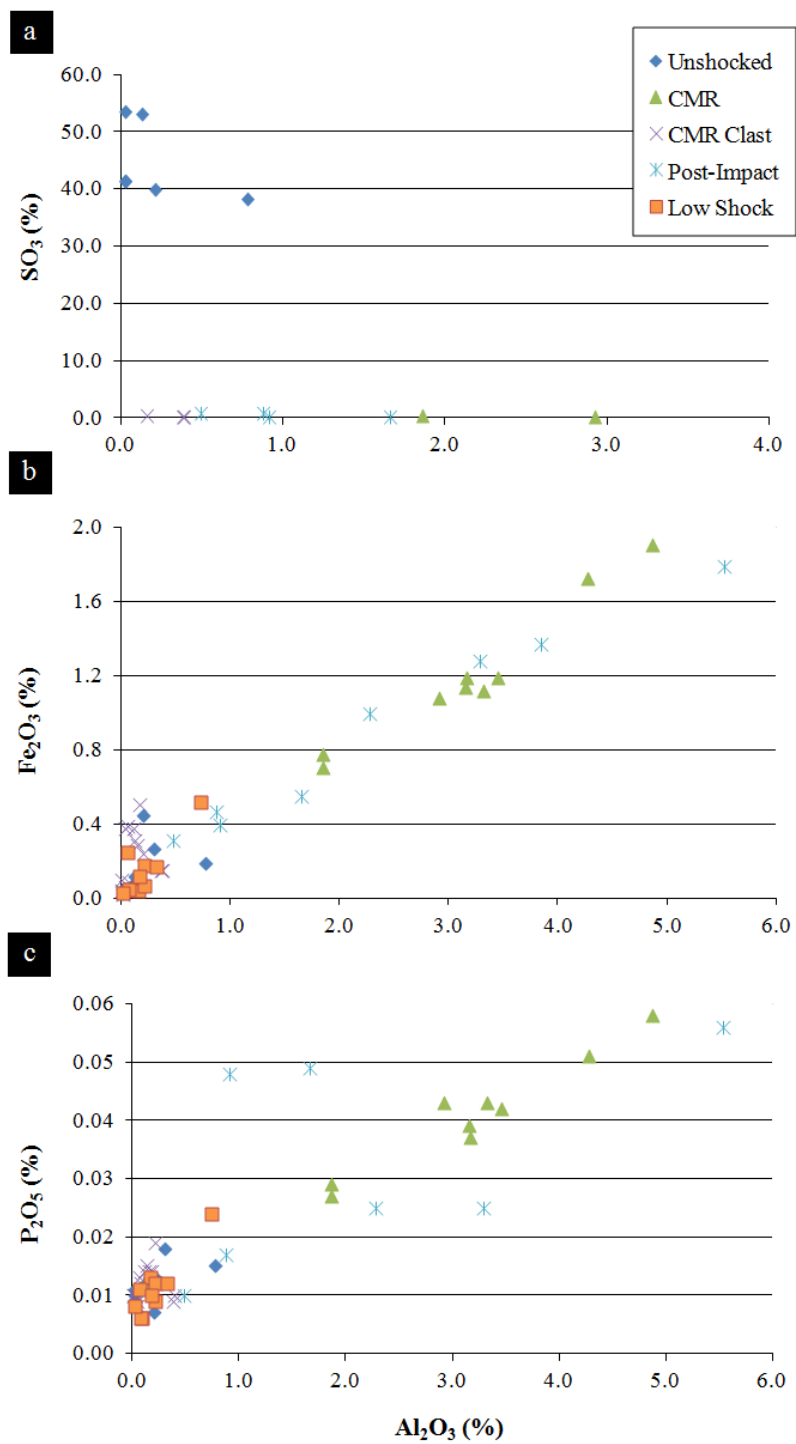


Figure 2-3. Graphs showing XRF data of sedimentary lithologies for some biologically relevant elements, plotted against Al_2O_3 . In (b) and (c), a linear trend for CMR is visible with R^2 values of 0.9707 and 0.9742 respectively.

2.3.3 *Crystalline Samples*

Fifty samples of both shocked and unshocked gneiss from in and around Haughton were analysed using XRF and ICP, the data of which was plotted together, as the two methods were found to be in good agreement (Appendices A4 and A5). From both the major oxide and trace element data collected, no fine-scale correlation between shock level and elemental composition was found. Indeed, samples from low shock and high shock levels frequently had the same composition (Figure 2-4). Elemental composition was also plotted against broad-range shock levels (i.e. unshocked vs. low shock), which revealed a reduction in elemental concentration with increasing shock pressure. The pre-impact composition of the gneisses in and around the Haughton Structure are quite variable, with at least 11 different types of gneiss identified (Metzler et al., 1988). This heterogeneity of target materials is represented in our own sample set of 10 unshocked basement rocks, where Si content varied from 50% to 80%, and Fe ranged from 1% up to 9%. In addition, data sets were also plotted as a set of means for each major oxide and trace element analysed, standard deviations are available in Appendix A7. For all of the major oxides, with the exception of SiO₂ and CaO, the mean concentration decreased with increasing shock level, revealing a polynomial distribution (Figure 2-5). A polynomial trendline was fitted to the data, with the highest correlation being MgO, $R^2 = 0.8625$, see Figure 2-4. The highest concentration levels were observed not in the unshocked samples, but in samples from shock level 3 (10-30 GPa range), which was found to be a statistically different population, $p < 0.05$ from all of the other samples (see Appendix A7 for probability calculations).

2.3.4 *SEM-BSE and EDS*

Though changes in bulk chemical composition were minor, it is evident that there was significant redistribution of these elements, especially at higher shock levels. BSE images from shock levels 5 and above (Figure 2-6), show large amounts of feldspar mineral glasses. Generally these glasses contain quartz clasts that still preserve their grain shapes, as well as partially melted plagioclase and K-feldspar clasts (Figure 2-6a). In some cases the glasses contain small, 1–10 µm-scale, iron and titanium-rich clasts (Figure 2-6b). We were not able to determine the mineralogy of these clasts.

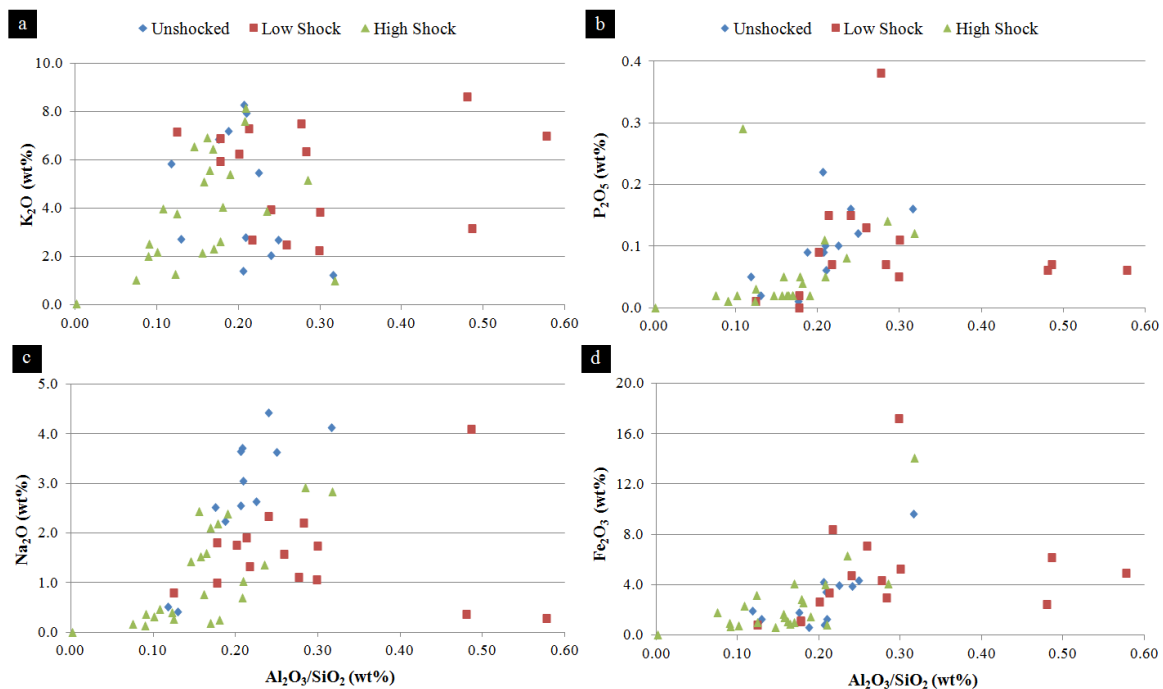


Figure 2-4. Graphs showing combined XRF and ICP data for crystalline rocks of various elements plotted against the ratio of $\text{Al}_2\text{O}_3/\text{SiO}_2$. With the exception of Na_2O , the other graphs show no significant difference between unshocked and low shock populations. All four plots show a statistical difference ($p < 0.01$) between the low shock and high shock populations which reveal a reduction in concentration for the given element.

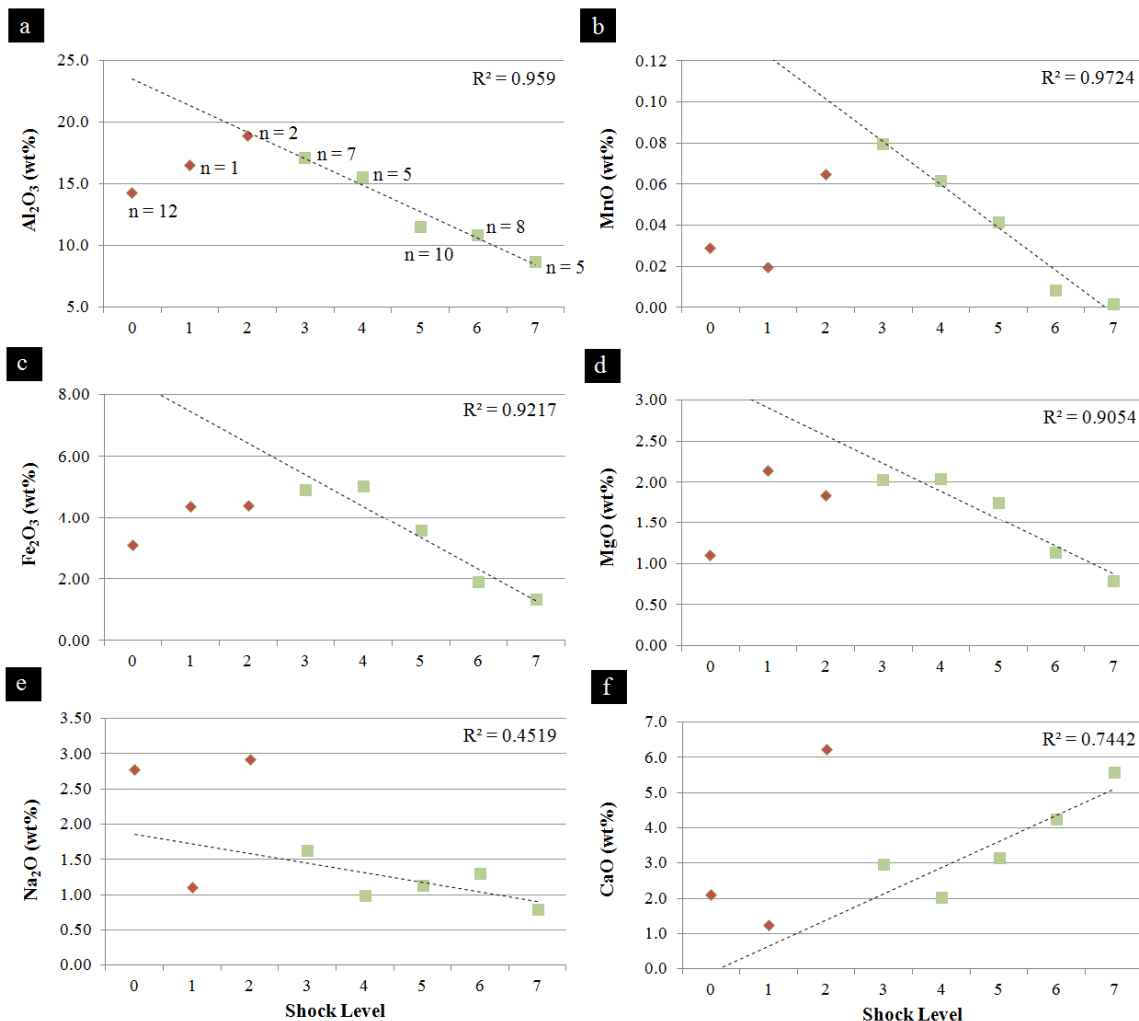


Figure 2-5. Graphs showing the means of several different elements, compiled from XRF and ICP data (see Appendix A5). A linear regression has been applied to data from shock levels 3–7. Shock levels 0,1 and 2 (shown here as diamonds) have been omitted from this analysis, as they either comprise samples outside of the crater or, in the case of the low shock levels, only comprise 1 and 2 samples, respectively, and as such, are subject to a significant amount of bias. For all of the graphs the unshocked samples were shown to be statistically different from shock level 3 samples. A significant difference was also observed between shock level 3 and 7 sample populations. See Appendix A7 – for all p-value calculations.

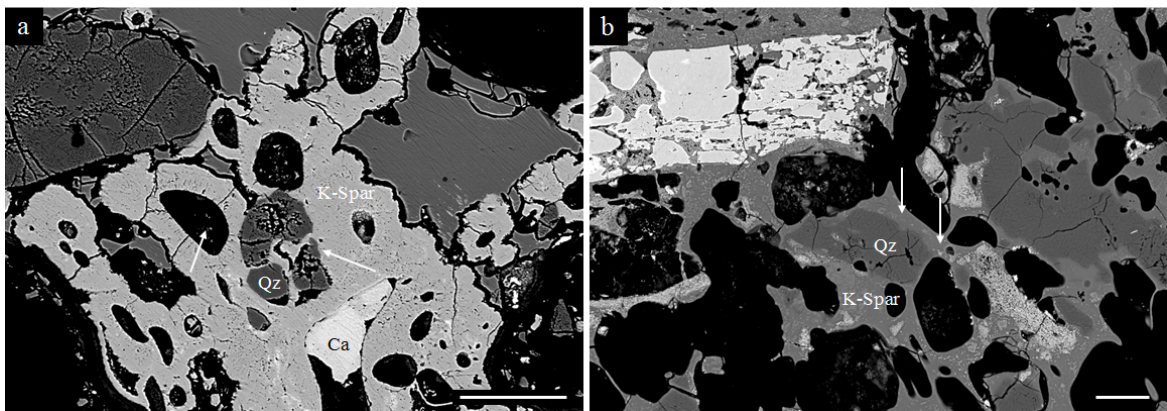


Figure 2-6. SEM-BSE micrographs of shocked gneiss. Both images show quartz (Qz) clasts within a mineral glass derived from potassium feldspar (K-Spar). In (a), the left-most arrow highlights a vesicle, and the right-most, an area where the quartz crystal has been disaggregated into “rafts” within the glass. In (b), the arrows indicate where small amounts of iron have been mobilized within a feldspar mineral glass. Scale bars are 100 μm and 10 μm , respectively.

2.4 Discussion

As the shockwave passed through the pre-impact target of the Haughton structure, temperatures and pressures upwards of 2000°C and ~80 GPa, respectively, were likely attained (Osinski et al., 2005b). One hypothesis is that the intense volatilization and melting that occurred as a result of this impact and the concomitant loss of material would have a similar effect on labile elements in the target substrates, i.e., a depletion of oxides, resulting in brecciated samples that were composed primarily of Si and O. This would of course have significant deleterious effects on the ability of microorganisms to inhabit such environments. We find, however, that this is not the case. In our analysis of over 100 samples of sedimentary and crystalline rocks, no systematic change between differing shocked samples in either the major oxide or trace element data sets were observed when plotted as ratios. For some of the major oxides within the crystalline samples, a significant difference was noted between unshocked and highly shocked samples, and in some cases between low shock and high shocked samples (Figure 2-4a,c).

Alternatively, within the sedimentary samples, some of the values are actually found to be higher within shocked samples (Figure 2-3a). In the case of phosphorus, the higher levels of the shocked samples may be the result of phosphate deposition from hydrothermal fluids or could be derived from input of the basement materials (e.g., from apatite-bearing granitic lithologies). Another potential source of phosphorus within the rocks analysed could, intuitively, be due to the phosphorus within the colonizing organisms, all of which require phosphorus for cellular function (Oberson and Joner 2003). This would also explain why the hydrogeochemically-isolated CMR clasts do not show an increase in phosphorus, since the CMR clasts would not be exposed to endolithic colonization. However, it does not address the issue of initial microbial access to phosphorus. If the source of phosphorus came from the host rock, then isolated CMR clasts should have been similarly enriched.

Mean values of the data for all samples (both sedimentary and crystalline) were calculated, but it was only when plotting the means of the major oxides for the crystalline samples that a decrease in concentration with shock level was observed (see Figure 2-5). This was not seen in either the trace element data for the crystalline samples, or in any of the sedimentary material. The explanation for this is unclear. It is possible that the trace

elements themselves are generally a part of more stable phases within the rock and thus are not so readily volatilized. However, with the sedimentary data, this is likely not the case. One important difference between the sedimentary and crystalline data, however, is the classification system that is used. The lack of a fine-scale, i.e. μm -scale, categorization of shock level in sedimentary lithologies then, may be limiting our ability to detect changes occurring within the current broad categorization used.

Curiously, most of the oxides for the crystalline samples experience a peak in mean concentration at shock level 3 and then begin to decrease beyond this. As noted previously, we have assumed that the basement samples collected from Sverdrup Inlet (representing unshocked gneiss) have the same composition as those beneath the impact structure. Given that most of the unshocked samples (with the exception of Figure 2-5f) plot below the shocked samples, it is likely that some heterogeneity is present. Shock level 0 samples were shown to be statistically different from the shock level 3 suite of rock, but frequently were considered to be quite similar to the shock level 7 grouping (see Appendix A7). Given that shock level 3 was statistically different from shock level 7, we believe that this clearly shows that the unshocked basement outside the crater is not ideally representative of the pre-impact basement beneath the crater. Unfortunately, there is no other way to access the pre-impact basement and so we must use the values collected. In some of the graphs (e.g., Figures 2-5a,d), the values for shock levels 1 and 2 (which were omitted from the trend line due to insufficient sample numbers) plot above the higher shock levels, supporting the idea that the lower shock levels (i.e., shock levels 1-3) possess increased nutrients relative to their more highly shocked counterparts (this does not, however, inhibit endolithic growth; Cockell et al., 2002b). The lack of low-shock samples in this study is representative of the fact that there is a significant paucity of low-shock samples available from the Haughton structure in general. This deficiency has been noted in previous studies of the structure (e.g., Metzler et al., 1988), but to date the reasons are still unclear. It should also be noted that the decrease seen in the mean data could have alternative explanations. It is possible, for example, that the decrease is representative of the path of the shockwave, travelling through different lithologies as it radiates out from a central point.

When examining the major physical changes occurring in the crystalline samples, significant change is found to occur at the transition from shock levels 4 and 5. At this point, one can see the formation of diaplectic glasses as well as selective melting of some minerals. It follows then that at this stage there could be mobilization of elements occurring within the samples, which would explain any decrease in oxide composition. Indeed, at shock level 6 we observed feldspathic- and silica-rich glasses that were intermingled, though still appearing to maintain distinct boundaries (Figure 2-6b). Within these melts we also observed small titanium and iron-rich clasts that were possibly mobilized as a result of the heat and pressure. Taking into account the problems inherent with collecting sufficient chemical data for the lower shock levels, it is plausible that concentrations might actually remain fairly consistent up until shock level 4, and then begin to experience a more significant decrease. Finally, it is noted that in Figure 2-5f, there is actually an increase in the concentration of CaO with shock level. There could be several reasons for this. Firstly, the CaO could be present as carbonate melt inclusions, which forms the groundmass to the impact melt rocks (Osinski et al. 2005a). Alternatively, these elevated CaO levels could be the result of post-impact alteration (either through hydrothermal or modern-day weathering), where increased pore space with increasing shock levels would allow for more significant amounts of secondary carbonate deposition.

The TOC data from the carbonate clasts of the CMR exhibit a similar pattern. The results from the total organic carbon (TOC) analysis and the mass balance calculation of carbon in the target before impact and carbon preserved in the carbonates shows that the organic carbon levels actually increase. The carbon in put to the CMR from the pre-impact target, however, is highly dependent on the carbonate target rock, since 74% of the target succession is composed of carbonate. The results from the TOC analyses show that the carbon content of the carbonate target varies significantly between different samples (0.07 – 0.30% TOC), while the carbon content of the melt rock is more constant (0.10 – 0.17% TOC) which is not a significant change. This is likely a result of the fact that the melt rock is a mix of all target rocks, and therefore the %TOC is averaged out here. These values are consistent with previous studies that have shown that despite the high initial temperatures of the impact melt rocks (> 1750°C for Haughton (Osinski et al.,

2005b)), organic carbon is preserved in the impact melt breccia, including in the lithic carbonate clasts (Parnell et al., 2005).

2.5 Biological Implications

The ability of organisms to derive nutrients from the lithosphere (nutrients that are largely unavailable to many living organisms) has been long documented (Barker et al., 1997; Ehrlich 1998; Welch et al., 1999; Bennet et al., 2001; de los Ríos et al., 2002; Konhauser 2008). Many microorganisms are capable of secreting a wide range of organic acids and chelators to liberate elements from mineral surfaces. Exopolysaccharide (EPS) can maintain acidity levels and act as binding sites for mineral formation (Barker et al., 1997, Douglas and Beveridge 1998). Some minerals, however, can prove difficult to dissolve due to the stability of their crystal structure. The observation that levels of microbial growth tend to increase with shock level (e.g. Cockell and Osinski 2007) correlates, in part, with the occurrence of glasses within the impact shocked rocks. The answer for this may lie in the amorphous nature of glasses, which are more easily weathered due to the lack of a stable crystalline framework, promoting the growth of these microorganisms. For example, the mobilization of iron into the melt would intuitively make it more accessible to the microbial community (Figure 2-6). In addition, during mobilization and potential volatilization of hydrous minerals, the corresponding elements, such as K, Na, and Mg that are left behind, might preferentially coat the insides of vesicles (Fike et al., 2003).

2.6 Concluding Remarks

This study has shown that, though initially very destructive, a meteorite impact event does not cause impoverishment of the target substrate with respect to elements essential for life (as we know it). Coupled with the formation of possible hydrothermal systems, an increase in available habitat for endolithic organisms and the generation of heating over a long (million-year) period of time, it is possible that impact craters could serve as habitats for life on other planets than our own. As these hydrothermal environments began to cool down and eventually disappeared entirely, putative microbial colonies could have migrated into these newly-created endolithic habitats where they would be protected from UV radiation, temperature shifts, and dessication. If this hypothesis

proves accurate, is it plausible that dormant or fossilized colonies of such organisms exist today, buried under overlying millennia of deposition.

2.7 References

Ames, D. E., Watkinson, D. H., and Parrish, R.R. 1998. Dating of a regional hydrothermal system induced by the 1850 Ma Sudbury impact event. *Geology* **26**: 447–450.

Barker, W., Welch, S. A., and Banfield, J. A. 1997. Biogeochemical weathering of silicate minerals. *Reviews in Mineralogy and Geochemistry* **35**: 391–428.

Boston, P. J., Ivanov, M. V., and McKay, C. P. 1992. On the possibility of chemosynthetic ecosystems in subsurface habitats on Mars. *Icarus* **95**: 300–308.

Boison, G., Mergel, A., Jolkver, H., and Bothe, H. 2004. Bacterial life and dinitrogen fixation at a gypsum rock. *Applied and Environmental Microbiology* **70**: 7070–7077.

Bunch, T. E., Grieve, R. A. F., Lee, P., McKay, C. P., Rice, J. W. Jr., Schutt, J. W., and Zent A. 1997. Haughton-Mars 97 - II: preliminary observations on highly shocked crystalline basement rocks from the Haughton impact crater: *Lunar and Planetary Science XXIX*.

Chao, E. C. T. 1968. Pressure and temperature histories of impact metamorphosed rocks, based on petrographic observations. *Neues Jahrbuch fuer Mineralogie. Abhandlungen* **108**: 209–246

Cockell, C. S., and Lee, P. 2002. The biology of impact craters – a review. *Biological Reviews* **77**: 279–310.

Cockell, C. S., Lee, P., Osinski, G. R., Horneck, G., and Broady, P. 2002. Impact-induced microbial endolithic habitats. *Meteoritics & Planetary Science* **37**:1287–1298.

Cockell, C. S., McKay, C. P., and Omelon, C. 2003. Polar endoliths – an anticorrelation of climactic extremes and microbial diversity. *International Journal of Astrobiology* **1**: 305–310.

Cockell, C. S. 2004. Impact-shocked rocks – insights into archaean and extraterrestrial microbial habitats (and sites for prebiotic chemistry?). *Advances in Space Research* **33**: 1231–1235.

Cockell, C. S., Lee, P., Broady, P., Lim, D. S. S., Osinski, G. R. R., Parnell, J., Koeberl, C., Pesonen, L., and Salminen, J. 2005. Effects of asteroid and comet impacts on habitats for lithophytic organisms – A synthesis. *Meteoritics & Planetary Science* **40**:1901–1914.

Cockell, C.S., and Osinski, G.R. 2007. Impact-induced impoverishment and transformation of a sandstone habitat for lithophytic microorganisms. *Meteoritics & Planetary Science* **42**:1985–1993.

de los Ríos, A. Wierzchos, J., Sancho, L. G., and Ascaso, C. 2002. Microhabitats and chemical microenvironments under saxicolous lichens growing on granite. *Microbial Ecology* **43**:181–188.

Douglas, S., and Beveridge, T. J. 1998. Mineral formation by bacteria in natural microbial communities. *FEMS Microbiology Ecology* **26**:79–88.

Fike, D. A., Cockell, C. S., Pearce, D., and Lee, P. 2003. Heterotrophic microbial colonization of the interior of impact-shocked rocks from Haughton impact structure, Devon Island, Nunavut, Canadian High Arctic. *International Journal of Astrobiology* **1**: 311–323.

French, B. M. 1998. *Traces of Catastrophe: A Handbook of Shock-Metamorphic Effects in Terrestrial Meteorite Impact Structures*. Lunar and Planetary Institute, Houston, TX, pp. 17–30.

Friedmann, E. I., and Ocampo, R. 1976. Endolithic blue-green algae in the dry valleys: Primary producers in the Antarctic desert ecosystem. *Science* **193**:1274–1279.

Friedmann, E. I. 1980. Endolithic microbial life in hot and cold deserts. *Proceedings of the fourth College Park Colloquium on Chemical Evolution: Origins of Life* **10**:223–235.

Hirsch, P., Eckhardt, F. E. W., and Palmer, Jr. R. J. 1995. Methods for the study of rock-inhabiting microorganisms – A mini review. *Journal of Microbiological Methods* **23**: 143–167.

Konhauser, K. 1998. Diversity of bacterial iron mineralization. *Earth-Science Reviews* **43**: 91–121.

Konhauser, K. 2007. *Introduction to Geomicrobiology*. Blackwell Publishing, Malden, MA, pp. 1–35, 192–292.

Lindgren, P., Parnell, J., Bowden, S. A., Taylor, C., Osinski, G. R., and Lee, P. 2007. Preservation of organic carbon in impact melt breccias, Haughton impact structure. *LPSC XXXVIII*: 1142.

Mann, H. B., and Whitney, D. R. 1947. On a test of whether one of two random variables is stochastically larger than the other. *The Annals of Mathematical Statistics* **18**:50–60.

Martin, W., Baross, J., Kelley, D., and Russel, M. J. 2008. Hydrothermal vents and the origins of life. *Nature Reviews: Microbiology* **6**:805–814.

- McKnight, P. E., and Najab, J. 2010. Mann-Whitney U Test. In *Corsini Encyclopedia of Psychology*, edited by Weiner I.B. and Craighead W.B. Online: John Wiley & Sons. pp. 1.
- Metzler, A., Ostertag, R., Redeker, H. -J., and Stöffler, D. 1988. Composition of the crystalline basement and shock metamorphism of crystalline and sedimentary target rocks at the Haughton Impact Crater, Devon Island, Canada. *Meteoritics* **23**:197–207.
- Naumov, M. V. 1996. Impact-generated hydrothermal activity: the record in terrestrial craters. *Lunar and Planetary Science* **27**:935.
- Oberson, A., and Joner, E. J. 2003. Microbial turnover of phosphorous in soil. In *Organic Phosphorous in the environment*. Edited by Turner, B.L., Frossard, E. and Baldwin, D.S. Cambridge, MA: CABI Publishing, p. 147.
- Omelson, C. R. 2008. Endolithic microbial communities in polar desert habitats. *Geomicrobiology Journal* **25**:404–414.
- Osinski, G. R., Lee, P., Spray, J. G., Parnell, J., Lim, D. S. S., Bunch, T. E., Cockell, C. S., and Glass, B. 2005a. Geological overview and cratering model for the Haughton impact structure, Devon Island, Canadian High Arctic. *Meteoritics & Planetary Science* **40**:1759–1776.
- Osinski, G. R., Lee, P., Parnell, J., Spray, J., and Baron, M. 2005b. A case study of impact-induced hydrothermal activity: The Haughton impact structure, Devon Island, Canadian High Arctic. *Meteoritics & Planetary Science* **40**:1859–1877.
- Osinski, G. R. 2007. Impact metamorphism of CaCO₃-bearing sandstones at the Haughton structure, Canada. *Meteoritics & Planetary Science* **42**:1945–1960.
- Osinski, G. R., Cockell, C. S., Lindgren, P., and Parnell, J. 2010. The effect of meteorite impacts on the elements essential for life. *AbSciCon* 2010:5252.
- Osinski, G. R., Tornabene, L. L., Banerjee, N. R., Cockell, C. S., Flemming, R., Izawa, M. R. M., McCutcheon, J., Parnell, J., Preston, L., Pickersgill, A. E., Pontefract, A., Sapers, H. M., and Southam, G. 2012. Impact-generated hydrothermal systems on Earth and Mars. *Icarus* **224**:347–363.
- Parnell, J., Osinski, G. R., Lee, P., Green, P. F., and Baron, M. J. 2005. Thermal alteration of organic matter in an impact crater and the duration of postimpact heating. *Geology* **33**: 373–376.
- Parnell, J., Boyce, A., Thackrey, S., Muirhead, D., Lindgren, P., Mason, C., Taylor, C., Still, J., Bowden, S., Osinski, G. R., and Lee, P. 2010. Sulfur isotope signatures for rapid colonization of an impact crater by thermophilic microbes. *Geology* **38**:271–274.

Singleton, A. C., Osinski, G. R., McCausland, P. J. A., and Moser, D. 2011. Shock induced changes in density and porosity in shock metamorphosed crystalline rocks, Haughton- impact Structure. *Meteoritics & Planetary Science* **46**:1774–1786.

Stöffler, D. 1966. Zones of impact metamorphism in the crystalline rocks of the Nördlinger Ries crater. *Contributions to Mineralogy and Petrology* **12**:15–24.

Stöffler, D. 1971. Progressive metamorphism and classification of shocked and brecciated crystalline rocks at impact craters. *Journal of Geophysical Research* **76**:5541–5551.

Versh, E., Kirsimäe, K., and Jõelet, A. 2006. Development of potential ecological niches in impact-induced hydrothermal systems: The small-to-medium size impacts. *Planetary and Space Science* **54**:1567–1574.

Vestal, R. J. 1988. Biomass of the cryptoendolithic microbiota from the Antarctic Desert. *Applied and Environmental Microbiology* **54**:957–959.

Wackett, L. P., Dodge, A. G., and Ellis, L. B. M. 2004. Microbial genomics and the periodic table. *Applied and Environmental Microbiology* **70**:647–655.

Wierzchos, J., and Ascaso, C. 2001. Life, decay and fossilisation of endolithic microorganisms from the Ross desert, Antarctica. *Polar Biology* **24**:863–868.

Chapter 3 : Impact-generated endolithic habitats within crystalline rocks of the Haughton impact structure, Canada

Alexandra Pontefract, Gordon R. Osinski, Charles S. Cockell and Gordon Southam.

3.1 Introduction

The colonization of rocks by microorganisms (referred to as endolithic) has long been documented (Friedmann, 1980) and is seen as an advantageous trait, especially in environments such as hot or cold deserts, where temperature shifts, low water availability and high UV indices pose a significant problem (Bell 1993; Cockell et al., 2003; Omelon et al., 2007). In these situations, rocks can provide a refuge for both photosynthetic and chemosynthetic organisms, forming complex endolithic communities only millimetres below the surface (Walker and Pace 2007). The word endolith (here encompassing cryptoendoliths) refers specifically to organisms dwelling within the rock with no obvious point of entry, distinctive from epiliths, which are surface dwelling organisms and hypoliths, which are found on the underside of rocks. Both the porosity and the translucency of the rock have a significant impact on the extent of colonization possible because organisms are dependent on the connectivity of pore spaces (or permeability) beneath the surface as well as the penetration depth of photosynthetically active radiation (PAR) (Walker and Pace 2007). For this reason, the majority of these communities can be found residing in sedimentary lithologies such as sandstones, or in evaporitic rocks such as gypsum and halite, generally 1 mm beneath the surface where the increased depth allows water retention and provides sufficient UV protection (Stivaletta et al., 2010; Wierzchos et al., 2011). The colonization of sandstones in Antarctica has received significant attention (Pointing et al., 2009). In this polar desert, endolithic assemblages can constitute the majority of viable biomass, reproducing at very slow rates with doubling times on the order of thousands of years (Friedmann et al., 1993).

Given that endolithy is a viable strategy in such extreme environments, it is plausible that if life existed on other terrestrial bodies in our solar system, such as Mars, these organisms might adopt a similar approach to survival (Wynn-Williams and Edwards 2000). We cannot, however, be assured that the geological processes that produce

lithologies capable of providing endolithic habitats (e.g., quartz-rich sandstones or evaporites) on Earth would operate on other planetary bodies. Meteorite impacts are one such mechanism that occurs throughout our solar system and is a fundamental geological process on all rocky and icy planetary bodies (Melosh 1989; Napier and Clube 1979; Osinski and Pierazzo 2013). Though initially detrimental to biology, an impact event can favourably change the availability and habitability of a substrate for endolithic organisms, which can then colonize micro-fractures and pore spaces created during the impact (Cockell 2006; Cockell et al., 2002). In these instances, impact structures could provide refuge to endolithic organisms. Cockell and Osinski (2007) have shown the increase of microbial biomass with increasing exposure to shock pressure in sedimentary targets, which was found to be related to increases in porosity and translucency. During an impact event, however, the opening of pore spaces is transient and sedimentary targets experience a collapse of pore spaces at pressures over 35 GPa (Cockell and Osinski 2007), and thus do not support endolithic colonization at pressures higher than this. This is not the case for other substrate types. Singleton et al. (2011) showed that unlike sedimentary targets, the porosity of crystalline samples (specifically gneisses) increases until vaporization, creating a habitat where before none existed.

Early work by Cockell et al. (2002), Cockell et al. (2004) and Fike et al. (2003) revealed that shocked gneisses do indeed provide a unique and viable habitat for endoliths, providing a moisture-retaining and UV-protected environment. This is of increased relevance for astrobiology than the existence of endolithic habitats in shocked sedimentary rocks due to the dominance of crystalline rocks on all other terrestrial planets in the solar system. The original work by Cockell et al. (2002) investigated the degree of light penetration as well as UV protection between low shock versus high shock samples of gneiss, where the degree of shock was denoted by the absence of amphibole banding at high pressure. The study revealed that within the high shock class of samples the light penetration depth at 680 nm – the absorption maximum for chlorophyll *a* – increased by an order of magnitude. Despite this, however, it was shown that 1 mm of the shocked gneiss was capable of reducing spore inactivation in *Bacillus subtilis* by UV radiation by two orders of magnitude. Work by Fike et al. (2002) looked at both the heterotrophic community of these rocks, as well as nutrient availability, and was the first to note a

potential loss of biologically relevant elements. In Chapter 2 it was shown that nutrient availability in terms of bioessential elements in these crystalline lithologies does decrease with increasing shock level, however, not significantly enough to inhibit microbial growth. The question then is: does microbial biomass trend with this increase in porosity, or are there other factors determining abundance? To answer this question, we have employed a multi-faceted approach: conducting cell counts, along with Scanning Electron Microscopy (SEM) and Confocal Scanning Laser Microscopy (CSLM) to reveal the morphology and extent of subsurface growth as well as to identify “hot-spots” of microbial growth *in situ*.

3.2 Methods

3.2.1 Field Site

The Haughton impact structure is located in the northwestern region of Devon Island, Nunavut, in the Canadian High Arctic archipelago at 75°08'N, 87°51'W (Osinski et al., 2005a). Haughton was formed approximately 39 Ma and has an apparent diameter of ~23 km, with a final crater rim estimate of 16 km in diameter (Osinski et al., 2005b). The target rocks are almost entirely sedimentary and represent lower Paleozoic rocks of the Arctic Platform. This ~1880 m sequence (pre-impact thickness) is comprised of marine carbonates, with lesser amounts of evaporites, sandstone and shale, overlaying gneisses of the Precambrian basement of the Canadian Shield. The most identifiable feature of the impact structure is the pale-grey crater-fill (clast-rich impact melt rocks) deposits (Figure 3-1a,b), which form a discontinuous layer throughout the centre of the structure, having a maximum thickness today of ~125 m, covering ~60 km² (Osinski et al., 2005b). Another salient feature of the structure is the hydrothermal deposits, seen in the form of several alteration products, such as selenite and marcasite, as well as the presence of hydrothermal vugs (Osinski et al., 2005a; Osinski et al., 2001).

3.2.2 Sample Collection and Processing

Samples of shocked gneiss were collected during the seasons of 2008 and 2010 from a large number of locations within the crater on several of the impact melt rock hills located both near the crater rim and towards the central uplift (Figure 3-1b,d), coordinates for which are listed in Appendix B1. A notation of which surfaces were exposed was also

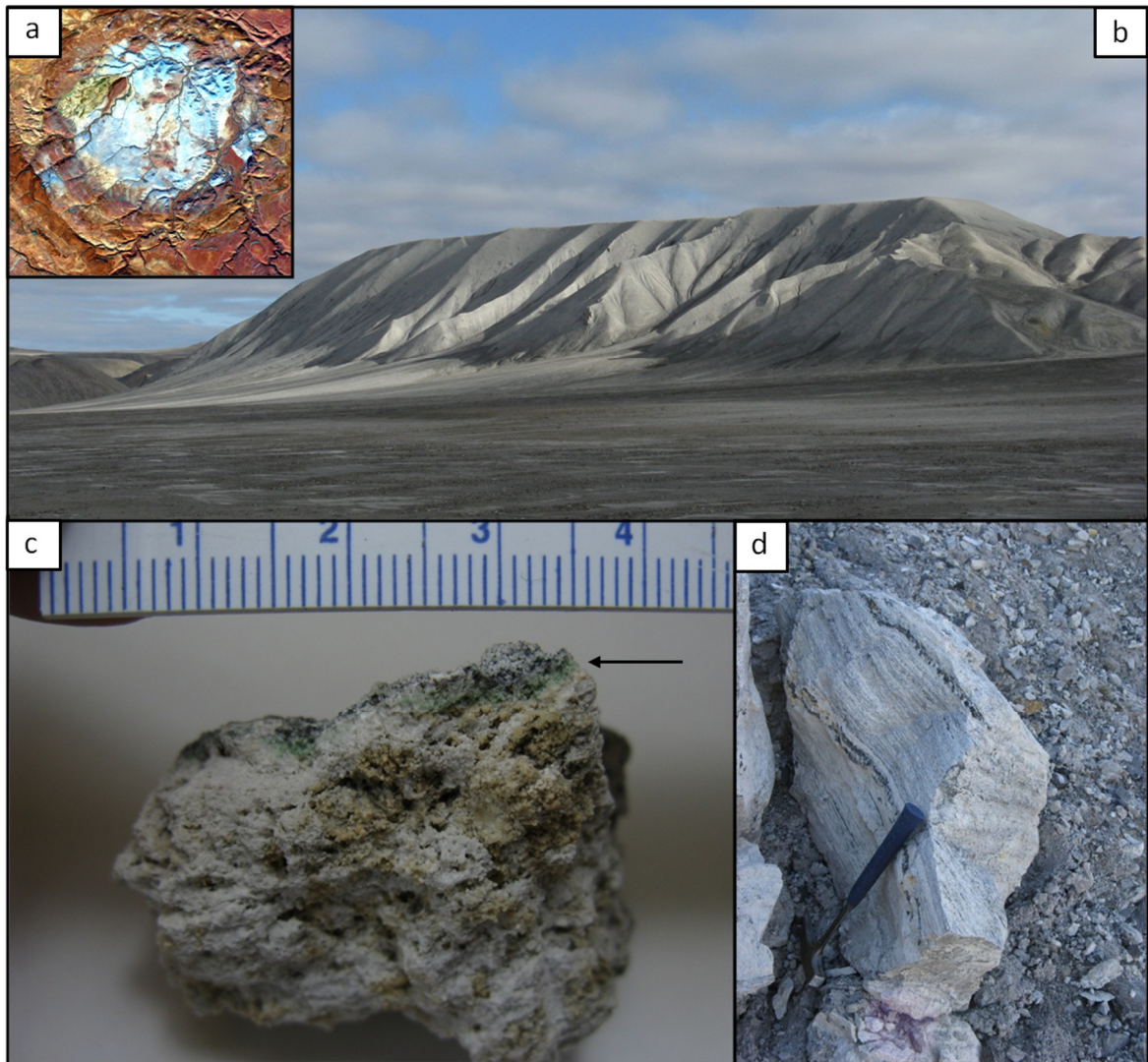


Figure 3-1. (a) Landsat image of the Haughton Crater, Devon Island, Canada, courtesy of G.R. Osinski. (b) Bruno Escarpment, a breccia hill located south-west in the crater, approximately 1 km in length. (c) Fragment of shocked gneiss used for embedding in CSLM and SEM imaging. Endolithic band is visible 1-2mm beneath the surface (arrow), scale is in centimetres. (d) Example of large gneiss breccia within the crater, Easting for scale.

made where possible. Each sample was thin sectioned and studied under a petrographic microscope (Nikon Eclipse LV100POL Compound Petrographic Microscope) in order to determine shock level. This was necessary in order to correlate the amount of growth seen in the rocks with the pressure that the rock was exposed to. In this paper, we have used the classification system created by Singleton et al. (2011) for rocks at the Haughton structure as well as the estimated porosity values for each shock level (Table 3-1). It should be noted that in this paper broad terms referring to shock are sometimes used, i.e. “unshocked” refers to shock level 0 samples, “low shock” to shock levels 1–2, “moderate shock” to levels 3–4 “high shock” to shock levels 5–6, and “very high shock” to level 7 samples (Figure 3-2).

3.2.3 Bulk Cell Counts

For each shock level, excepting levels 1 and 2 (which were omitted due to the scarcity of samples available from within the crater), 3 samples were selected for bulk cell counts. As the cell counts of solely the endolithic community were to be tallied, any surface crust which could possibly be housing epilithic communities was removed using a sterile pick and chisel. Samples were then hand crushed to a fine sand grain size using an alumina mortar and pestle (CoorsTek, Colorado, USA #60370). One gram of sample was then suspended in 20 ml of a 5 mM sodium pyrophosphate solution (Buss et al., 2003; Haldeman et al., 1993; Hirsch et al., 1995), vortexed briefly and then sonicated on low power for 5 min. Five hundred microlitres of the solution was then suspended in 1 mL dH₂O and was counted using a Petroff-Hausser stage in a Zeiss Axio Imager Z1 Microscope. Counts of five different grids were conducted based on methods from Hausser Scientific used to determine the average cell number per 1 mm² (Vukosavljevic, 2010). The number of cells per ml was then calculated using equation (1).

$$\text{Number of cells/ml} = \text{Dilution Factor} \times 50,000 \times \text{number of cells/1mm}^2 \quad (1)$$

The total number of cells in the initial volume was then calculated and divided by the total number of grams of rock for the given sample to achieve a value in cells/g.

Table 3-1. Classification of shock level in gneisses based on petrographic analysis along with observations from microscopic and confocal images and scanning electron micrographs, adapted from Pontefract et al. (2012) and Singleton et al. (2011). Porosity values were calculated from raw data from Singleton et al. (2011), and are used as the estimated porosity for samples in this study.

Shock Stage	Pressure Range (GPa)	Rock Features, Mineral Effects and Colonization Potential	Avg. Porosity (%)
0	-	Unshocked substrate. Colonization is purely epilithic.	0.5
1	2-5	Beginning of fracturing. Formation of shatter cones and kink banding in Biotite. Colonization is epilithic.	n/a
2	5-10	Extensive planar fracturing (PFs) along with distinctive checkerboard pattern in plagioclase. Colonization is epilithic.	1
3	10-30	The first microscopic deformations begin to form within quartz as planar deformation features (PDFs), along with a toasted appearance and phase transitions of quartz to stishovite. Macrofractures are extensive at this stage. Colonization is still mainly epilithic but with some infilling within the first 1000 μm of the rock.	1.5
4	30-35	Extensive PDF formation, loss of pleiochromism in biotite. Shatter cones are now no longer present. Quartz transitions to coesite also with optically homogeneous extinction. Colonization is still mainly epilithic but with some infilling within the first 1000 μm of the rock.	10.5
5	35-55	Diaplectic glass formation begins (mineral outline still present) to vesiculated glass and partial melting. Loss of extinction in quartz and loss of PDFs. Endolithic colonization is extensive down to 4 mm in depth at the upper end of the pressure range.	18.5
6	55-60	Significant vesicularization of the substrate and the beginning of flowed glass features in both quartz and feldspars. Biotite is absent. Endolithic colonization is extensive throughout all samples.	44.0
7	60-80	Complete melting of all minerals along with visible flow and differentiation of mafic and felsic materials, connections between pore spaces begin to close. Endolithic colonization is still extensive within the first 1000 μm , but is not readily present at other depths except near the presence of macrofractures. Complete vaporization of rocks past 80 GPa.	63.0

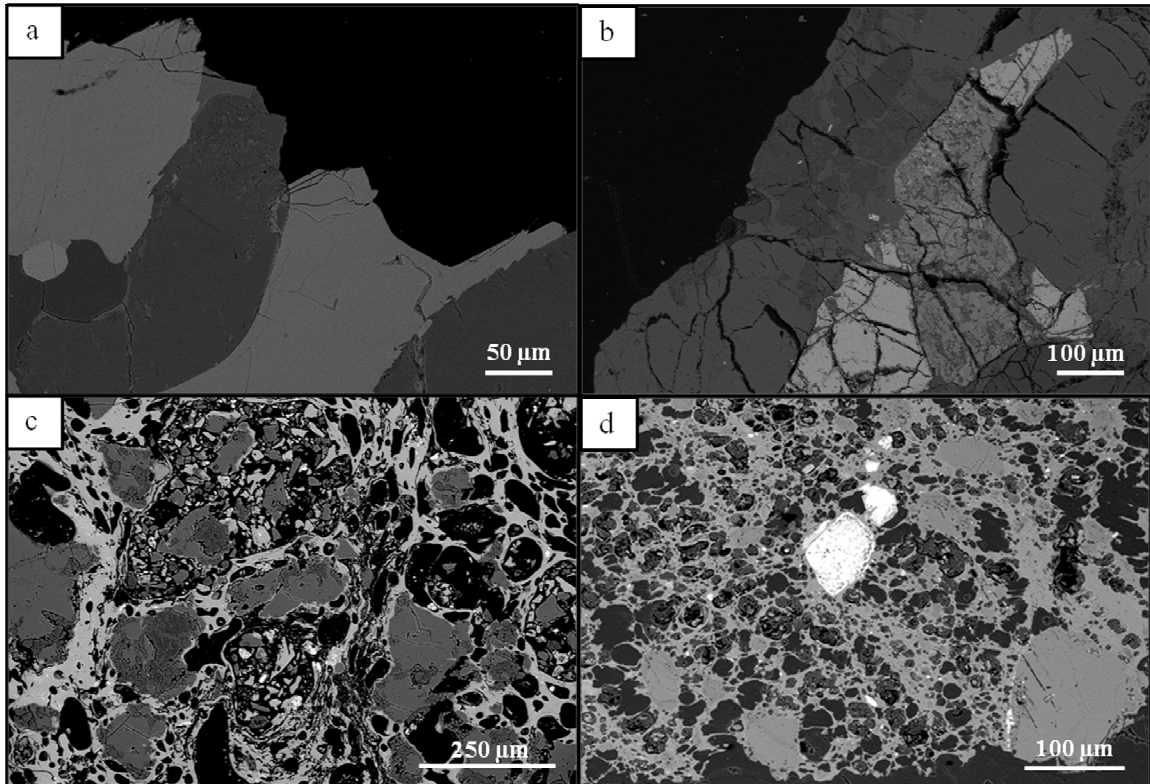


Figure 3-2. SEM-BSE micrographs of unshocked and shocked gneisses from the Haughton impact structure. Black regions within the micrographs represent embedding resin. (a) Unshocked basement gneiss from Sverdrup Inlet (b) moderately shocked gneiss, exposed to pressures between 20-30 GPa, (c) high shocked gneiss (~45 GPa), and (d) very highly shocked sample (~60 GPa). Note extensive flow of potassium-rich phases (light colour) in (c) and extensive porosity and homogeneity of the substrate in (d).

3.2.4 *Confocal Scanning Laser Microscopy*

A total of 16 samples were analysed using Confocal Scanning Laser Microscopy (CSLM), consisting of: 2 unshocked, 2 low shock, 4 moderate shock, 4 high shock and 2 very high shock, in order to visualize *in situ* microbial colonization of the rocks and as an analysis of levels of biomass. From each field sample, subsamples measuring approximately 1–2 cm³ were broken off using a sterile chisel and hammer. These subsamples were then split in half using the same sterile technique in order to expose an inner cross-section of the rock (Figure 3-1c). For imaging endolithic cells *in situ*, a method was adapted from de los Ríos et al. (2005) and Wierzos et al. (2004). The fresh rock surface was stained with LIVE/DEAD *Baclight* L7007 from Invitrogen (Molecular Probes, Eugene, OR). This is a fluorescent stain containing two types of nucleic binding fluorophores; SYTO 9 which is membrane permeable and will bind to all cells, and a propidium iodide (PI) counterstain, which is restricted to cells with damaged membranes. Two hundred microlitres of the mixture was pipetted onto the fresh surface and was incubated in the dark at room temperature for 1 hour. Each sample was then fixed in 2% glutaraldehyde for 1 hour, dehydrated with ethanol (15 min each at 50%, 75%, 100% and 100%) and then embedded in resin (LR White, Electron Microscopy, Hattfield, PA) using the cold cure method from Electron Microscopy. These cured pucks were then polished and mounted for imaging. The unshocked samples were used as the control as an unshocked crystalline rock was presumed to only have epilithic (surface) growth, which was confirmed with microscopic observations. SEM Electron Dispersive Spectroscopy (EDS) was used to confirm absence of non-specific binding.

3.2.5 *CSLM Image Acquisition and Processing*

For each puck, representing one sample, three transects of the rock were taken using the CSLM (Zeiss LSM 5 Duo, Software: Zen 2009 v.5.5 SP2) from the top of the sample (exterior face) to the bottom (interior face) representing an increase in depth, at 20x magnification. This magnification was used because higher magnification did not allow for the necessary working distance with the sample. Based on SEM imaging of the rocks and observations of *in situ* colonization, the average cell size was calculated at 2–3 μm which correlates with one pixel. Images were acquired using three lasers: green

fluorescence (SYTO 9 / live stain) with excitation/emission of 488/510–530 nm using an argon laser; red fluorescence (PI / dead stain) with excitation/emission of 543/620–750 nm, using an HeNe laser; and rock surface reflectance was imaged using a 633 HeNe laser. Images were processed using Image Pro (v.7.0), wherein each transect was tiled and then split into its respective channels (i.e. Rock, SYTO 9 and PI) for enumeration. The rock channel was used as a representation of background noise and was subtracted from the SYTO 9 and PI channels. Bins of 500 μm in length (with a constant area of 150,000 μm^2), were constructed and overlaid on each transect channel to count pixels (corresponding with individual cells) for both SYTO 9 and PI channels respectively. These counts were then averaged to provide an overall approximation for cellular abundance with increasing depth for each rock.

3.2.6 *Scanning Electron Microscopy*

Samples of shocked gneiss were either fractured into small pieces using a sterile technique and imaged directly using secondary electrons (SE2), or were embedded in plastic for back-scattered electron microscopy (SEM-BSE) and EDX (energy dispersive X-ray spectroscopy). Fractured pieces were fixed in glutaraldehyde, dehydrated in ethanol and critical-point dried to preserve membrane structure, platinum coated using a Denton Vacuum Desk II sputter coater at 12 mA for 150 sec and imaged. Embedded samples were first prepared using the same methodology as for CSLM samples. Fresh faces were exposed and the entire sample was then fixed in 2% glutaraldehyde for 24 hours and then rinsed for 15 min in a Na-cacodylate buffer. Samples were then stained using a 0.1M OsO_4 -cacodylate buffer for one hour. An ethanol dehydration series was performed (15 min each at 50%, 75%, 100% and 100%), followed by 2 rinses @ 15 min of 100% acetone. Samples were then embedded with EmBed following the protocol from Electron Microscopy, Hattfield, PA and (Dykstra and Reuss, 2003). The osmium tetroxide serves as a lipid membrane stain and makes imaging of cells possible when using electron back-scattering (SEM-BSE).

3.3 Results

3.3.1 Bulk Cell Counts

Results for bulk microbial cell counts from shocked gneisses are shown in Figure 3-3. Shock level 0 values begin at 10^7 cells/g, representing surface (epilithic) growth, and then increase by an order of magnitude at shock levels 2-4, increasing again past shock level 4. A linear regression was fit to the data, having an R^2 value of 0.92. A 4th order polynomial was also fit to the data with an R^2 of 0.97. Both regressions were compared for statistical significance using the Akaike Information Criterion (AIC), and the linear regression was found to have a better goodness of fit for the data, though the difference was negligible.

3.3.2 CSLM

CSLM images can be seen in Figure 3-4. It can be seen that in all cases, growth from the epilithic community was observed to continue into the rocks, following fissures and fractures within the rock. Figure 3-5b shows average cell number with increasing depth and increasing shock level. In this instance, shock levels have been grouped into broader categories as use of the previously mentioned fine scale was not able to reveal growth trends within the samples. The first data point indicates a range of 0–500 μm beneath the surface, and so on with increasing depth. Shock level 0 shows an initial spike in microbial abundance at the surface and then diminishes with increasing depth. The subsequent increasing shock levels show a concomitant increase in biomass. Shock level 7 (very high shock) shows lower biomass overall than the “high shock” samples, though with increased variability indicated by sharp increases and decreases in abundance values. Figure 3-5a gives a comparison of total microbial biomass for each category, showing that the high shock samples (levels 5 and 6) have the highest overall biomass in comparison with the other samples, this data fits a linear correlation with an R^2 of 0.61, with the Akaike criterion again showing that the linear fit was negligibly more significant than the polynomial. Figure 3-6 shows a comparison of the overall biomass counts conducted with the bulk and *in situ* methods.

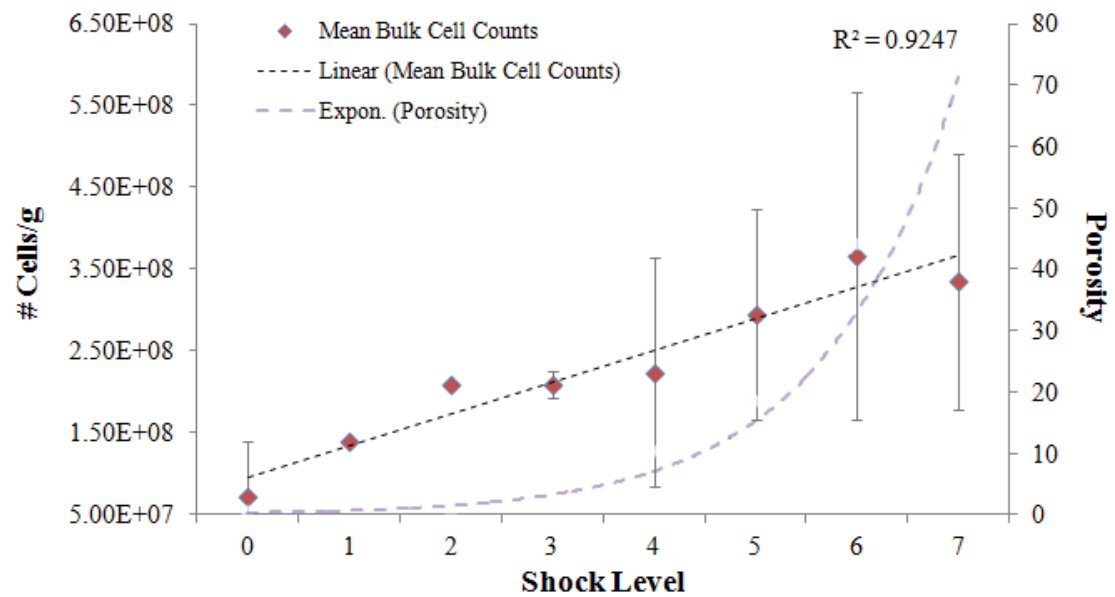


Figure 3-3. Average number of cells/g and porosity plotted versus shock level. Dashed line represents the exponential increase seen in porosity for gneisses, data adapted from Singleton et al. (2011). Standard deviation values are not shown for shock levels 1 and 2 for cells/g due to insufficient sample numbers.

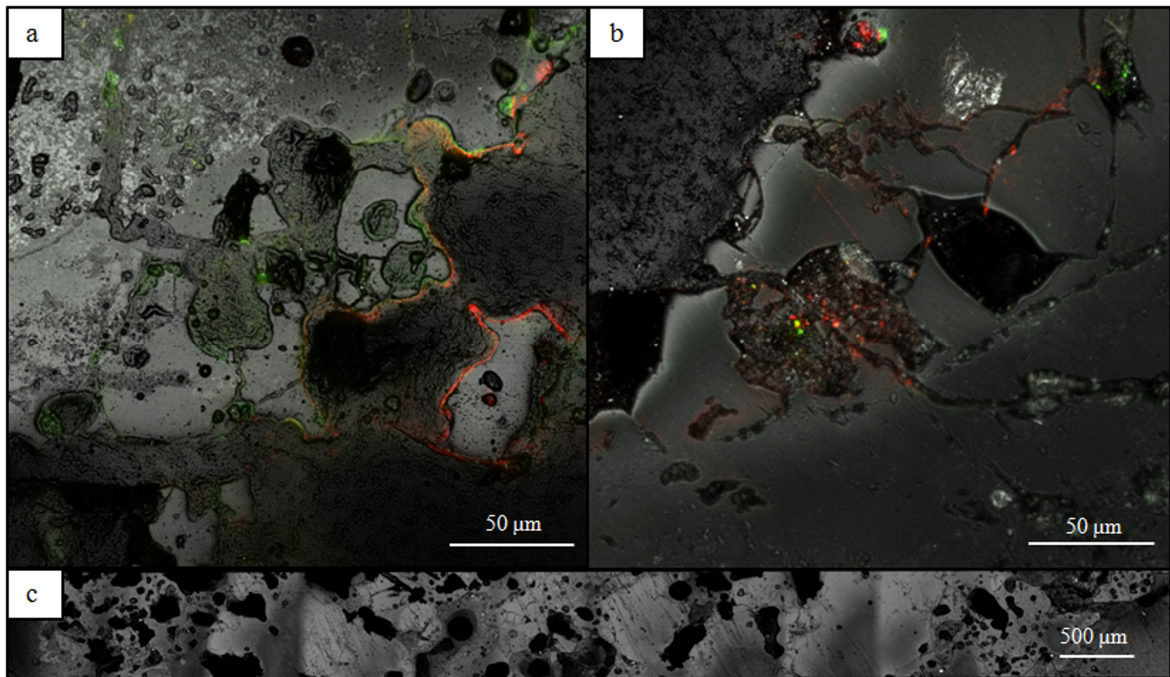


Figure 3-4. (a) and (b) show CSLM micrograph with live (green)/dead (red) stain and reveal epilithic and endolithic colonization of fractures and vesicles within the rock. The mottled dark-grey substrate (ex. (b) top left) is embedding resin. (c) is a stitched transect in the “rock” channel showing extensive porosity and fracturing throughout the sample at shock level 6.

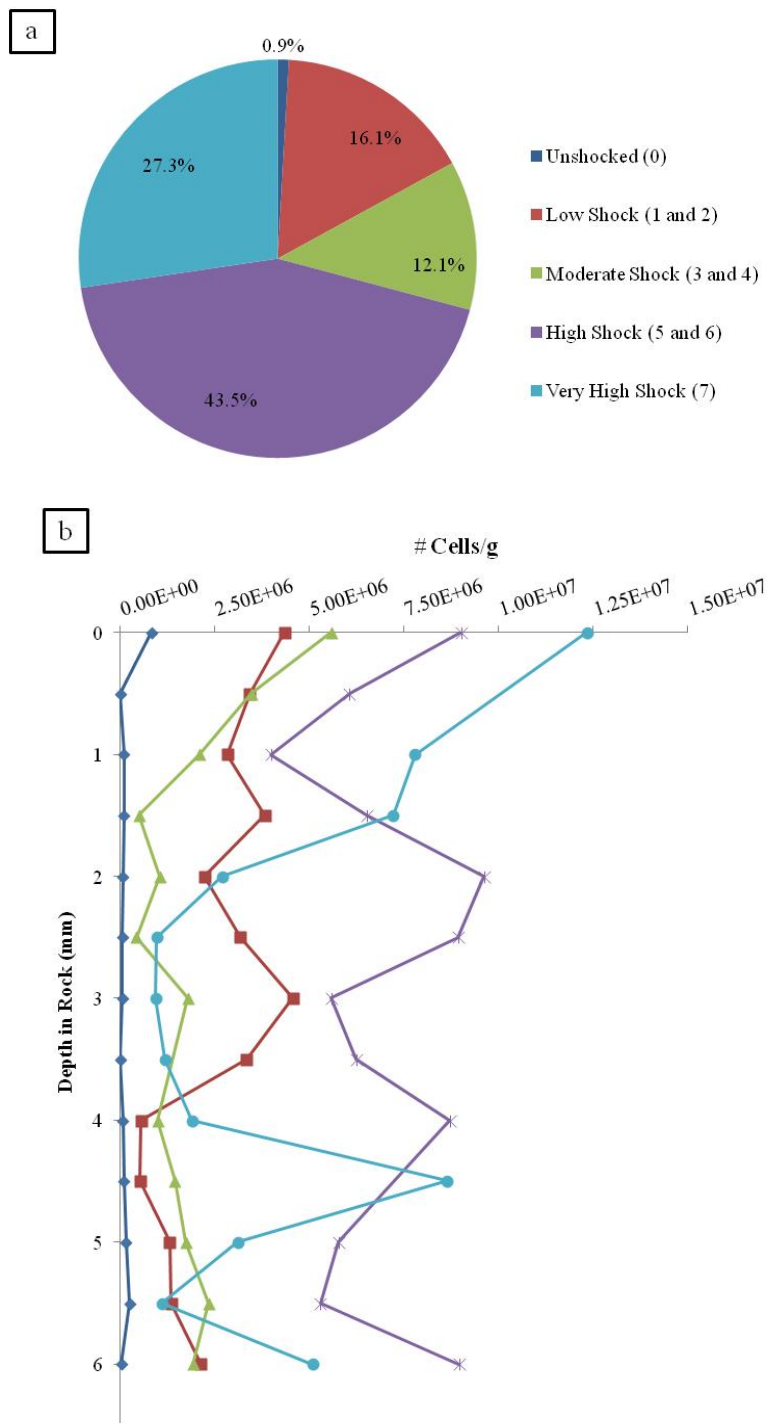


Figure 3-5. Average # cells/g plotted versus shock level (a) and depth within the substrate (b) through *in situ* analysis. (a) Biomass levels for each shock category, where 100% indicates the total biomass from all samples. (b) Graph shows increasing shock level from left to right, and variations with increasing depth. Note that each data point represents a bin sum of $150,000 \mu\text{m}^2$, therefore the first data point is indicative of surface epilithic growth and growth associated with macrofractures. The primary photosynthetic zone is indicated (right) as well as zones for heterotrophic and epilithic colonization.

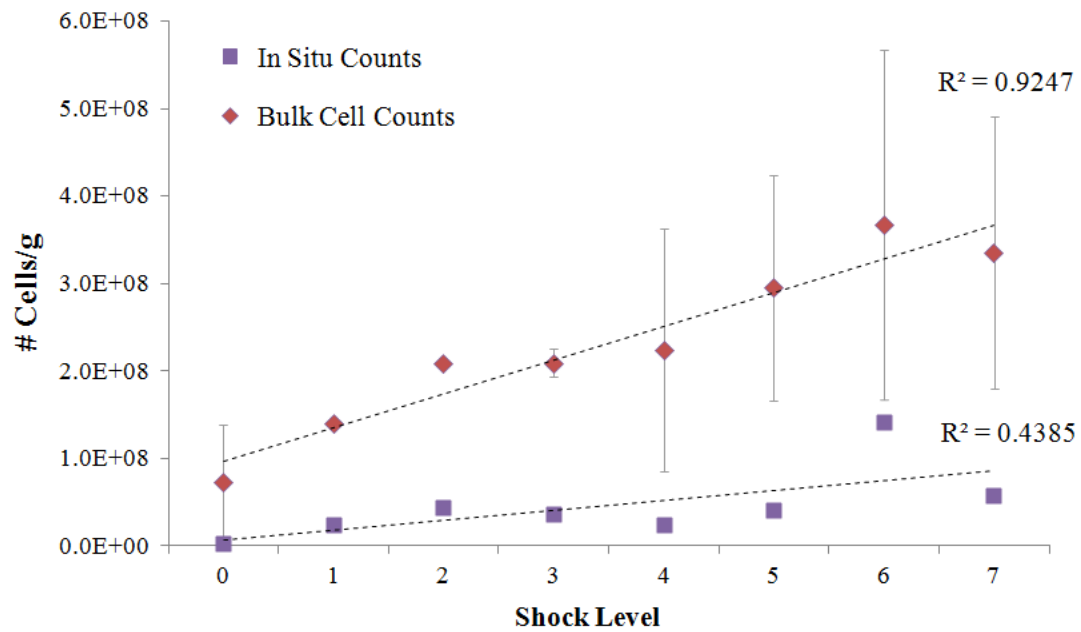


Figure 3-6. Plot of bulk cell counts vs. *in situ* counts. Both data sets show a peak in cell numbers at shock level 6 and a corresponding decrease at shock level 7. When *in situ* cell count data is plotted as a function of broad shock ranges, a linear fit has a correlation coefficient of 0.6140. Error bars show standard deviations, which were omitted for shock levels 1 and 2 as only 1 sample was available in each case. Error bars for the *in situ* counts are too small to be visible in this graph.

3.3.3 SEM

Scanning electron microscopy shows that shock level 5 (high shock) samples are characterized by extensive microbial colonies *in situ* showing both rod and coccoid-shaped cells (Figure 3-7). SEM-BSE images of the same confocal transects used to construct Figure 3-4 was also imaged to provide substrate information for the colonies. Because of the sheer size of these images, full transects are not shown, instead Figure 3-8 shows one tile each of a confocal and back-scattered image for comparison of cell-growth vs. substrate type.

3.4 Discussion

The Haughton impact initially heated a portion of the target rocks to temperatures in excess of 2000°C (Osinski et al. 2005a), cooling down over time to allow the formation of a hydrothermal system, and finally dissipating to leave behind the impact melt rock hills situated within barren arctic tundra that are observed today (Cockell and Lee, 2002). The microorganisms within these rocks are representative of a contemporary environment (Cockell et al., 2002), though calcified cells are present within the lithology (image not shown). Building on earlier work by Cockell et al (2002, 2004) and Fike et al. (2003), we have provided the first systematic investigation of the relationship between microbial colonization of crystalline rock and level of shock, with samples categorized into 7 shock levels – previous studies classified samples as either “low shock” or “high shock”. It can be seen that the epilithic environment reveals stratification, with dead cells comprising the outermost layer, giving protection to the active photosynthetic layer. Inwards, cohesive colonization becomes more prevalent with an increasingly shocked target, peaking in the shock level 6 samples (Figure 3-3), corresponding to a pressure exposure of between 40–50 GPa and a mean porosity of 44% (Singleton et al. 2011). SEM images also reveal extensive colonization (Figure 3-7) at these high shock stages, which is not seen in lower shock level samples, which is similarly reinforced by the CSLM *in situ* counts (Figure 3-5), which show a peak in microbial cell abundance at the high shock range.

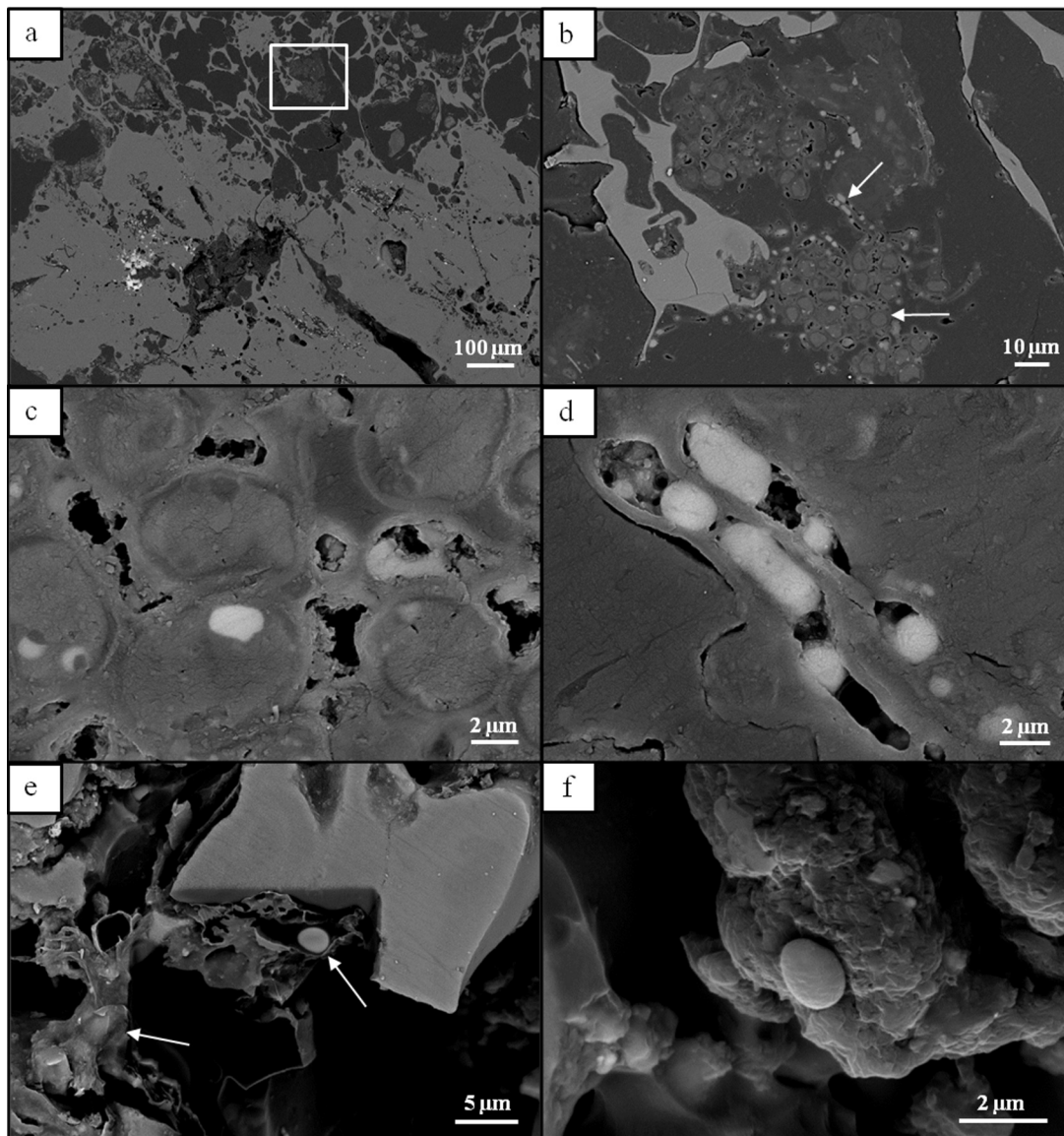


Figure 3-7. SEM-BSE micrographs of endolithic organisms within shocked gneiss. (a) Low magnification micrograph of lithic substrate shocked to ~50 GPa. Square shows area of interest for (b), (c) and (d). (b) Endolithic colony. Arrows indicate (c) (bottom) and (d) (top). Darker region between the rock and colony is the embedding resin. Lighter color encapsulating colony is EPS. (c) Micrograph showing cocci cells. White spot is a concentration of OsO_4 . (d) Rod shaped cells preserved within the EPS. (e) and (f) show the nature of the colony along the fractures where resin did not infill. (e) shows a cell coated with EPS (left) and a cell revealed via the use of a focused ion beam (FIB) within the EPS (right).

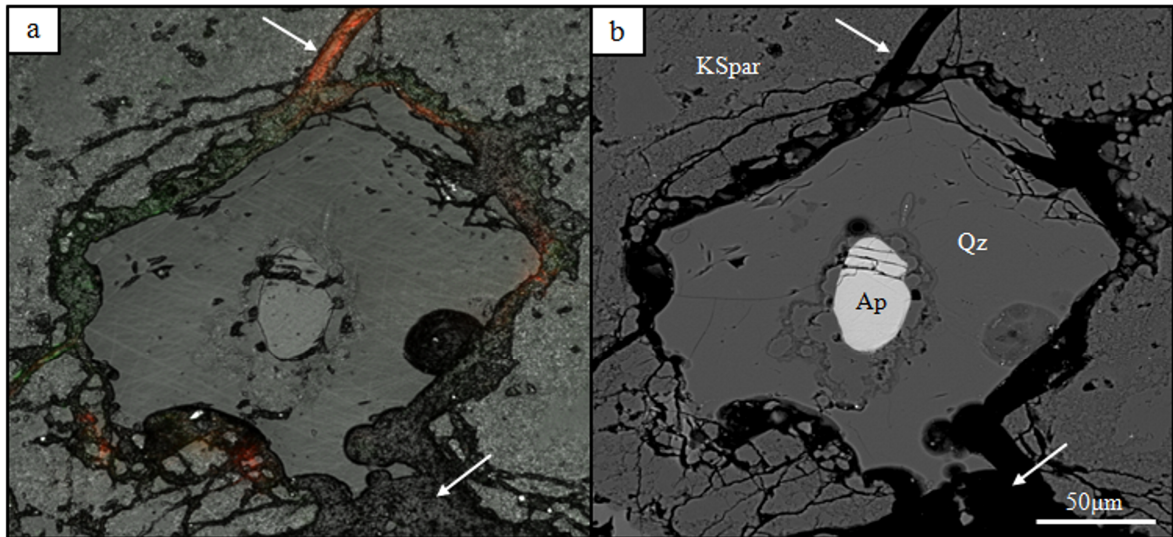


Figure 3-8. (a) CSLM micrograph with *in situ* LIVE/DEAD Baclight stain. Arrow (top) shows fluorescence of propidium iodide, and bottom arrow points to embedding resin. Compare with (b), an SEM-BSE micrograph, where both areas indicated in (a) are atomic-lows. Substrate is variable with a feldspathic glass (KSpar), a quartz glass (Qz) and an apatite crystal (Ap).

3.4.1 *Microbial Biomass and Shock Metamorphism*

The bulk microbial cell counts for these samples reveal a linear trend with increasing shock metamorphism of the target. There are, however, several factors controlling the abundance of biomass for each shock level, such as: porosity, permeability, translucency, friability and substrate type (e.g. glass vs. crystalline mineral). Though possible that these factors combine in such a way as to confer a linear relationship between biomass and shock level, the data do also support a more complex multi-factored model. When considering the biomass levels in terms of the above-mentioned factors using a non-linear fit, two distinct plateaus in the data become apparent. The first plateau occurs over shock levels 2–4, where large-scale macrofractures are occurring in the rock allowing for an increase in chasmoendolithic growth; however, porosity of the substrate is still below 10% of the total bulk volume (see Table 3-1), and translucency is still markedly low, allowing approximately 1.8% of incident PAR to penetrate more than 0.5 mm (Cockell et al. 2002). Porosity does not begin to increase rapidly until shock level 5, which corresponds with the next jump in biomass values.

Interestingly, the shock level 7 values dip below that of the previous shock level. Though not a significant difference, *in situ* cell counts also showed a corresponding lowering of biomass levels at the highest shock level (Figure 3-5a). That both methodologies reveal a concomitant loss of biomass points to something more complex influencing microbial growth at these pressures, and it is unlikely that this result is an artefact. One possible hypothesis that would account for this loss is that though porosity is increasing rapidly at this stage, going from 44% at shock level 6 to over 60% at shock level 7, what is unknown is the corresponding change in permeability of the rock, where extensive flow of melt within these samples may act to effectively isolate pore spaces. Currently, however, there is no supporting work which investigates this phenomenon. Given these notable changes in biomass levels and the several known factors which affect growth, it is plausible that the relationship between biomass and shock level is more complex than a linear relationship and that the current data set is too small reveal such trends.

Though *in situ* imaging using CSLM did not show a strong linear correlation, a polynomial regression for the data revealed a good correlation and again the linear fit was

as a negligible improvement over the polynomial using AIC. Though the data did not fit a linear correlation using the fine-scale shock classification system, they were significant when grouped into the broader categories used in Figure 3-5a,b. It is likely that a more robust sample set would more clearly reveal trends in biomass increases; however, given the time-intensive process using this method, performing bulk cell counts is the preferred method. What the CSLM micrographs did reveal, however, were a clear progression of biomass levels with shock level and the expansion of habitation depth with shock level. In all shocked samples, colonization of the rock down to 2 mm was fairly consistent and cell numbers increase with shock accordingly. Below this point, however, cell numbers drop by an order of magnitude in all but the high shock samples which show a large range in variability with increasing depth likely due to the friability of the substrate and connectivity of pore spaces.

3.4.2 *Subsurface Morphology*

Using SEM-BSE spectroscopy in conjunction with the CSLM transects (Figure 3-8); we were able to correlate areas of growth with substrate type to ascertain whether or not some substrates, such as feldspathic glasses, may provide increased nutrients to microbial colonies over other possible surfaces. Interestingly, we found that there was no such preference seen in over 42 transects studied. It would appear that the microbial colonies within these gneisses are following both macro- and microfractures to the interior of the rock, eventually colonizing the interiors of vesicles. In the study by Fike et al. (2002), it was hypothesized that the volatilization process could effectively concentrate bioessential nutrients along the inside of these vesicles, allowing for increased levels of colonization.

Given that no infiltration of glasses was seen in any of the SEM-BSE and CSLM images, and that much of the glass is quartz-rich, it is unlikely that the impact formed glasses provide much nutrient to the microbial colonies. In this way, “hot spots” of growth that are observed are governed by three main factors: 1) The trade-off between the depth of PAR for a given sample vs. the ability to act as a sufficient UV shield – the depth of which seems to occur 1-2 mm beneath the surface, 2) the connectivity of pore spaces within the rock, and 3) the connectivity of these spaces with macro- and microfractures to the surface, allowing the percolation of pore waters, nutrients and microbiota. It is

possible that over time, weathering of the substrate could reveal nutrient-loaded regions of the rock. In Figure 3-7, for example, we see an apatite crystal surrounded by quartz glass. Given that phosphate can be limiting for microbial ecosystems, these apatite crystals could act as a localized source of nutrients.

3.5 Concluding Remarks

Based on the results presented in this paper, we find that impact shocked gneisses provide an excellent habitat for microbial endoliths in harsh environmental conditions. We see that microbial biomass levels reach maximum values within gneisses exposed to between 55 and 65 GPa and that higher shocked targets may not be as suitable a habitat due to potential losses in permeability of the rock at such high pressures. Given the dominance of shocked crystalline lithologies on every terrestrial body in the solar system, it is plausible that if life existed elsewhere, that endolithic colonization of impact craters would have occurred beyond Earth. Currently, many of these shocked lithologies are buried under multiple layers of ejecta, protected from high levels of UV radiation and low atmospheric pressures, and provide an excellent target for future life detection missions.

3.6 References

- Bell, R. A. 1993. Cryptoendolithic algae of hot semiarid lands and deserts. *Journal of Applied Phycology* **29**:133–139.
- Buss, H. L., Brantley, S. L. and Liermann, L. J. 2003. Nondestructive methods for removal of bacteria from silicate surfaces. *Geomicrobiology Journal* **20**:25–42.
- Cockell, C. S. 2004. Impact-shocked rocks - Insights into archean and extraterrestrial microbial habitats (and sites for prebiotic chemistry?). *Advances in Space Research* **33**:1231–1123.
- Cockell, C.S. 2006. The origin and emergence of life under impact bombardment. *Philosophical Transactions of the Royal Society B* **361**:1845–1856.
- Cockell, C. S. and Lee, P. 2002. The biology of impact craters - a review. *Biological Reviews* **77**:279–310.
- Cockell, C. S., Lee, P. Osinski, G. R., Horneck, G. and Broady, P. 2002. Impact-induced microbial endolithic habitats. *Meteoritics & Planetary Science* **37**:1287–1298.

- Cockell, C. S., McKay, C. P. and Omelon, C. R. 2003. Polar endoliths - an anti correlation of climatic extremes and microbial diversity. *International Journal of Astrobiology* **1**:305–310.
- Cockell, C. S. and Osinski, G. R. 2007. Impact-induced impoverishment and transformation of a sandstone habitat for lithophytic microorganisms. *Meteoritics & Planetary Science* **42**:1985–1993.
- de los Ríos, Wierzchos, A., J., Sancho, L. G., Green, T. G. A. and Ascaso, C. 2005. Ecology of endolithic lichens colonizing granite in continental Antarctica. *The Lichenologist* **37**:383–395.
- Dykstra, M. J. and Reuss, L. E. 2003. *Biological Electron Microscopy: Theory, Techniques and Troubleshooting* 2nd. Edition. Kluwer Academic / Plenum Publishers, New York. pp.1-31, 86, 101.
- Fike, D. A., Cockell, C. S., Pearce, D. and Lee, P. 2003. Heterotrophic microbial colonization of the interior of impact-shocked rocks from Haughton impact structure, Devon Island, Nunavut, Canadian high Arctic. *International Journal of Astrobiology* **1**:311–323.
- Friedmann, E. I. 1980. Endolithic microbial life in hot and cold deserts. *Origins of Life* **10**:223–235.
- Friedmann, E. I., Kappen, L., Meyer, M. A. and Nienow, J. A. 1993. Long-term productivity in the cryptoendolithic microbial community of Ross Desert, Antarctica. *Microbial Ecology* **25**:51–69.
- Haldeman, D. L., Amy, P. S., Ringelberg, D. and White, D. C. 1993. Characterization of the microbiology within a 21m³ section of rock from the deep subsurface. *Microbial Ecology* **26**:145–159.
- Hirsch, P., Eckhardt, F. E. W. and Palmer Jr., R. J. 1995. Methods for the study of rock inhabiting microorganisms - a review. *Journal of Microbiological Methods* **23**:143–167.
- Melosh, H. J. 1989. *Impact Cratering: A Geologic Process*. Oxford University Press, London.
- Napier, W. M. and Clube, S. V. M. 1979. A theory of terrestrial catastrophism. *Nature* **282**:455–459.
- Omelson, C. R., Pollard, W. H. and Ferris, F. G. 2007. Inorganic species distribution and microbial diversity within high Arctic cryptoendolithic habitats. *Microbial Ecology* **54**:740–752.

Osinski, G. R., Lee, P., Parnell, J., Spray, J. G. and Baron, M. 2005a. A case study of impact-induced hydrothermal activity: the Houghton impact structure, Devon Island, Canadian High Arctic. *Meteoritics & Planetary Science* **40**:1859–1877.

Osinski, G. R., Lee, P., Spray, J. G., Parnell, J., Lim, D. S. S., Bunch, T. E., Cockell, C.S., and B. Glass. 2005b. Geological overview and cratering model for the Houghton impact structure, Devon Island, Canadian high Arctic. *Meteoritics & Planetary Science* **40**:1759–1776.

Osinski, G. R. and Pierazzo, E. editors. 2013. *Impact Cratering: Processes and Products*. Blackwell Publishing, Oxford. pp. 330.

Osinski, G. R., Spray, J. G., and Lee, P.. 2001. Impact-induced hydrothermal activity within the Houghton impact structure, arctic Canada: Generation of a transient, warm, wet oasis. *Meteoritics & Planetary Science* **36**:731–745.

Pointing, S. B., Chan, Y., Lacap, D. C., Lau, M. C. Y., Jurgens, J. A. and Farrell, R. L. 2009. Highly specialized microbial diversity in hyper-arid polar desert. *Proceedings of the National Academy of Sciences* **106**:19964–19969.

Singleton, A. C., Osinski, G. R., McCausland, P. J. A., and Moser, D. E. 2011. Shock induced changes in density and porosity in shock-metamorphosed crystalline rocks, Houghton impact structure, Canada. *Meteoritics & Planetary Science* **46**:1774–1786.

Stivaletta, N., López-García, P., Boihem, L. and Millie, D. F. 2010. Biomarkers of endolithic communities within gypsum crusts (Southern Tunisia). *Geomicrobiology Journal* **27**:101–110.

Vukosavljevic, D. 2010. Laboratory model of microbial growth on serpentized and non serpentized mineral surfaces: insight into Archaen life. University of Western Ontario, London.

Walker, J. J. and Pace, N. R.. 2007. Endolithic microbial ecosystems. *Annual Reviews in Microbiology* **61**:331–347.

Wanger, G., Southam, G., and Onstott, T. C. 2006. Structural and chemical characterization of a natural fracture surface from 2.8 kilometers below land surface: biofilms in the deep subsurface. *Geomicrobiology Journal* **23**:443–452.

Wierzchos, J., Cámara, B., de los Rios, A., Davila, A. F., Sánchez Almazo, I. M., Artieda, O., Wierzchos, K., Gómez-Silva, B., McKay, C. and Ascaso, C. 2011. Microbial colonization of Ca-sulfate crusts in the hyperarid core of the Atacama Desert: implications for the search for life on Mars. *Geobiology* **9**:44–60.

Wierzchos, J., de los Rios, A., Sancho, L. G. and Ascaso, C. 2004. Viability of endolithic micro-organisms in rocks from the McMurdo Dry Valleys of Antarctica established by confocal and fluorescence microscopy. *Journal of Microscopy* **216**:57–61.

Wynn-Williams, D. D. and Edwards, H. G. M. 2000. Antarctic ecosystems as models for extraterrestrial surface habitats. *Planetary and Space Science* **48**:1065–1075.

Chapter 4 : Microbial community composition within impact-generated endolithic habitats in crystalline rocks

Alexandra Pontefract, Gordon R. Osinski, Charles S. Cockell and Gordon Southam.

4.1 Introduction

The colonization of rocks was first noted almost a century ago (Diels, 1914); however, it was not until the discovery of extensive endolithic (within-rock) colonization in the Dry Valleys of Antarctica that widespread interest in these environments was engendered (Friedmann and Ocampo, 1976). Previously thought to be uninhabited, the Dry Valleys are characterized by extreme cold and dry conditions, where any precipitation generally sublimates, providing very minimal water input for organisms (Pointing et al., 2009). Since the initial discovery, microbial endolithy has been widely recognized as a beneficial adaptation to environmentally harsh conditions, and is generally found to be the primary mode of survival for microorganisms in either cold or hot desert environments (Friedmann 1980). Rocks are an ideal substrate in such environments due to their ability to serve as a UV shield, protect from large temperature swings, act as a concentrating mechanism for air-blown nutrients and water, and generally providing a higher relative humidity than the surrounding environment (Cockell et al., 2005). Typically, only rocks with a high level of porosity and translucency experience endolithic colonization, such as sedimentary rocks or evaporites (e.g., Wierzchos et al., 2011). More opaque rocks, such as granites and gneisses, will only see chasmoendolithic or epilithic growth (Cockell and Stokes 2006).

Since the initial survey in the late 1970's, much work has also been done to attempt to characterize the microbial diversity of endolithic communities in polar and non-polar deserts around the world (e.g., de la Torre et al., 2003; Friedmann 1980, 1982; Friedmann et al., 1993; Friedmann and Kibler 1980; Omelon 2008; Pointing et al., 2009; Wierzchos and Ascaso 2001; Wierzchos et al., 2006; Wierzchos et al., 2011). In a review by Walker and Pace (2007) focusing on RNA-based studies, the authors point out that these communities are extremely simple in terms of diversity and share compositional similarities with other desert environments. One such example can be found in the genus

Chroococciopsis, a cyanobacterium that is common in endolithic communities worldwide (Friedmann 1980). Other members of the Cyanobacteria are also prevalent in both Arctic and Antarctic endolithic ecosystems such as: *Leptolyngbya*, *Gloeocapsa*, *Trebouxia*, *Oscillatoria* and *Nostoc spp.* (Omelon et al., 2006; Pointing et al., 2009). This supports the hypothesis that these endolithic environments are highly specialized and that only a small reservoir of organisms from the globally-distributed microbial pool are capable of colonizing them (Pointing et al., 2009; Jungblut et al., 2010; Fierer and Lennon 2011). It is believed that the physical and chemical conditions of the rock – such as porosity, translucency, hygroscopic properties and rock type – have a much higher influence on the composition of the microbial community than geography (Walker and Pace 2007).

In the last decade a new habitat has been added to the list of substrates capable of hosting endolithic communities, in the form of impact-metamorphosed lithologies. Meteorite impacts are a fundamental, though often overlooked, geological process that affects all rocky and icy planetary bodies. The extreme heat and pressure generated by a meteorite impact event results in the formation of microfractures, vesicularization and increased translucency within the substrate, favourably altering the target rock for endolithic colonization. Of particular interest is the creation of endolithic habitats in crystalline rocks, specifically gneisses, which before the impact, were not capable of being colonized. Early work showed the prevalence of endolithic communities in shocked gneisses from the Houghton impact structure, Canada (Cockell et al., 2002; Cockell 2004; Cockell et al., 2005). Recent work has shown that biomass levels increase with increasing shock level as a function of porosity and translucency, with the unshocked rocks – mainly comprised of an epilithic community – having cell counts at $\sim 10^6$, whereas moderate and high shocked samples reached levels of $\sim 10^8$ and $\sim 10^9$ respectively (Chapter 2). The biodiversity of these impact-created habitats, however, has yet to be characterized fully. Fike et al. (2003) performed a preliminary study of the heterotrophic organisms inhabiting shocked versus unshocked lithologies based on rock-isolates and showed that most of the organisms within this habitat shared similar metabolic strategies. Community complexity was increased in the shocked gneisses, relative to host impact breccias from the same area, which were dominated by three genera: *Arthrobacter*, *Pseudomonas* and

Stenotrophomonas. Alternatively, shocked samples contained organisms from the bacterial genera *Arthrobacter*, *Pseudomonas*, *Bacillus*, *Stenotrophomonas*, *Planococcus*, *Caulobacter* and *Janthinobacter*, with approximately equal levels of abundance. This initial research suggested that the impact event created an environment with its own unique selectional pressures, affecting the species abundance and distribution of microorganisms within the endolithic community. In this study we show that shock metamorphism does effect the composition of the endolithic community, especially with reference to phototrophic bacteria. Here, the first culture-independent genomic analysis of microbial diversity within shocked gneisses from the Houghton impact structure is presented, expanding on a new type of environment within the arctic tundra as well as elucidating the selectional pressures related to shock metamorphism. The promotion of endolithic habitats within impact craters is also discussed, especially with reference to the potential for past-endolithic environments on other terrestrial bodies in the solar system, such as Mars.

4.2 Methods

4.2.1 Field Site

Samples were collected from multiple sites within the Houghton impact structure, located in the northwestern region of Devon Island, Nunavut (75°08'N, 87°51'W), in the Canadian High Arctic archipelago (Osinski et al., 2005a) (see Appendix B1 for sample locations). Hand-sized samples of shocked gneiss from a range of different shock levels were collected and placed in sterile sample bags and stored at 4°C. Endolithic banding was occasionally visible to the naked eye, but this was not a criterion for sample selection. It should be noted that determination of shock level in the field is difficult owing to the high level of variation in the types of gneisses present as well as the range of porosity experienced within each shock level. Estimations of density as well as visual observations of mafic banding or complete loss of mafic minerals aided sample selection. A more stringent characterization was then made in the laboratory through the use of petrographic thin sections to characterize shock effects at the microscopic level (see Appendix A1 for a description of shock characterization). Once characterized, samples

were then placed at either -20°C for DNA extraction or at 4°C for storage for culturing or various imaging techniques.

4.2.2 *DNA Extraction, Sequencing and Statistical Analysis*

Twenty-two samples, divided into three populations, comprising unshocked (0), moderate shock (levels 3 and 4) and high shock (levels 6 and 7), were examined for Bacterial 16S DNA, and 3 samples (1 per population) for Fungal and Eukaryal 18S analysis. Ten grams of sample was weighed out and powdered using a sterile alumina mortar and pestle in a laminar flow hood. DNA extraction was then performed using PowerMax® Soil DNA Isolation Kit (MoBio, Carlsbad, CA) according to the manufacturer's instructions. Samples were sequenced for Bacterial, Eukaryotic and Fungal 18S rDNA using 454 Pyrosequencing (Research and Testing Laboratories, Austin, TX). Alpha diversity indices (Shannon's Index, Simpson's Index and Pielou's Evenness) were calculated using untransformed data at the class level for each of the Bacterial, Eukaryotic and Fungal sequences and as a community. Primer v.5 was used to run a one-way ANOSIM (Analysis of Similarity) and to generate an NMDS (Non-Metric Multi-Dimensional Scaling Plot) using Bray-Curtis similarities to graphically represent similarities between populations.

4.2.3 *Culturing*

Small, 1 cm³ rocks from varying shock levels were placed in BG-11 media for enrichment of the phototrophic community at 24°C for 1 month using a 16h daylight:8h dark. Enrichments were then plated on BG-11 agar to isolate species, which were then imaged using a Nikon Eclipse LV100POL Compound Microscope. Identification of isolates was made using either Castenholz and Waterbury (1989) or Wehr (2003). Isolates were also plated on NO₃-deficient agar plates to identify nitrogen fixers within the community (for a list of all nitrogen fixers see Sprent and Sprent (1990)). Finally, samples of gneiss were placed in distilled water for over 6 months at room temperature (16h daylight:8h dark) to see if growth would occur in un-enriched conditions in which the organisms make use of only the nutrients present within the inoculated rocks.

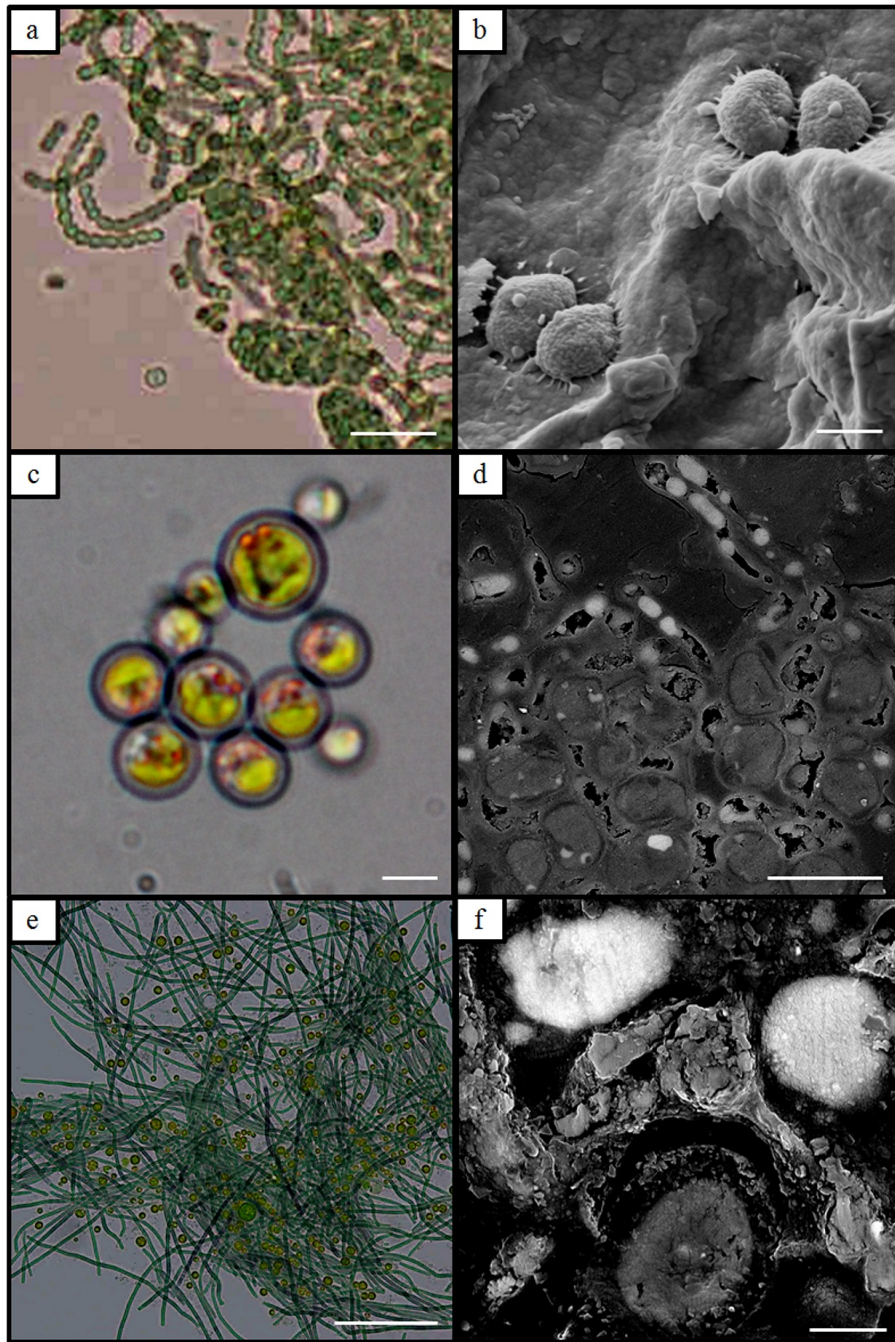


Figure 4-1. Micrographs of cultured isolates from shocked gneisses (left side) and SEM micrographs of *in situ* colonization within highly shocked gneisses (right side). (a) Micrograph of *Anabaena* spp.; bar is 25 μ m. (b) Secondary electron image of bacterium with EPS; bar is 600 nm. (c) Micrograph of coccoid algae, *Chlorella* spp., bar is 10 μ m. (d) SEM-BSE image of an endolithic colony consisting of large coccoid organisms and rod shaped bacteria; bar is 10 μ m. (e) Micrograph of culture from shocked gneiss in BG-11 with *Chlorella* and a filamentous Cyanobacterium; bar is 100 μ m. (f) SEM-BSE image of endolithic bacterium fossilized in calcium; bar is 2 μ m.

4.3 Results

4.3.1 Culturing

Samples of shocked gneiss placed in BG-11 nutrient media showed considerable growth after one month. In most cases, growth of cyanobacteria and algae within the flasks completely engulfed the rock, which was frequently no longer visible. Culturing methods revealed several species of cyanobacteria, which could be determined to the class level: *Oscillatoria spp.*, *Nostoc spp.*, *Anabaena spp.*, *Gloeocapsa spp.*, *Chroococciopsis spp.*, *Leptolyngbya spp.* and one species of alga, *Chlorella sp.* which was confirmed through sequencing (Figure 4-1). Rocks incubated in distilled water for over 6 months showed no discernible growth and no isolates could be detected when medium was plated on BG-11 nutrient agar (Appendix C1), indicating that the rock was a nutrient-limiting substrate.

4.3.2 16S Analysis and Diversity Calculations

Pyrosequencing yielded 300,000 reads per sample at 442 bp per fragment and were identified using a custom database derived from NCBI (Research and Testing, 2012). Analyses of the total bacterial 16S rDNA at class level showed large statistical differences between the unshocked and shocked communities (Figure 4-2a), revealing some general trends. The unshocked samples consisted primarily of three classes of bacteria: Actinobacteria (40%), Gammaproteobacteria (29%) and Alphaproteobacteria (21%), with a small contribution from the Clostridia and Bacilli, with the total population consisting of 23 different classes. Among the different shock levels, Actinobacteria and Fusili classes were ubiquitous throughout; however, the Alphaproteobacteria and Gammaproteobacteria both decrease by almost an order of magnitude with increasing shock. Algal and fungal sequencing was completed for only three samples (one from each shock population). Within the Algae, only the moderate and high shock samples were able to be amplified and low and moderate shock samples failed to generate amplicons for fungal analysis. As such, these data were omitted from the statistical analysis and serve only as an indicator of species present. The moderately shocked sample analysed for algae was dominated entirely by a species belonging to the Chlorophyta, most closely affiliated with *Rosenvingiella radicans*. The highly shocked sample for the same analysis showed more taxonomic diversity, consisting of nine species most closely affiliated with

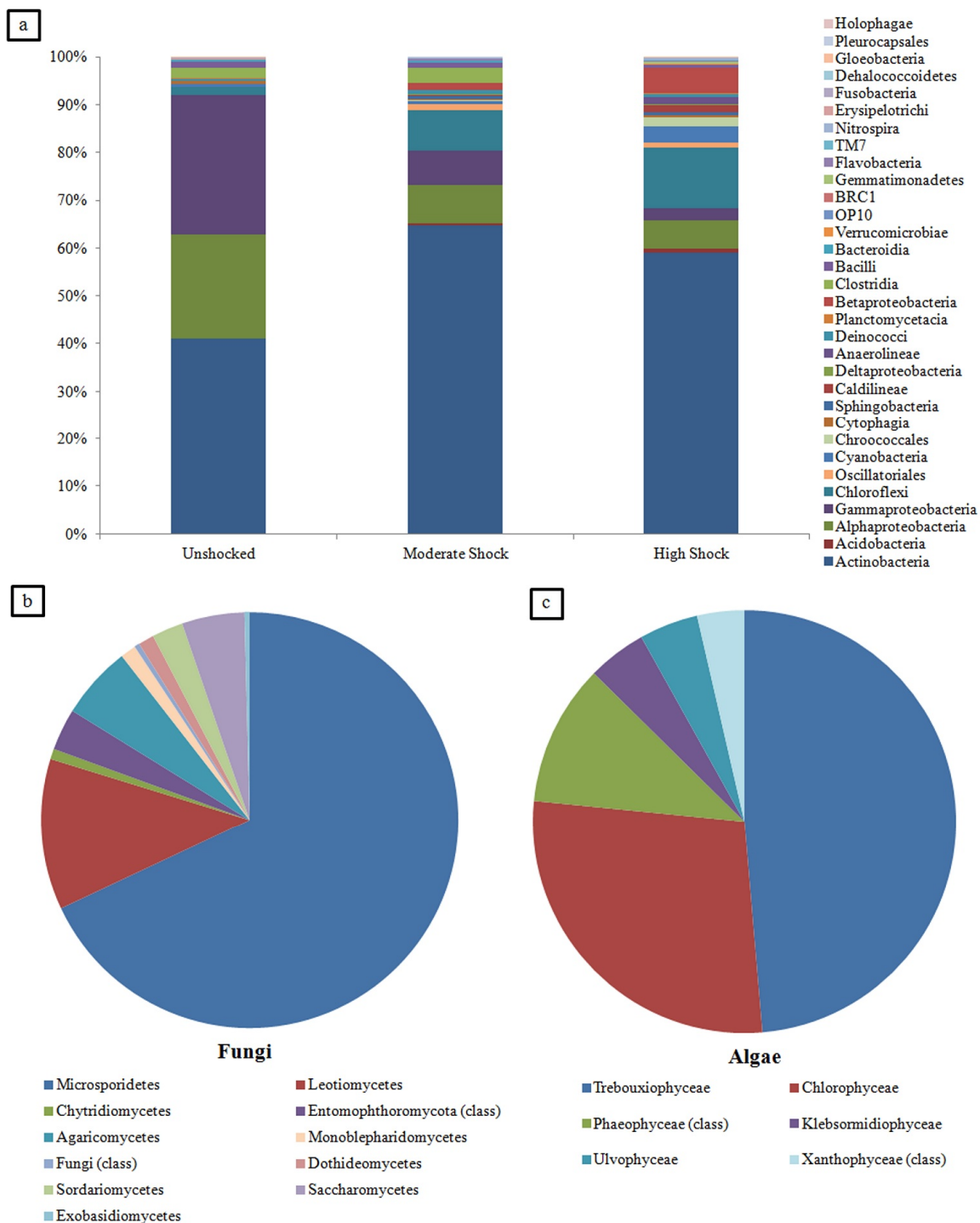


Figure 4-2. (a) Percentage abundances of 16S DNA for the bacterial communities from unshocked, moderate shock and highly shocked gneisses. (b) Percentage abundance of ssu DNA for the fungal community of a highly shocked gneiss. (c) Percentage abundance of 16S rDNA for the algal community from the same highly shocked sample as in (b). All data are represented at the class level.

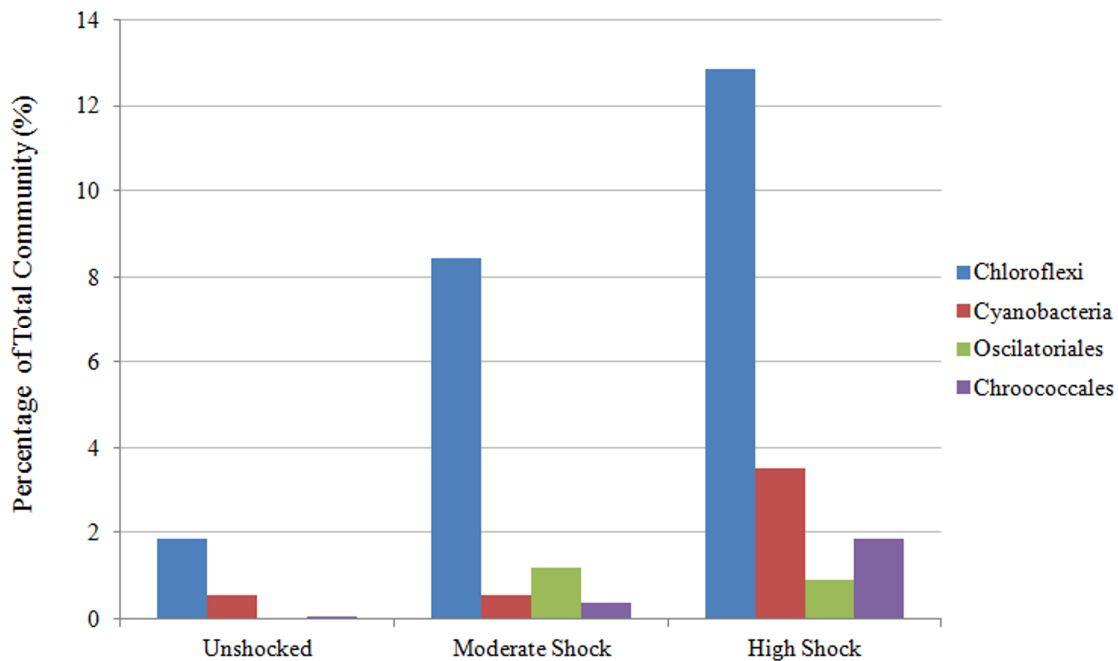


Figure 4-3. Percentage abundance of the phototrophic bacterial communities from the unshocked, moderately shocked and highly shocked gneisses, presented at the class level as a function of the percentage of the total bacterial community.

species within the Chlorophyta (though still dominated by *R. radicans* as well as *Bracteacoccus cohaerens*) and 1 of Streptophyta: *Klebsormidium flaccidum*, a filamentous green-alga (Figure 4-2c). The fungal sequences were dominated by the Ascomycota, consisting primarily of sequences most closely affiliated with *Thelidium decipiens* and *Placidiopsis cinerascens*, and the Microsporidia (*Systemostrema alba*), a parasitic fungi of animals, with a small contribution from the Basidiomycota in the form of mushroom forming spores such as *Cortinarius sodagnitus* (Figure 4-2b). Focusing solely on the bacterial phototrophic community; the largest contributor within the rocks came from the Chloroflexi (class) which was present at 2% in the unshocked lithologies, increasing to well over 12% in the high shock samples (Figure 4-3). The Cyanophyta (phylum) were not largely present (though counts did increase by an order of magnitude between each of the unshocked, moderate shock and high shock samples) having a minor contribution from the Chroococales and Oscillatoriales, the latter of which was only present within the shocked lithologies.

Statistical analysis based on alpha diversity using the Shannon Index, Simpson's Index and Pielou's Evenness did not reveal any large differences between the shocked and unshocked populations for the bacterial community (Table 4-1), where all populations were equally uneven and only the high shock population showed a slightly elevated H' value of 1.63. Using a multivariate analysis, ANOSIM showed that the unshocked population was significantly different from the moderate shock level population with $p < 0.10$, and from the high shock populations with $p < 0.01$. There was no significant difference between the moderate and high shock level populations, $p < 0.30$. Similarly, the NMDS plot (Figure 4-4) showed that the shocked samples were generally a discrete group from the unshocked samples, with the exception of one outlier, WSR001A2. Beyond this, however, samples did not appear to group as a function of shock or in terms of geographical location within the crater. See Appendix C3 for full pyrosequencing results.

Table 4-1. List of diversity statistics and phylum abundances for unshocked, moderate shock and high shock populations.

	Unshocked	Moderate Shock	High Shock
Alpha Diversity Indices*			
Shannon's Index	1.4	1.4	1.6
Simpson Diversity Index	0.8	0.9	0.9
Pielou's Evenness	0.4	0.4	0.5
Bacterial Phylum Abundance (%)			
Actinobacteria	41.1	65.2	59.4
Acidobacteria	0.1	0.4	0.8
Proteobacteria	51.1	16.9	13.9
Firmicutes	3.3	4.3	0.7
Bacteroidetes	1.0	1.6	1.4
Deinococcus	0.5	0.5	0.5
Planctomycetes	0.1	0.1	0.2
Verrucomicrobia	0	0	0.1
Armatimonadetes	0	0	0
BRC1	0	0	0
Gemmatimonadetes	0	0.1	0.3
Nitrospirae	0	0.1	0.4
Fusobacteria	0.2	0	0
Chloroflexi	1.9	8.7	15.9
Cyanobacteria	0.7	2.2	6.4
Algal Phylum Abundance (%)			
Phaeophyceae	—	0	10.8
Xanthophyceae	—	0	3.6
Chlorophyta	—	100	81.1
Streptophyta	—	0	4.5
Fungal Phylum Abundance (%)			
Microsporidia	—	—	22.2
Ascomycota	—	—	74.0
Chytridiomycota	—	—	0.7
Entomophthoromycota	—	—	1.1
Basidiomycota	—	—	2.0
Fungi (phylum)	—	—	0.1

* Alpha indices calculated only for the bacterial 16S genomes.

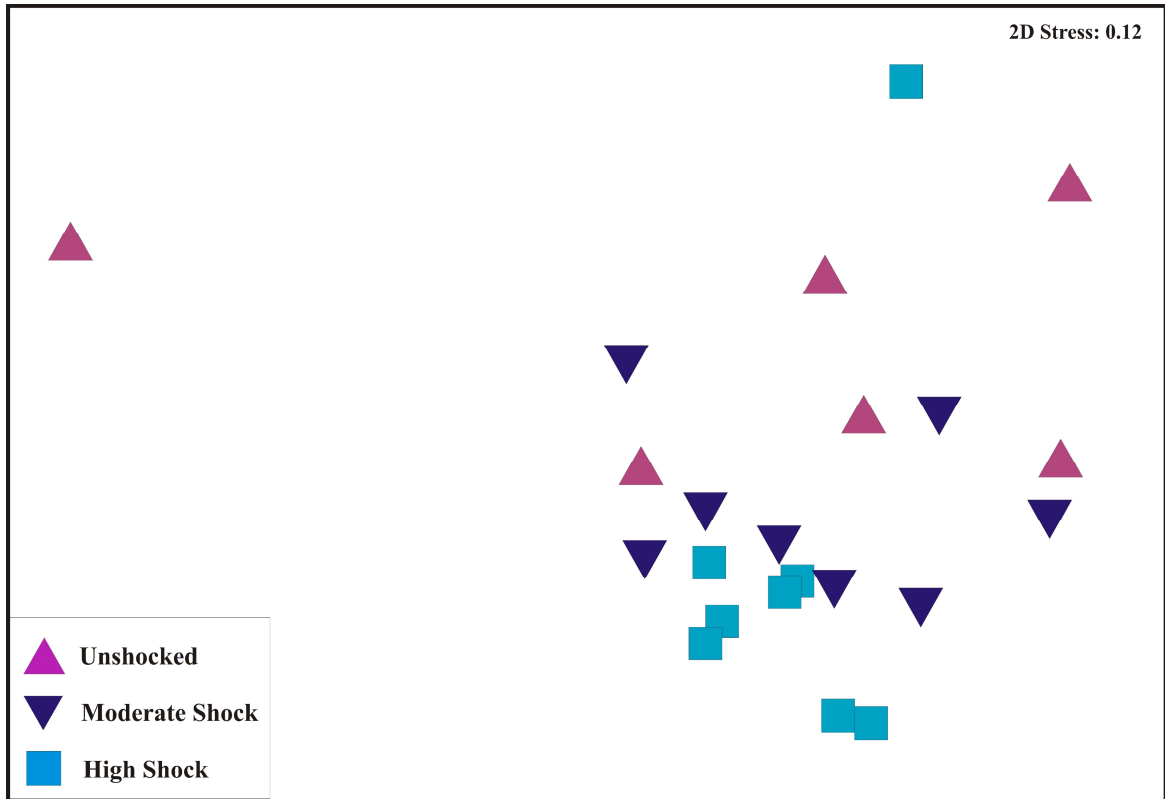


Figure 4-4. Nonmetric multidimensional scaling plot (NMDS) for bacterial 16S rDNA from unshocked, moderately shocked and highly shocked populations (ANOSIM, $n=22$, $p < 0.1$ for division in a pairwise comparison between unshocked and highly shocked populations, and $p < 0.3$ for pairwise between unshocked and moderate shock). High shock samples (squares) do appear to show some grouping distinct from the unshocked communities, but plot very closely with moderate shock samples.

4.3.3 *N*₂ Fixation

Metagenomic analysis showed 22 species present within the populations belonging to genera that are known to have N₂-fixing representatives, such as *Rhizobium*, *Chroococales*, *Nostoc*, *Oscillatoria*, *Calothrix*, *Prochlorales*, *Rhodospirillales*, *Burkholderiales* and *Chromatiales*. Isolates from the rocks grown in BG-11 were all plated on nitrogen-deficient BG-11 agar and grown for 3 weeks. Growth of *Lyngbya* and *Anabaena* were both observed, but no other isolate showed growth, indicating that the species of *Oscillatoria* in culture was not capable of N₂ fixation.

4.4 Discussion

This study represents the first comprehensive assessment of a microbial colony within impact metamorphosed rocks and also represents one of the few culture-independent studies of land-based Arctic microbial communities (e.g., Nemergut et al., 2005; Yergeau et al., 2010; Deslippe et al., 2012;). This impact-created endolithic environment is a valuable habitat within polar deserts, which has important implications for the potential for viable habitats on other terrestrial bodies in our solar system – especially in instances where impact cratering may be one of the only active geologic processes.

As in Arctic soils, the Actinobacteria were the largest contributors to the community at all three shock levels; however, the unshocked lithologies contained the closest values to typical soil microbiota (Deslippe et al., 2012; Yergeau et al., 2010), having abundant Proteobacteria (specifically within the Alphaproteobacteria and Gammaproteobacteria – both of which contain N₂-fixing species) and low (< 3%) levels of the Firmicutes, Bacteroidetes and Chloroflexi. Interestingly, the Gemmatimonadetes (gram-negative aerobic bacteria), which are generally quite prevalent in Arctic soils, were found only within the high shock level samples. Within endolithic communities, it has been suggested that nitrogen fixation is generally rare (Friedmann 1982). We do not find this to be the case in our study; although the N₂-fixing species, such as *Rhizobium*, were found only within the shocked lithologies and was also accompanied by an increase in the phototrophic communities, several species of which are diazotrophs. Presumably some nitrogen input for the community was also likely provided through atmospheric fixation and deposition (Walker and Pace 2007).

The most profound effects of shock on the microbial community were seen within the phototrophic organisms, spanning four phyla within the bacteria. The Chloroflexi were the dominant phototroph in each shock level (2%, 9% and 16% respectively), over the Cyanophyta, which, even at the high shock levels only reached an abundance of 6%. In addition there was a very small addition to the phototrophic community in the *Rhodospirilloceae*, a photoorganoheterotroph from the purple non-sulfur bacteria. This in contrast to current literature on Antarctic and alpine endolithic communities that has consistently found cyanobacteria to be the dominant phylotype (up to 56%; Pointing et al., 2009), with Chloroflexi present in either very low numbers (Walker and Pace 2007), or being completely absent (Pointing et al., 2009).

Of the five metagenomic studies available on terrestrial arctic microbial communities (Zhou et al., 1997; Neufeld and Mohn 2005; Nemergut et al., 2005; Yergeau et al., 2010; Deslippe et al., 2012) only the Deslippe study mentions the presence of Chloroflexi within soils, present at a low abundance. In the shocked gneiss community the cyanobacteria consist of the Chroococcales, Nostocales, Oscillatoriales, few of which were able to be cultured in the lab. Cyanobacteria from Antarctica appear to be much more diverse, containing 112 distinct species, many of which are unknown (Pointing et al., 2009), compared to 62 in the shocked gneisses. This is unusual considering the fact that the Arctic environment is considerably less extreme than that of the Antarctic, receiving much larger amounts of precipitation throughout the year and experiencing warmer temperatures, resulting in less stringent selectional pressures (Omelon et al., 2006). In addition, the sandstones of Antarctica have a porosity of between 2.3% and 13.0% (Cockell et al., 2003), in comparison to the shocked gneisses which can reach porosities of over 60% (Singleton et al., 2011). That the level of porosity does affect the colonization of shocked gneisses by phototrophs is evidenced both by the marked increase in the bacteria with increasing shock and by the presence of eukaryotic algae and large filamentous cyanobacteria, such as Oscillatoriales within only the shocked lithology, where increased porosity would allow for such relatively large organisms.

In this instance, as neither porosity, light penetration nor climate are apparent barriers to phototrophic colonization, it is plausible that because of the large presence of both the Actinobacteria and Proteobacteria due to more clement conditions, the phototrophic

community is out-competed and is simply not able to reach the large abundances seen in Antarctic communities. Neither the algal nor fungal species within these samples appeared to be strong contributors to the overall community, existing at very low abundances, which is in keeping with previous microscopic observations by Cockell et al. (2003) and Omelon et al. (2006), though work on a larger sample size must be completed. As a whole, the community is dominated by heterotrophic bacteria with the phototrophs supplying, at most, 12% of the total active community. This suggests that the organisms must also rely on an exogenous form of carbon input from the environment, likely along with other nutrients such as phosphorus and nitrogen. The fungal community is a clear indicator that the sequenced DNA of these samples is not necessarily representative of the active community. Without knowing the entire composition of the active community, it is difficult to surmise the metabolic diversity of these Arctic endolithic communities, and an investigation of the active community should be completed. The presence of so many bacterial species in such a harsh environment, as well as a plausible reliance on external sources of nutrients, indicates that few species might occupy metabolic niches, with the rest of the population potentially using similar metabolic pathways (Fierer and Lennon 2011). The dominant presence of *Actinobacteria* within all of the samples does show that a significant amount of carbon turnover is possible within these communities, made more likely by the wetter conditions experienced in the Arctic.

Overall, a significant change in microbial community composition with increasing shock pressure in the gneisses was observed, revealing the presence of distinct populations based on the level of created porosity and translucency within the rock. Due to the fact that the sample size was small, that communities were highly uneven and that the relative abundances remained fairly similar between populations, analyses using alpha diversity indices were unable to statistically reveal changes in microbial diversity. ANOSIM was able to show that there is a distinct difference in community composition between the unshocked and shocked populations; however, due to the high variability inherent in the samples the moderate- and high-shocked communities showed no significant difference from each other. This is likewise reflected in the NMDS plot (Figure 4-4), which, aside from showing a more distinct difference between unshocked and shocked populations, is not able to resolve any further patterns related to shock

metamorphism. Indeed, some of the samples collected from opposite regions within the crater plot together, while samples collected near each other along the same escarpment do not. Comparison of NMDS plots with calculated porosity values for those samples (data not shown) did not reveal any correlation, indicating that the grouping of samples seen within this plot may instead be related to specific wind patterns within the crater, and other factors such as drainage patterns along escarpments, sun exposure, and the prevalence of macrofractures within the sample. Future work in this area requires a detailed ecological study of the crater region so as to determine the effects of variable light incidence and precipitation on shocked lithologies and how these variables may interact to influence community composition.

4.5 Concluding Remarks

A wide range of studies spanning polar and non-polar desert endolithic communities has shown that such populations are highly specialized and, in many cases, ideally adapted to surviving such harsh conditions (Friedmann et al., 1993; de la Torre et al., 2003; Wierzchos et al., 2006; Walker and Pace 2007; Omelon 2008). As a result of this, these organisms tend to be remarkably persistent over long periods of geologic time (Pointing et al., 2009). What does this mean for life elsewhere in our solar system? On Mars for example – which is essentially a polar desert, albeit an extreme one – impact cratering and the generation of shocked lithologies as well as transient hydrothermal systems (Osinski et al., 2013) is an important geological process. If life existed on Mars in the early Noachian, it is plausible that as conditions on the planet began to deteriorate, and transitioned into a cold, dry planet that life may have survived in the abundant endolithic environments afforded by impact craters. Not only within the surficial brecciated deposits, but also likely in the deep fractured subsurface beneath these craters (Boston et al., 1992; Ascaso and Wierzchos 2002; Cockell et al., 2012). Future infilling of these deposits may then have preserved these organisms, making these brecciated lithologies an attractive target for future life detection missions.

4.6 References

Abramov, O. and Kring, D. A., 2005. Impact-induced hydrothermal activity on early Mars. *Journal of Geophysical Research* **110**:1–19.

Abramov, O. and Mojzsis, S. J., 2009. Microbial habitability of the Hadean Earth during the late heavy bombardment. *Nature* **459**:419–422.

Alvarez, L. W., Alvarez, W., Asaro, F. and Michel, H. V., 1980. Extraterrestrial Cause for the Cretaceous-Tertiary Extinction. *Science* **208**:1095–1108.

Ascaso, C., and Wierzchos, J., 2002. New approaches to the study of Antarctic lithobiontic microorganisms and their inorganic traces, and their application in the detection of life in Martian rocks. *International Journal of Microbiology* **5**:215–222.

Barker, W. W., Welch, S. A., and Banfield, J., 1997. Biogeochemical weathering of silicate minerals, *in* Banfield, J., and Nealson, K.H., eds., *Geomicrobiology: Interactions Between Microbes and Minerals*, Volume 35. *Reviews in Mineralogy*: Atlanta, Mineralogical Society of America, pp. 391–428.

Bell, R. A., 1993. Cryptoendolithic algae of hot semiarid lands and deserts. *Journal of Applied Phycology* **29**:133–139.

Boston, P. J., Ivanov, M. V. and McKay, C. P., 1992. On the possibility of chemosynthetic ecosystems in subsurface habitats on Mars. *Icarus* **95**:300–308.

Brack, A., Horneck, G., Cockell, C. S., Bérces, A., Belisheva, N. K., Eiroa, C., Henning, T., Herbst, T., Kaltenegger, L., Léger, A., Liseau, R., Lammer, H., Selsis, F., Beichman, C., Danchi, W., Fridlund, M., Lunine, J., Paresce, F., Penny, A., Quirrenbach, A., Röttgering, H., Schneider, J., Stam, D., Tinetti, G. and White, G. J. 2010. Origin and Evolution of Life on Terrestrial Planets. *Astrobiology* **10**:69–76.

Burt, J. B., Pope, M. C., and Watkinson, A. J., 2005. Petrographic, X-ray diffraction, and electron spin resonance analysis of deformed calcite: Meteor Crater, Arizona. *Meteoritics & Planetary Science* **40**:297–306.

Buss, H. L., Brantley, S. L. and Liermann, L. J., 2003. Nondestructive methods for removal of bacteria from silicate surfaces. *Geomicrobiology Journal* **20**:25–42.

Chao, E. C. T., 1968. Pressure and temperature histories of impact metamorphosed rocks - Based on petrographic observations. *N. Jb. Miner. Abh.* **108**:209–246.

Cockell, C. S., 2004. Impact-shocked rocks - Insights into archaic and extraterrestrial microbial habitats (and sites for prebiotic chemistry?). *Advances in Space Research* **33**:1231–123.

Cockell, C. S., 2006. The origin and emergence of life under impact bombardment. *Philosophical Transactions of the Royal Society B* **361**:1845–1856.

Cockell, C. S. and Lee, P., 2002. The biology of impact craters - a review. *Biological Reviews* **77**:279–310.

Cockell, C. S., Lee, P., Broady, P., Lim, D. S. S., Osinski, G. R., Parnell, J., Koeberl, C., Pesonen, L. and Salminen, J., 2005, Effects of asteroid and comet impacts on habitats for lithophytic organisms - a synthesis. *Meteoritics & Planetary Science* **40**:1901–1914.

Cockell, C. S., Lee, P., Osinski, G. R., Horneck, G. and Broady, P. 2002. Impact-induced microbial endolithic habitats. *Meteoritics & Planetary Science* **37**:1287–1298.

Cockell, C. S., McKay, C. P. and Omelon, C. R. 2003. Polar endoliths - an anti-correlation of climatic extremes and microbial diversity. *International Journal of Astrobiology* **1**:305–310.

Cockell, C. S. and Osinski, G. R. 2007. Impact-induced impoverishment and transformation of a sandstone habitat for lithophytic microorganisms. *Meteoritics & Planetary Science* **42**:1985–1993.

Cockell, C. S., and Stokes, M. D. 2006. Hypolithic Colonization of Opaque Rocks in the Arctic and Antarctic Polar Desert. *Arctic, Antarctic and Alpine Research* **38**:335–342.

Cockell, C. S., Voytek, M. A., Gronstal, A. L., Finster, K., Kirshtein, J. D., Kallmeyer, J., Kelly, L. and Powars, D. S. 2012. Impact disruption and recovery of the deep subsurface biosphere. *Astrobiology* **12**:231–246.

de la Torre, J. R., Goebel, B. M., Friedmann, E. I. and Pace, N. R. 2003. Microbial diversity of cryptoendolithic communities from the McMurdo Dry Valleys, Antarctica. *Applied and Environmental Microbiology* **69**:3858–3867.

de los Ríos, A., Wierzchos, J., Sancho, L. G., Green, T. G. A., and Ascaso, C. 2005. Ecology of endolithic lichens colonizing granite in continental Antarctica. *The Lichenologist* **37**:383–395.

Deslippe, J. R., Hartmann, M., Simard, S. W., and Mohn, W. W. 2012, Long-term warming alters the composition of Arctic soil microbial communities. *FEMS Microbiology Ecology* **82**:303–315.

Diels, L., 1914. Die Algen-Vegetation der Südtiroler Dolomitriffe. Bericht der Deutschen botanischen Gesellschaft, **32**:502–526.

Douglas, S., and Beveridge, T. J. 1998. Mineral formation by bacteria in natural microbial communities. *FEMS Microbiology Ecology* **26**:79–88.

Dykstra, M. J. and Reuss, L. E. 2003. *Biological Electron Microscopy: Theory, Techniques and Troubleshooting* 2nd. Edition: New York, Kluwer Academic / Plenum Publishers. pp.1-31, 86, 101.

Fairén, A. G., Davila, A. F., Lim, D. S. S., Bramall, N., Bonaccorsi, R., Zavaleta, J., Uceda, E. R., Stoker, C., Wierzchos, J., and Dohm, J. M. 2010. Astrobiology through the ages of Mars: the study of terrestrial analogues to understand the habitability of Mars. *Astrobiology* **10**:821-843.

- Fedo, C. M. and Whitehouse, M. J. 2002. Earth's Earliest Life. *Science* **296**:1448–1452.
- Fierer, N. and Lennon, J. T. 2011. The Generation and Maintenance of Diversity in Microbial Communities. *American Journal of Botany* **98**:439–448.
- Fike, D. A., Cockell, C. S., Pearce, D. and Lee, P. 2003. Heterotrophic microbial colonization of the interior of impact-shocked rocks from Haughton impact structure, Devon Island, Nunavut, Canadian high Arctic. *International Journal of Astrobiology* **1**:311–323.
- French, B. 1998. Traces of Catastrophe: A Handbook of Shock-Metamorphic Effects in Terrestrial Meteorite Impact Structures. Houston, Lunar and Planetary Institute. pp.17–30.
- French, B. and Koeberl, C. 2010. The convincing identification of terrestrial meteoritic impact structures: What works, what doesn't, and why. *Earth-Science Reviews* **98**:123–170.
- Friedmann, E. I. 1980. Endolithic microbial life in hot and cold deserts. *Origins of Life* **10**:223–235.
- Friedmann, E. I. 1982, Endolithic Microorganisms in the Antarctic Cold Desert. *Science* **215**:1045–1053.
- Friedmann, E. I., Kappen, L., Meyer, M. A. and Nienow, J. A. 1993. Long-term productivity in the cryptoendolithic microbial community of Ross Desert, Antarctica. *Microbial Ecology* **25**:51–69.
- Friedmann, E. I. and Kibler, A. P. 1980. Nitrogen economy of endolithic microbial communities in hot and cold deserts. *Microbial Ecology* **6**:95–108.
- Friedmann, E. I. and Ocampo, R. 1976. Endolithic Blue-Green Algae in the Dry Valleys: Primary Producers in the Antarctic Desert Ecosystem. *Science* **193**:1247–1249.
- Gault, D. E., Oberbeck, V. R. and Quaide, W. L. 1968. Impact cratering mechanics and structures. In French, B., and Short, N.M., eds., *Shock Metamorphism of Natural Materials*: Baltimore, Mono Book Corporation, pp. 87–99.
- Haldeman, D. L., Amy, P. S., Ringelberg, D. and White, D. C. 1993. Characterization of the microbiology within a 21m³ section of rock from the deep subsurface. *Microbial Ecology* **26**:145–159.
- Hirsch, P., Eckhardt, F. E. W. and Palmer Jr., R. J. 1995. Methods for the study of rock-inhabiting microorganisms - a review. *Journal of Microbiological Methods* **23**:143–167.
- Jungblut, A. D., Lovejoy, C. and Vincent, W. F. 2010. Global distribution of cyanobacterial ecotypes in the cold biosphere. *The ISME Journal* **4**:191–202.

- Karl, D. M. 1995. *The Microbiology of Deep-sea Hydrothermal Vents*. Boca Raton, CRC Press. pp. 35-124.
- Konhauser, K. O. 2007. *Introduction to Geomicrobiology*. Malden, MA, Blackwell Publishing. pp. 1–35, 192–292.
- Konhauser, K. O., Lalonde, S. V. and Phoenix, V. R. 2008, Bacterial biomineralization: Where to from here? *Geobiology* **6**:298–302.
- Lindgren, P., Parnell, J., Bowden, S., Taylor, C., Osinski, G. R., and Lee, P. 2007. Preservation of organic carbon in impact melt breccia, Haughton impact structure. *Lunar and Planetary Science*, v. XXXVIII.
- Martin, W., Baross, J., Kelley, D. and Russell, M. J. 2008. Hydrothermal vents and the origin of life. *Nature Reviews Microbiology* **6**:805–814.
- Melosh, H.J. 1989. *Impact Cratering: A Geologic Process*. London, Oxford University Press, 256 p.
- Melosh, H. J. and Ivanov, B.A. 1999. Impact Crater Collapse. *Annual Review of Earth and Planetary Science* **27**.
- Michalski, J. R., Cuadros, J., Niles, P. B., Parnell, J., Rogers, A. D. and Wright, S. P. 2013. Groundwater activity on Mars and implications for a deep biosphere. *Nature Geoscience* **6**:133–138.
- Morgan, J. and Warner, M. 1999., Chicxulub: The third dimension of a multi-ring impact basin. *Geology* **27**:407–410.
- Napier, W. M. and Clube, S. V. M. 1979. A theory of terrestrial catastrophism. *Nature* **282**:455–459.
- Naumov, M.V. 1996. Impact-generated hydrothermal activity: the record in terrestrial craters. *Lunar and Planetary Science*, v. XXVII:935–936.
- Nemergut, D. R., Costello, E. K., Meyer, A. F. and Pescador, M. Y. 2005. Structure and function of alpine and arctic soil communities. *Research in Microbiology* **156**:775–784.
- Neufeld, J. D., and Mohn, W. W. 2005. Unexpectedly high bacterial diversity in Arctic tundra relative to boreal forest soils, revealed by serial analysis of ribosomal sequence tags. *Applied and Environmental Microbiology* **71**:55710–5718.
- Nienow, J. A., McKay, C. and Friedmann, E. I. 1988. The Cryptoendolithic Microbial Environment in the Ross Desert of Antarctica: Light in the Photosynthetically Active Region. *Microbial Ecology* **16**:271–289.
- Omelson, C. R. 2008. Endolithic Microbial Communities in Polar Desert Habitats. *Geomicrobiology Journal* **25**:404–414.

Omelson, C. R., Pollard, W. H. and Ferris, F. G. 2006. Chemical and Ultrastructural Characterization of High Arctic Cryptoendolithic Habitats. *Geomicrobiology Journal* **23**:189–200.

Omelson, C. R., Pollard, W. H. and Ferris, F. G., 2007. Inorganic species distribution and microbial diversity within high Arctic cryptoendolithic habitats. *Microbial Ecology* **54**:740–752.

Osinski, G. R., 2007. Impact metamorphism of CaCO₃-bearing sandstones at the Haughton structure, Canada. *Meteoritics & Planetary Science* **42**:1945–1960.

Osinski, G. R., Cockell, C. S., Lindgren, P. and Parnell, J. 2010. The Effect of Meteorite Impacts on the Elements Essential for Life, *Astrobiology Science Conference 2010. Evolution and Life: Surviving Catastrophes and Extremes on Earth and Beyond*. Houston, Lunar and Planetary Institute. Abstract #5252.

Osinski, G. R., Lee, P., Parnell, J., Spray, J. G. and Baron, M. 2005a. A case study of impact-induced hydrothermal activity: the Haughton impact structure, Devon Island, Canadian High Arctic. *Meteoritics & Planetary Science* **40**:1859–1877.

Osinski, G. R., Lee, P., Spray, J. G., Parnell, J., Lim, D. S. S., Bunch, T. E., Cockell, C. S. and Glass, B. 2005b. Geological overview and cratering model for the Haughton impact structure, Devon Island, Canadian high Arctic. *Meteoritics & Planetary Science* **40**:1759–1776.

Osinski, G. R. and Pierazzo, E. 2013. In *Impact Cratering: Processes and Products*. Eds. Osinski, G. R., and Pierazzo, E. Oxford, Blackwell Publishing, pp. 330.

Osinski, G. R., Spray, J. G. and Lee, P. 2001. Impact-induced hydrothermal activity within the Haughton impact structure, arctic Canada: Generation of a transient, warm, wet oasis. *Meteoritics & Planetary Science* **36**:731–745.

Parnell, J., Boyce, A., Thackrey, S., Muirhead, D., Lindgren, P., Mason, C., Taylor, C., Still, J., Bowden, S., Osinski, G. R. and Lee, P. 2010. Sulfur isotope signatures for rapid colonization of an impact crater by thermophilic microbes. *Geology* **38**:271–274.

Pointing, S. B., Chan, Y., Lacap, D. C., Lau, M. C. Y., Jurgens, J. A., and Farrell, R. L. 2009. Highly specialized microbial diversity in hyper-arid polar desert. *Proceedings of the National Academy of Sciences* **106**:19964–19969.

Research and Testing. 2012. *Data Analysis Methodology*. Houston, Research and Testing, p. 17.

Singleton, A. C., Osinski, G. R., McCausland, P. J. A. and Moser, D. E. 2011. Shock-induced changes in density and porosity in shock-metamorphosed crystalline rocks, Haughton impact structure, Canada. *Meteoritics & Planetary Science* **46**:1774–1786.

Spray, J. G. and Elliot, B. 2013. Earth Impact Database. Fredericton, Planetary and Space Science Centre.

Sprent, J. I. and Sprent, P. 1990. Nitrogen Fixing Organisms. Pure and Applied Aspects: New York, Chapman and Hall, 256 p.

Steven, B., Briggs, G., McKay, C. P., Pollard, W. H., Greer, C. W. and Whyte, L. G. 2007. Characterization of the microbial diversity in a permafrost sample from the Canadian high Arctic using culture-dependent and culture-independent methods. *FEMS Microbial Ecology* **59**:513–523.

Stivaletta, N., López-García, P., Boihem, L. and Millie, D. F. 2010. Biomarkers of endolithic communities within gypsum crusts (Southern Tunisia). *Geomicrobiology Journal* **27**:101–110.

Stöffler, D. 1966. Zones of Impact Metamorphism in the Crystalline Rocks of the Nördlinger Ries Crater. *Contributions to Mineralogy and Petrology* **12**:15–24.

Stöffler, D. 1971. Progressive Metamorphism and Classification of Shocked and Brecciated Crystalline Rocks at Impact Craters. *Journal of Geophysical Research* **76**:5541–5551.

Vestal, R.J. 1988. Biomass of the cryptoendolithic microbiota from the Antarctic desert. *Applied and Environmental Microbiology* **54**:957–959.

von Engelhardt, W. and Beetsch, W. 1969. Shock Induced Planar Deformation Structures in Quartz from the Ries Crater, Germany. *Contributions to Mineralogy and Petrology* **20**.

Vukosavljevic, D. 2010. Laboratory model of microbial growth on serpentinized and non-serpentinized mineral surfaces: insight into Archaean life: London, University of Western Ontario.

Wackett, L. P., Dodge, A. G. and Ellis, L. B. M. 2004. Microbial genomics and the periodic table. *Applied and Environmental Microbiology* **70**:647–655.

Walker, J. J. and Pace, N. R. 2007. Endolithic microbial ecosystems. *Annual Reviews in Microbiology* **61**:331–347.

Wanger, G., Southam, G. and Onstott, T. C. 2006. Structural and chemical characterization of a natural fracture surface from 2.8 kilometers below land surface: biofilms in the deep subsurface. *Geomicrobiology Journal* **23**:443–452.

Wierzchos, J. and Ascaso, C. 2001. Life, decay and fossilisation of endolithic microorganisms from the Ross Desert, Antarctica. *Polar Biology*, v. 24, p. 863–868.

Wierzchos, J., Ascaso, C. and McKay, C. P. 2006. Endolithic Cyanobacteria in Halite Rocks from the Hyperarid Core of the Atacama Desert. *Astrobiology* **6**:415–422.

Wierzchos, J., Cámara, B., de los Rios, A., Davila, A. F., Sánchez Almazo, I. M., Artieda, O., Wierzchos, K., Gómez-Silva, B., McKay, C. and Ascaso, C. 2011. Microbial colonization of Ca-sulfate crusts in the hyperarid core of the Atacama Desert: implications for the search for life on Mars. *Geobiology* **9**:44–60.

Wynn-Williams, D. D. and Edwards, H. G. M. 2000. Antarctic ecosystems as models for extraterrestrial surface habitats. *Planetary and Space Science* **48**:1065–1075.

Yergeau, E., Hogues, H., Whyte, L. G. and Greer, C. W. 2010. The functional potential of high Arctic permafrost revealed by metagenomic sequencing, qPCR and microarray analyses. *ISME* **4**:1206–1214.

Zhou, J., Davey, M. E., Figueras, J. B., Rivkina, E., Gilichinsky, D. and Tiedje, J. M. 1997. Phylogenetic diversity of a bacterial community determined from Siberian tundra soil DNA. *Microbiology* **143**:3913–3919.

Chapter 5 : The habitability of shocked gneisses within a post-impact hydrothermal system

Alexandra Pontefract, Gordon R. Osinski, Charles S. Cockell, Sophie Nixon, and Gordon Southam.

5.1 Introduction

Meteorite impact events generate extreme temperatures and pressures within planetary crusts and, in the case of a water- or ice-bearing target, are capable of generating transient hydrothermal systems (Naumov 2002, 2005; Osinski et al. 2013), which can last from thousands to millions of years depending on the size of the impactor (Ames et al. 1998, Abramov and Kring 2005). The development and succession of a hydrothermal regime due to an impact event can be divided into three main stages (Osinski et al. 2001): Early (vapour dominated), Main (vapour and liquid) and Late stage (liquid). Following an impact event, water rushes in laterally and vertically to replace that which was displaced and/or vaporized during crater formation. Depending on the target (i.e., land versus marine) these waters are typically meteoric or seawater. The impact melt rocks, which represent the main source of heat for the generation of hydrothermal systems within impact craters, cools fairly quickly below the liquidus, down to temperatures characteristic of the Early stage, somewhere between 200°C and 600°C (Osinski et al. 2005). Within the Haughton impact structure on Devon Island, the Main stage is characterized by temperatures between 200°C and 80°C. Though these values would differ for each impact crater, depending on the size of the impact and the rate of cooling of the substrate and the permeability of the target rock (Abramov and Kring 2005), it is at the end of the Main stage and into the Late Stage of an impact-induced hydrothermal system that temperatures become low enough to potentially be able to support life.

Currently, the first life on Earth is thought to be hyperthermophilic, as these organisms generally branch deeply within the Bacteria and Archaea (Pace 1991). Some have hypothesized that life originated in deep-sea hydrothermal vents where the rich outflow of organics and potential reductants could have provided the energy necessary for the formation of complex life (e.g., Holm 1992). There are, of course, problems proving

this theory, based both in the fact that there is no geological record of this happening and due to the fact that most biochemical compounds decompose at temperatures above 100°C (Miller and Lazcano 1995), where the ocean would then tend to disperse any organic compounds that were synthesized (Lazcano and Miller 1996). The earliest known life on Earth has been dated to 3.5 Ga (Schopf and Packer 1987) with some claims of life at 3.8 Ga (Mojzsis et al., 1996) coinciding with the end of the Late Heavy Bombardment, and it has been hypothesized that impact cratering may either have had a hand in the origins of life here on Earth (Farmer 2000), or perhaps acted as a bottlenecking event resulting in the selection of hyperthermophilic organisms (Maher and Stevenson 1988, Gogarten et al., 1995). Impact-generated hydrothermal systems are potentially an ideal setting for the evolution and potential origin of life (Osinski et al., 2013). Rock-water interactions promote disequilibrium chemistry, and possible serpentinization in mafic targets causing the release of H₂ and CH₄ (Michalski and Niles 2010). Water interacting with impact melt breccias also promotes the dissolution of glasses and the formation of clays which are then able to hold onto organic compounds, and may have acted as a template for the origins of life (Cairns-Smith and Hartman 1986). Finally, impact craters act as a natural concentrating mechanism through which these aforementioned interactions could occur. To date, no microbial evidence has been found that can be shown to be the result of an impact-generated hydrothermal system; however, given that the hydrothermal phase of large impact structures would likely be quite extensive, it is conceivable that microbial communities could develop. Indeed, within the Haughton impact structure, Parnell et al. (2010) showed that significant sulfur isotope fractionation of the hydrothermal sulfide provides a strong case for the presence of thermophilic sulfate-reducing bacteria during the formation of these deposits.

On Mars, there is evidence for the presence of crater-related hydrothermal deposits (Marzo et al., 2010; Osinski et al., 2013) as well as associated clays (Mustard et al., 2008; Ehlmann et al., 2011), which are currently thought to be the most ideal substrate for yielding evidence of past life on Mars (e.g., Ehrenfreund et al., 2011). Another, and potentially equally viable habitat, may lie in impact-metamorphosed target rocks present as clasts in impact breccias and melt rocks. Given the porous nature of these rocks and that they provide a viable endolithic environment (Cockell et al., 2002, Cockell et al.,

2003, Osinski and Cockell 2007, Chapter 3, Chapter 4), it is possible that interactions of these rocks with hydrothermal fluids may provide an excellent habitat to organisms suspended in the water column by providing a nutrient source as well as a physical substrate with increased surface area for colonization. Currently, no work has been done investigating the interactions of impact-metamorphosed lithologies with hydrothermal fluids and the effect this may have on associated biology. As no post-impact hydrothermal system currently exists on Earth, it is difficult to assess the potential reactions and level of habitability of such an environment. In this paper we investigate the interaction of impact-processed gneisses from the Haughton impact structure, Canada, in hydrothermal systems generated in a laboratory setting as well as naturally occurring systems in Iceland.

5.2 Methods

Samples of shocked gneiss were collected from the 39 Ma Haughton impact structure, located in the northwest of Devon Island, Nunavut, Canada in the high Arctic archipelago at 75°08'N, 87°51'W. These rocks were excavated from 1.8 km down and can now be found as a component of the impact melt breccia hills within this 16 km diameter crater. Subsets of these samples (see below) were subjected to a hydrothermal regime both in the field and within the laboratory. In the case of the field experiments, shocked gneisses, which had been characterized petrographically to into 8 shock levels (see Chapter 2), were suspended in two different springs for one week during the field seasons of 2011 and 2012, which represented a generic post-impact hydrothermal regime. In the laboratory, samples of shocked gneiss were placed into a simulated impact-generated hydrothermal system using geochemical parameters equivalent to those estimated for the Haughton impact structure, in an experiment lasting six weeks.

5.2.1 Field Experimental Method

Duplicate samples of shocked gneiss were selected for each shock level, either cut or fractured to $\sim 1\text{cm}^3$ in size, wrapped in foil packages and baked in an oven at 450°C for 24 hours to remove any organics (Sutherland 1998). Fifty millilitre falcon tubes were used as specimen holders for immersion within the hydrothermal springs and holes were drilled near the top and bottom of the tube to allow flow through of the water without loss

of the sample, wrapped in foil and autoclaved. Field sites (see below) were chosen both based on chemical qualities as well as ease of access as many springs were located in areas where approach was not safe. Samples were then suspended in the springs and collected after one week, placed in sterile whirlpack bags and stored at -20°C for analysis. Samples of mud from the stream bed and water column were also collected for DNA analysis, and sequenced using *454* pyrosequencing at Research and Testing Laboratories, Lubbock, TX. Finally geochemical data were collected at both sites using a Spectroquant Multi Calorimeter, Merck to detect sulfides, ammonium, nitrates, nitrites and ferric iron, and samples were collected for anion and cation analyses (Table 5-1). Samples were imaged using scanning electron microscopy (SEM) via secondary imaging (SE2) and back-scattered emission (BSE). For samples viewed under SEM-BSE, rocks were fixed with glutaraldehyde for 24 hours, stained with 1% OsO_4 in 0.1M Na-cacodylate buffer for 1 hour, and then embedded in Epon which was hardened at 60°C for 48 hours. SE2 samples were fixed with glutaraldehyde, ethanol dehydrated and then critical point dried. BSE samples were coated with a thick coating (10 nm) of carbon, whereas SE2 samples were coated 2X with 5 nm thicknesses of osmium.

5.2.2 *Krýsuvík (Seltún)*

Located in the Reykjanes peninsula in south-western Iceland ($63^{\circ}53.727\text{N}$, $22^{\circ}3.40\text{W}$), Krýsuvík is a region consisting of several geothermal fields, the most famous of which is Seltún. This area is typified by extensive hydrothermal pools and streams, and contains several maars (craters formed by the explosion of overheated groundwater) (Figure 5-1a). The temperature at the surface where water is fluid is close to 100°C , but reaches upwards of 300°C immediately beneath the surface, grading to a vapour regime (Sæmundsson and Karson 2006). The area between the pools is interconnected by extensive near-surface tunnels carrying superheated water and gasses, thus undermining the stability of the ground. The stream that was chosen for the experiment was approximately 20 m downstream from the outflow and had a temperature of 40°C and a pH of 2.2. This stream was chosen due to the depth of the pool, the ease of access, and that it was not close to any of the tourist paths, so would be less likely disturbed (Figure 5-1b). In this location, no visible biology within the stream was noted, though the banks of the stream were

Table 5-1. ICP/IC data collected from Seltún and Geysir.

Water Geochemistry (mg/L)															
Site	#	S₂ mg/L	Fe²⁺ Abs	NH₄ mg/L	NO₂ ug/L	NO₃ 0.13	SO₄	PO₄	Ca	Fe	K	Mg	Mn	Na	S
Seltún	1	nd	—	53	9	15.1	1400	3.05	112	127	2.53	65.5	2.74	32.0	645
	2	nd	—	41	7	16.4	1440	3.05	114	129	3.05	64.5	2.75	31.0	646
	3	nd	1170	60	8	—	—	—	—	—	—	—	—	—	—
	Avg	—	—	51.3	8	15.8	1420	3.05	113	128	2.79	65.0	2.75	31.5	646
	<i>S.D.</i>	—	—	<i>10.06</i>	<i>1</i>	<i>0.9</i>	<i>28</i>	<i>0</i>	<i>0.9</i>	<i>1.2</i>	<i>0.4</i>	<i>0.70</i>	<i>0.01</i>	<i>0.7</i>	<i>0.7</i>
Geysir	1	1.06	—	—	—	4.79	90.4	0.03	0.58	—	9.55	—	—	239	30.9
	2	1.24	—	—	—	5.28	87.3	0.06	0.58	—	9.31	—	—	248	29.5
	3	1.52	—	—	—	4.76	83.4	—	0.58	—	8.69	—	—	238	32.4
	Avg	1.27	—	—	—	4.94	87.0	0.04	0.58	—	9.19	—	—	242	30.9
	<i>S.D.</i>	<i>0.23</i>	—	—	—	<i>0.3</i>	<i>3.5</i>	<i>0.02</i>	<i>0</i>	—	<i>0.4</i>	—	—	<i>5.8</i>	<i>1.45</i>

Physical Properties				
	pH	T °C	O₂ mg/L	Ω μS/cm
Seltún	2.2	50.5	4.22	447
Geysir	8.14	95	5.23	1788

surrounded in thick algal mats. Upstream, near the source were black filamentous streamers indicating a strong presence of iron sulfides (Figure 5-1c). Identification of any mineral deposits within the shocked gneisses was conducted using electron dispersive spectroscopy (EDS) and/or micro-X-ray Diffraction (μ -XRD).

5.2.3 *Geysir*

Geysir is also located in the Reykjanes geothermal platform at (64°18.65N, 20°18.217W). Our field site was located above the main site due to the privacy of the location away from tourists, the depth of the pool, and the differing geochemical conditions (Figure 5-2a). The spring used was 99°C at the source, and 95°C at the location of suspension of the samples, with a pH of 8.1. As with Seltún, samples were placed in falcon tubes and suspended in the stream for a week (Figure 5-2b,c). Geochemical data was collected as stated above, as a soil sample for DNA analysis and identification of any mineral deposits within the shocked gneisses was conducted using EDS and/or μ -XRD.

5.2.4 *Simulated Haughton Hydrothermal System*

In the lab, two sets of samples of shocked gneiss were placed in a hydrothermal environment (one biotic, one abiotic – 6 vials each) at 65°C using extrapolated water geochemistry simulating the late-stage hydrothermal system at the Haughton impact structure. For the biotic experiment we used an anaerobic thermophilic sulfate-reducing bacterium (SRB): *Thermodesulfobacterium commune* (DMZ 2188), which has an optimal growth temperature (OGT) of 70°C, grown on media recipe ATCC 1249 (Modified Barr's), in order to investigate controlled colonization of different shock levels with different surface areas; this is due to the findings of biologically fractionated sulfur within the hydrothermal sulfide deposits at Haughton (Parnell et al. 2010). The “media” used to simulate the Haughton impact-generated hydrothermal system was extrapolated from current water geochemistry for waters in the Haughton region today (Lim and Douglas 2003). Given that the water chemistry is thought to not have changed measurably since the late-stage (Osinski et al. 2005), we were able to calculate the proposed chemistry at 70°C using solubility/temperature curves for the main constituents: CaSO_4 and $\text{Ca}(\text{Mg})\text{CO}_3$. The average increase in concentration was then applied to all other ions in

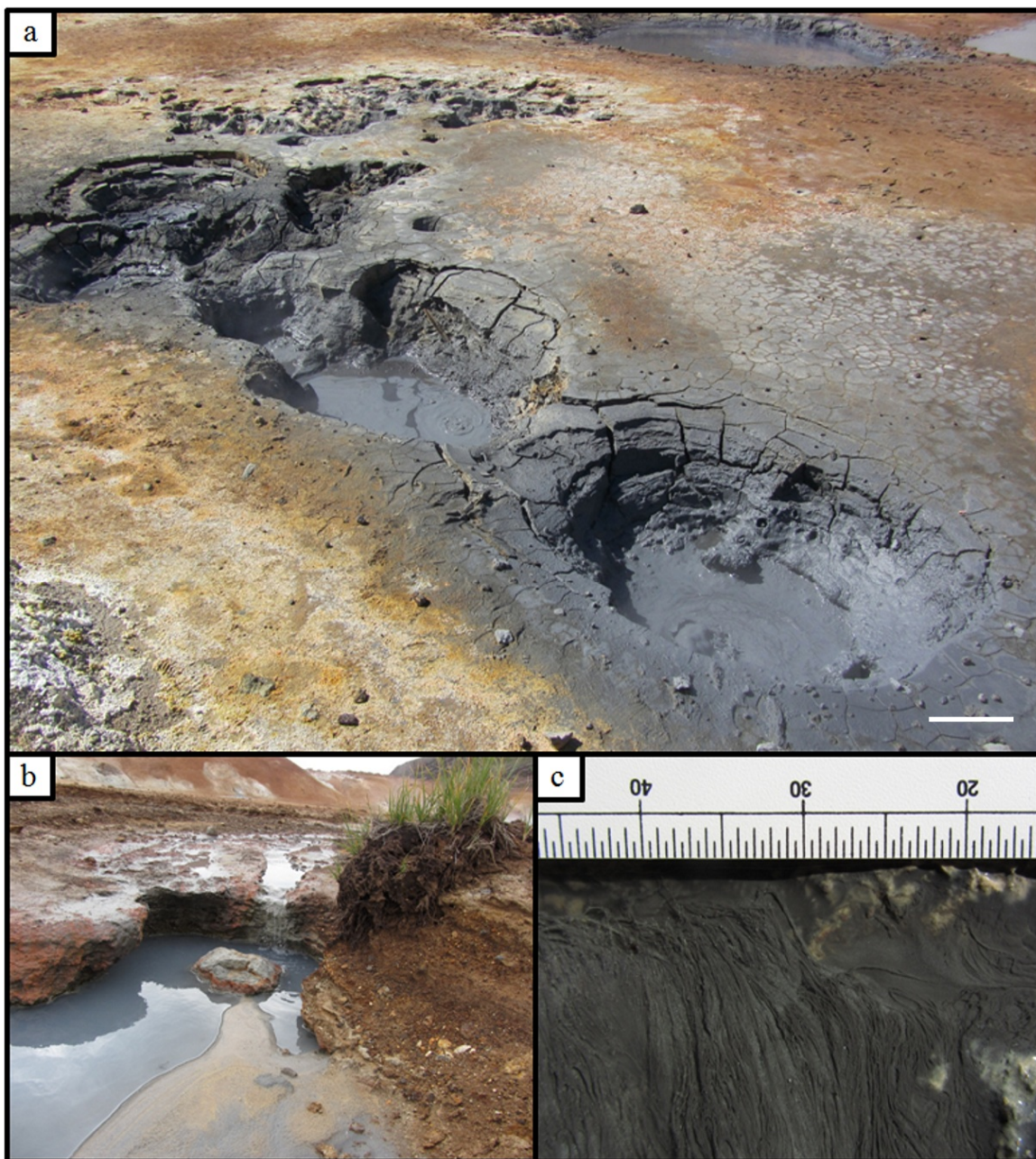


Figure 5-1. (a) Mudpots at Seltun, with a maar in the background, scale is 30 cm. (b) Hydrothermal pool used for experiment 50 m downstream from source. (c) Black filamentous streamers upstream of experiment, scale bar is in centimetres.

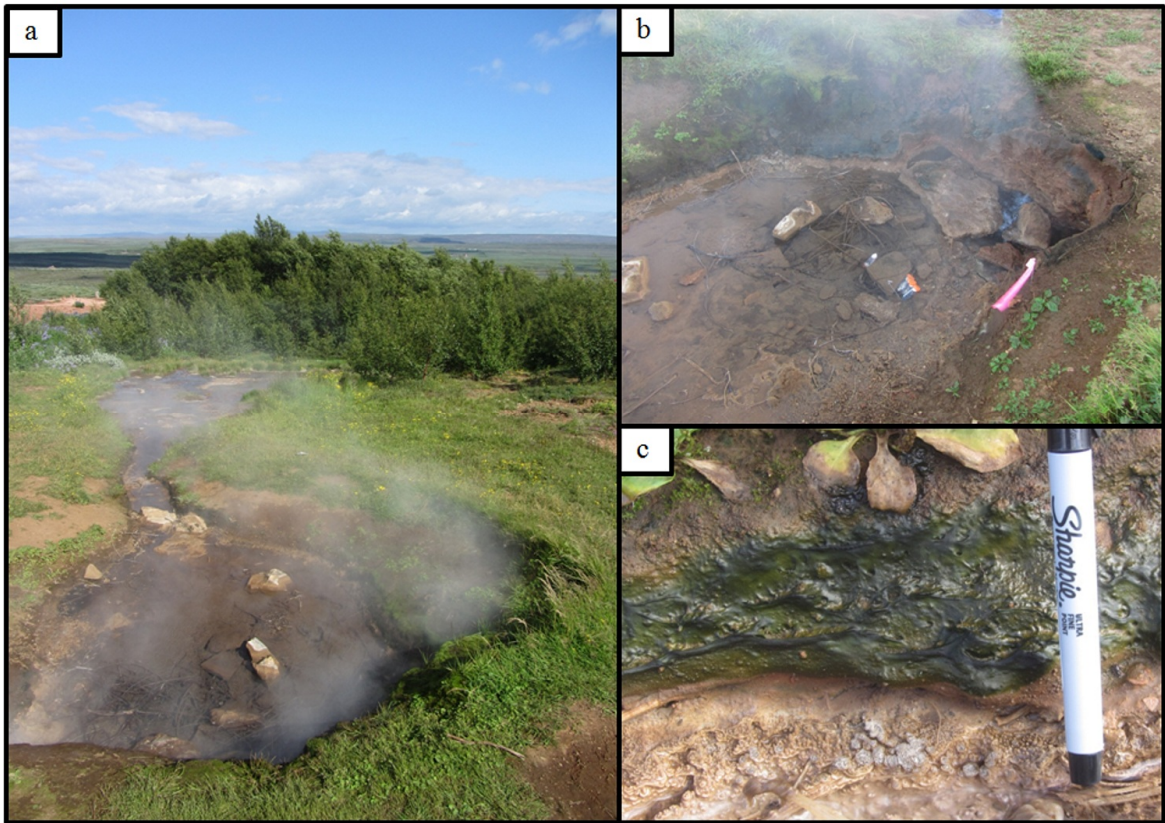


Figure 5-2. (a) Hydrothermal pool above Geysir showing outflow down the hill. Source is in foreground. (b) Experiment setup in pool, temperature is 94°C. (c) Pool had no visible growth within, however there were plants and thick algal mats lining the surroundings that were constantly bathed in steam.

solution. Sodium lactate and yeast extract from the ATCC medium were also include at 1/10 the normal concentration so as to provide a carbon and nutrient source for the SRBs. The final media concentrations were: 0.002 mg/L ZnSO₄; 0.004 mg/L CuCl₂; 2.45 mg/L Na₂CO₃; 0.018 g/L MgCl; 0.0262g/L CaSO₄; 0.1g/L NH₄Cl; 0.05 g/L KH₂PO₄; 0.01 g/L FeSO₄•7H₂O; 0.35 g/L Na Lactate; 0.1 g/L Yeast extract. One milligram per litre of Resazurin was used as a redox indicator. The pH was adjusted to 6 using NaOH as the acidity of the water during the late-stage system was circumneutral to slightly acidic (Osinski et al. 2001), filter sterilized and then stored at 65°C. After establishing SRB cultures on the ATCC medium, the bacteria were then established on the minimal Haughton medium until reaching a cell count of ~10⁸ per mL.

Samples for three shock groups – unshocked, moderate shock (3 and 4) and highly shocked (7) – were selected and crushed to represent two different clast sizes, pebble (coarse) or sand (fine) and then baked at 450°C to remove any organics. These samples were then placed into 22 mL serum vials (6 biotic vials and 6 abiotic vials sampled weekly, and 4 biotic vials, 2 coarse and 2 fine, sampled at 4 weeks and 8 weeks, respectively). Abiotic vials were filled with 18 mL of the Haughton media and sealed. Vials were then made anaerobic using RAS (0.75 g/100 mL of ascorbic acid: 0.75 g/100 mL of Na-thioglycollate) at a pH of 6, with a concentration of 1.2 mL RAS; 12 mL of media. At this point, 0.45 µm filter-sterilized 5% ferric ammonium sulfate was added to the vials to a final concentration of 0.01 mL/5.0 mL of media. For the biotic samples, 1 mL of inoculum at ~10⁸ cells was pipetted directly onto the serum vials under a pure nitrogen atmosphere and the vials were sealed. After incubating for half an hour so as to encourage attachment to the substrate, reduced media was then added to a final volume of 20 mL and placed in the oven at 65°C. Each of the 12 serum vials (biotic and abiotic) were sampled weekly for geochemical analysis through inductively coupled plasma atomic emission spectroscopy (ICP-AES/IC, The Biotron, University of Western Ontario), and half the medium replaced with fresh in order to simulate recharging within the system and promote growth within the substrate rather than suspended growth in the column. At week 4, two of the long-term vials were sampled for ICP/IC analysis, and several vials cracked and resealed to sample the substrate for imaging under SEM-BSE

and SE2 (same procedures as above). ICP values from week 5 and 6 were done using ICP-MS.

5.3 Results

5.3.1 Field Experiments – Seltún

After one week of submersion within the spring, the inside of the tubes for all samples had turned green and was also filled with a yellow clay-like substance. SE2 imaging showed extensive deposition of an iron sulfate bearing mineral (Figure 5-3a) held together by lattices of EPS, a bacterium with extensive branching and narrow diameters which resembles actinomycetes (Figure 5-3b), and mineralization by gypsum (Figure 5-3c). SEM-BSE imaging showed no noticeable internal colonization, but did show potential external colonization by a short filamentous bacterium (Fig 5-3d – *Leptosprillum*). Unshocked samples did not show the same deposition and colonization, suggesting that porosity (resulting from shock metamorphism) plays a key role in habitability. As the rocks were completely covered it was difficult to assess whether leaching of the rock had occurred, though at a pH of 2 this is highly likely for the glass-bearing shocked samples, which would tend to release more nutrients into the microenvironment surrounding the rock. Sequencing from the spring sediments showed bacteria from 9 different classes, belonging to acidophilic thermophiles using iron or sulfur species as energy sources. The most dominant species were: *Hydrogenobaculum* sp., *Acidimicrobium ferrooxidans*, *Desulfurella acetivorans*, *Acidiphilium* sp., and *Acidothiobacillus caldus*. The last organism is generally considered to be a weed in bioleaching operations, being the dominant reducer of inorganic sulfur (Hallberg et al. 1996). In contrast, DNA extracted from the newly colonized shocked gneisses, though showing similarities with the spring sediment did not reveal any colonization from bacteria associated with thermophilic classes such as Aquificae or Thermatogae. No DNA belonging to the Archaea was found (Table 5-2).

5.3.2 Field Experiments – Geysir

Unlike with Seltún, the tubes after one week did not exhibit much of a colour change, though some had been in-filled with the same type of mud-like sediment from the bottom

of the pool. Upon inspection of the rocks, the high shock level samples were very friable and the mud had permeated much of the structure. SEM-BSE revealed extensive mineralization by calcite, lining almost all vesicles within the shock level 7 rock (Figure 5-3e), showing that flow through of the rock by the hydrothermal system was achieved. However, only minor colonization of the substrate occurred (Figure 5-3f). The bacterial 16S rDNA sequenced from Geysir spring sediments held a surprisingly large number of classes though was very uneven and had a low Simpson diversity Index (Table 5-2), which is indicative of a high-temperature system. The sequences were mainly dominated by *Clostridium spp.* and *Fervidobacterium spp.*, the latter of which is a sulfur reducer. Though we are unsure as to the species for *Clostridium*, a common organism in Icelandic springs is *Clostridium thermocellum* isolated by Stainthorpe and Williams (1988). These bacteria are obligate anaerobes, normally rod shaped and have an OGT of 80°C. Sequenced DNA from the shocked gniesses showed that similar bacterial classes were colonizing the rocks in comparison to the sediments; however the population was much more even and had a higher Simpson Index. There was a large contribution from the Bacilli within the sample analysed, consisting of sequences most closely related to *Bacilli sp.* All Archaeal sequences belonged to the class Thermoprotei, with 85% of the counts consisting primarily of sequences most closely related to *Sulfophobococcus zilligii*, a strict anaerobe 3-5 µm in diameter that was originally isolated from an alkaline hot spring in Iceland (Hensel et al., 1997). The remaining 15% of counts consisted primarily of sequences belonging to the *Pyrobaculum*, specifically *Pyrobaculum sp.* and *Pyrobaculum islandicum*, the latter of which is a rod shaped bacterium with an OGT of 100°C and strictly uses sulfur as an electron acceptor (Huber et al., 1987). Similar to the samples Seltún, no colonization from either the Aquificae or Thermatogae occurred.

5.3.3 Simulated Haughton Hydrothermal System

Significant growth was detected within the first week of sampling, which was more obvious within the coarse substrate vials, having visible suspended bacteria versus the fine substrates which had a layer of FeS on or just below the surface of the substrate. pH measurements were collected for all vials, and was found to increase with increasing shock in the abiotic vials (Figure 5-4b). The highest pH modification occurred within

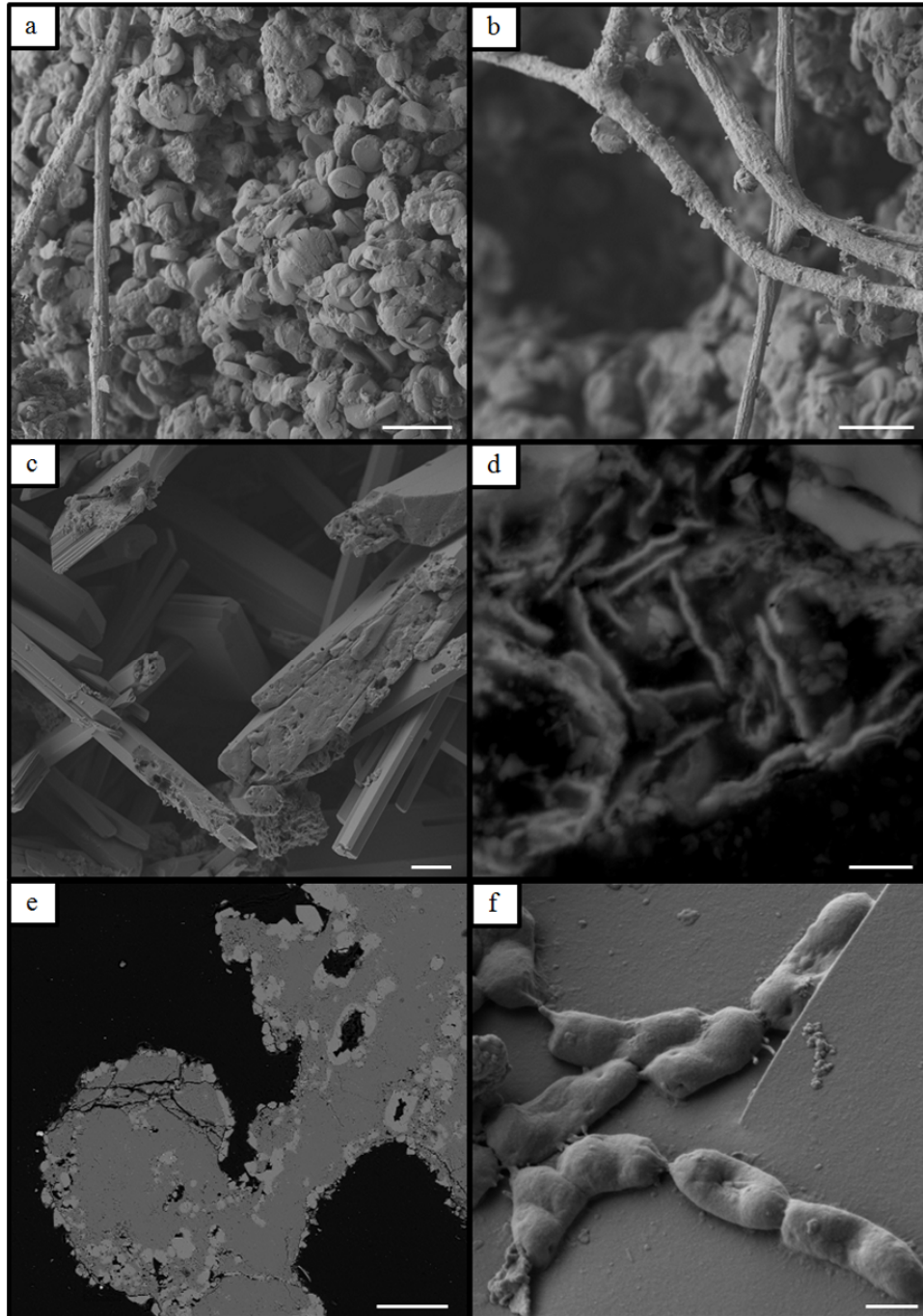


Figure 5-3. (a) SE2 micrograph showing iron sulphate deposits (likely jarosite) on shocked gneisses placed in Seltún, scale bar is 2 μm . (b) SE2 micrograph of branching within a filamentous algae or fungal like bacterium from Seltún, scale bar is 2 μm (c) Mineralization of gypsum, scale bar is 4 μm (d) SEM-BSE micrograph showing filamentous bacterium, possibly *Leptosprillum* from pool above Geysir, scale is 2 μm (e) SEM-BSE micrograph of calcite mineralization within rock from Geysir, scale at 100 μm . (f) SE2 micrograph of epilithic colonization by unknown bacterium from pool above Geysir, scale bar is 400 nm.

Table 5-2. 16S rDNA analysis of sediment samples and a high shocked colonized gneiss Seltun and Geysir using 454 pyrosequencing. Alpha diversity indices have been calculated for Bacteria only.

	Sediment		Shocked Gneiss	
	Seltún	Geysir	Seltún	Geysir
	Alpha Diversity Indices*		Alpha Diversity Indices*	
Shannon's Index	1.64	0.98	1.28	1.44
Simpson Diversity Index	0.79	0.54	0.52	0.71
Pielou's Evenness	0.75	0.35	0.53	0.62
	Bacteria		Bacteria	
Aquificae (class)	413	16	0	0
Actinobacteria (class)	132	0	96	289
Clostridia	8	1029	419	0
Deltaproteobacteria	459	0	82	0
Alphaproteobacteria	509	4	328	713
Sphingobacteria	0	7	0	20
Bacilli	19	12	0	1138
Gammaproteobacteria	471	1	83	0
Dictyoglomia	0	34	0	0
Thermotogae (class)	0	658	0	0
Anaerolineae	0	2	0	0
Cyanobacteria (class)	8	0	0	0
Betaproteobacteria	0	1	40	78
Ignavibacteria	0	3	0	0
Cytophagia	0	3	0	30
Nitrospira (class)	10	2	2	0
Deinococci	0	16	0	0
Thermodesulfobacteria (class)	0	4	0	0
Thermolithobacteria	0	2	0	0
	Archaea		Archaea	
Thermoprotei	N/A	N/A	0	3588

biotic vials and remained the most constant (when viewing the shock level 7 vials) (Figure 5-4a). ICP-AES/IC data show that significant leaching of Mg from the substrate occurred for the biotic vials ($\sim 30 \mu\text{g/L}$, where media contribution was measured to be $\sim 3 \mu\text{g/L}$) within the first week, which then declined gradually each week, a trend that was more pronounced within the fine substrate biotic vials (Figure 5-4e). Abiotic vials showed leaching at the higher shock levels of approximately $15 \mu\text{g/L}$ in the first week, lowering to below $10 \mu\text{g/L}$ in subsequent weeks (Figure 5-4f). Soluble potassium was between $\sim 60 \mu\text{g/L}$ and $\sim 110 \mu\text{g/L}$ for the biotic vials, and between $\sim 40 \mu\text{g/L}$ and $\sim 80 \mu\text{g/L}$ in the abiotic, compared to the media contribution of $\sim 20 \mu\text{g/L}$ (Figure 5-4c,d).

At both the moderate and high shock levels, extensive FeS deposition was observed. Macroscopically, the highly shocked coarse samples were completely black, and within 4 weeks, very little suspended bacteria were present. In contrast, the moderate shock level rocks were almost entirely coated in FeS, but the vials also supported a large amount of suspended growth. Under the SEM, however, it was difficult to distinguish the moderate samples from the high shock samples, as both were coated in significant amounts of FeS held together by extracellular polysaccharide (EPS), with SRBs throughout (Figure 5-5a,b). In addition to the extensive FeS deposition, the moderate shock coarse samples showed the formation of two carbonate minerals with the same chemical compositions, but different crystal habits (Figure 5-5c,d). Within the high shock sample however, we were able to observe infilling of pore spaces and, in some cases, leaching around the vesicle was observed when it was associated with large FeS-EPS deposits (Figure 5-5e,f). Unshocked samples had very little surface growth, which was restricted to areas of the rock that were relatively rough. Within the fine substrate vials, banding of FeS was visible, and only within the high shocked vials did we see significant suspended growth as well as coating of the inside of the vial.

5.4 Discussion

The dominant heat source for the hydrothermal system at the Haughton impact structure came from the impact melt rocks, which at over 300 m thick, led to the persistence of a hydrothermal system for upwards of 10,000 years (Osinski et al. 2001, 2005). The hydrothermal deposits within the crater are located in very specific geologic settings;

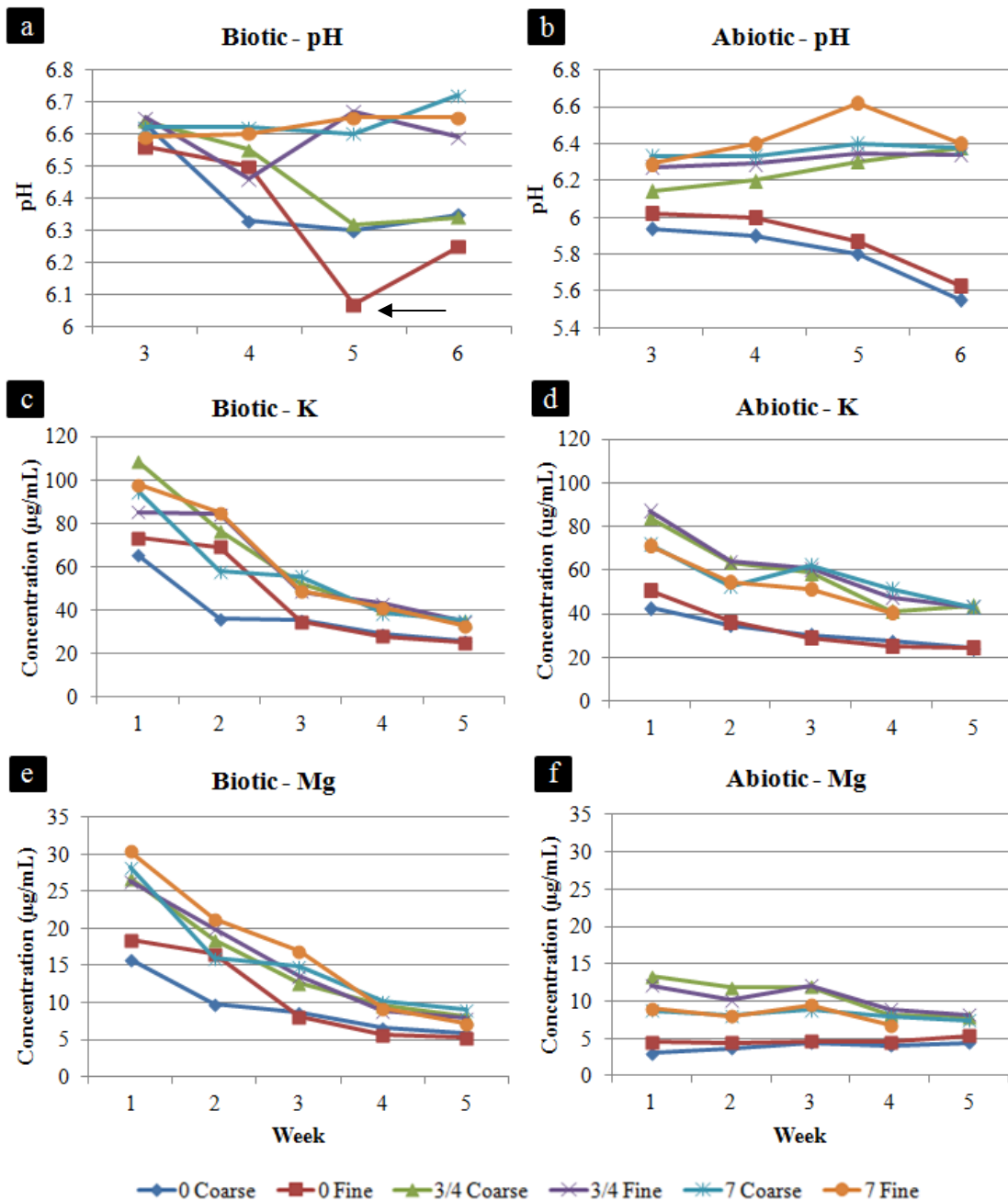


Figure 5-4. (a,b) pH measurements for weeks 3 through 6 of the experiment. The drop in pH (arrow) in the shock level 0 (fine vial) is the result of the vial being cracked in the previous week and slow recovery of the organisms in response to oxygen exposure. (c,d) ICP data for potassium (biotic and abiotic vials). (e,f) ICP data for magnesium (biotic and abiotic vials). Note that the abiotic vials have lower concentrations for both magnesium and potassium than the biotic.

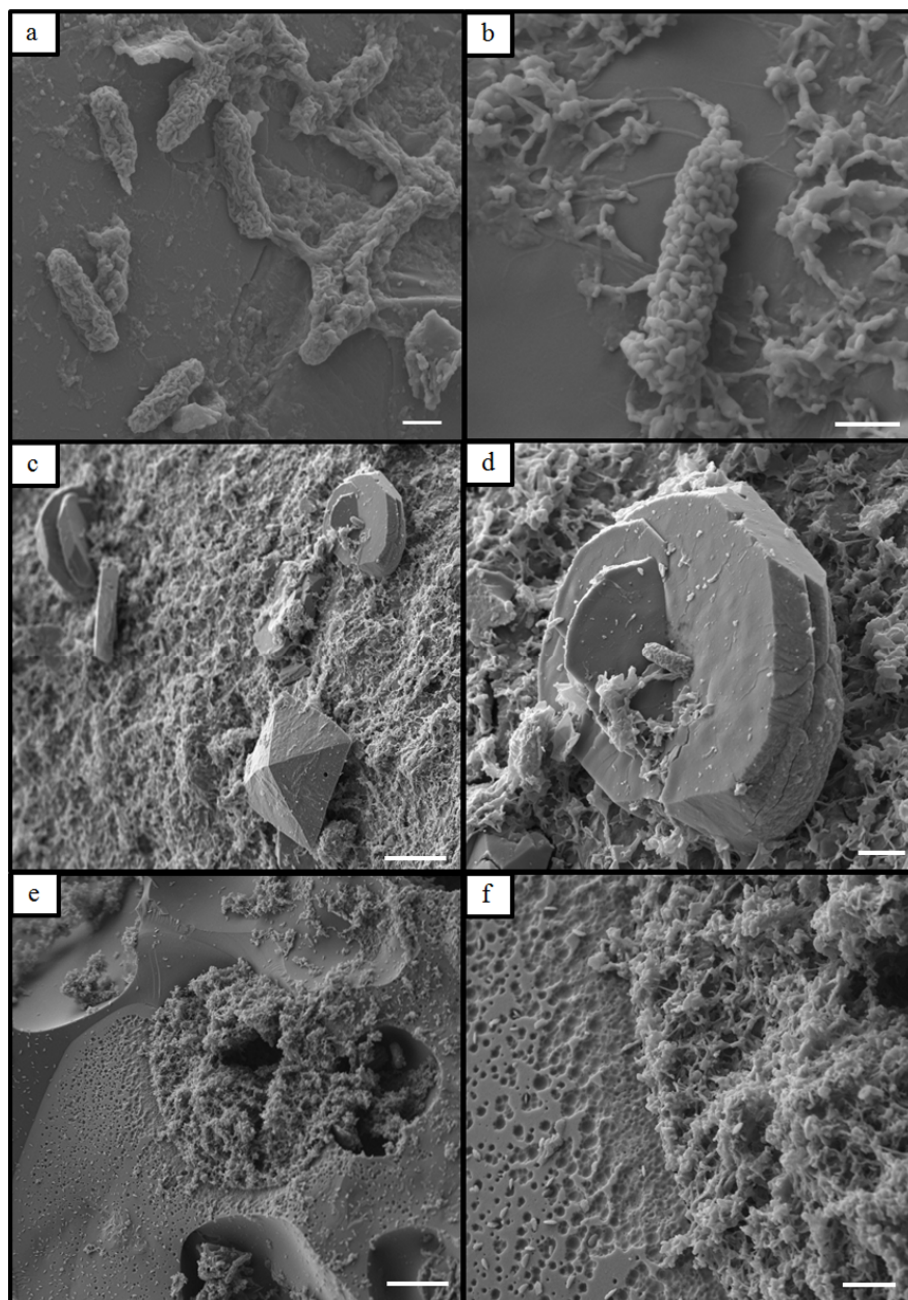


Figure 5-5. (a) SE2 micrograph of sulfate reducing bacteria on an unshocked coarse rock sample from the Haughton experiment. Fine coating on rock is EPS and FeS; scale is 500 μm . (b) SE2 micrograph of SRB on a high shock level sample; scale is 400 nm. (c) SE2 micrographs of two carbonate minerals on a bed of FeS on moderate shock coarse samples. EDS spectra indicate primarily Ca and O phases, mineral unknown; scale is 4 μm (d) Close up of (c) showing rounded hexagonal Ca mineral with SRB attached (centre); scale is 2 μm (e) Infilling of vesicles in a high shock sample with FeS; scale is 4 μm (f) Close up of (e) showing leaching of the substrate from generated H_2S within the FeS/EPS mass. Leaching revealed as a process of ethanol dehydration and critical point drying; scale is 1 μm .

found either as cavity and fracture fillings within the impact melt rocks, mineralization within the central uplift as well as fillings around the outer margin, and as hydrothermal pipe structures along faults in the crater rim region (Osinski et al. 2005). The interaction of these hydrothermal fluids with the target resulted in alteration phases such as gypsum, selenite, marcasite, pyrite and goethite (Osinski et al. 2005), while in other craters with more silicate-rich targets, phyllosilicates and clays are the dominant form (Allen et al. 1982; Naumov 2002).

In these experiments we examined how organisms would respond to a shocked crystalline rock – in this case gneiss – within a hydrothermal environment. Within the natural environments (Seltún and Geysir), which were quite different from each other in terms of pH and temperature, the same principles held true: shocked rocks provided the best substrate for colonization, with no significant difference in the level of colonization observed between the moderate shock levels (i.e., 3 and 4) and the higher shocked samples (5–7). Within the controlled lab experiments, the effects of shock metamorphism and substrate size on the growth of the sulfate reducing bacterium were more readily apparent. Though vials were initially all turbid with suspended growth, the moderate and highly shocked coarse samples rapidly became less turbid, with the latter eventually turning completely black and appearing to possess biofilms, with little to no visible suspended growth of the SRB. This would suggest that epilithic/endolithic growth was selective. SEM imaging shows infilling of all pore spaces with FeS and bacteria in an EPS lattice. Weathering of the rock around these areas was also observed, which was likely due to the production of acid as a by-product of FeS generation in these vesicular in-fills. Within the sand-sized biotic vials, growth of SRB's within the substrate was observed as coherent banding just beneath the surface. These bands became progressively thicker with time and did act to weakly cement the particles together, though not strongly enough to overcome surface tension when removed from the liquid medium. In the highly shocked sand vial, growth was so extensive that not only was the substrate almost completely black with iron sulfide, but significant suspended growth also began to occur, increasing in abundance each week.

Exposure of the shocked gneisses to the simulated hydrothermal system did produce weathering of the substrate, which was most evident within the first week. For example,

initial Haughton media levels included 20 $\mu\text{g/mL}$ of potassium, however, potassium levels in all vials (biotic and abiotic) showed higher dissolved values, with the highest levels seen in the moderate shocked vials (coarse and fine), and the highly shocked sand vials. Biotic vials showed 30% more K in solution than the abiotic vials, a pattern that was seen for Mg and Ca as well, which is likely due to increased production of HS^- in the biotic vials resulting in localized production of acids, leading to dissolution of the rocks. The fact that the moderately shocked vials showed consistently high levels of dissolved cations is likely due to the fact that many of the major oxides have been shown to decrease in concentration within these rocks with increasing shock (Chapter 2). As such, the highly shocked samples, though largely glass bearing and thus more easily dissolved have relatively less available nutrients than the moderately shocked rocks. Levels are still high, however, and are highest in the highly shocked sand vials due to increased surface area. In the unshocked samples, ICP revealed some leaching, but very little surface growth was observed, which is consistent with macroscopic observations as well as previous work on biomass levels in unshocked gneisses (Chapter 3). In the moderate shock level biotic coarse jars only, primary mineralization of two unidentified Ca-bearing phases occurred (see Figure 5-4). These minerals do not conform to any recognized calcium carbonate mineral, however, the precipitation of calcium carbonate in alkaline-SRB systems is expected and has been previously demonstrated (Castanier et al. 1999). The precipitation of calcite bearing phases in conjunction with iron sulfides does trend with the observations from the Haughton crater hydrothermal deposits, which reveal both layering and intermixing of these two mineral types (Osinski et al. 2005), though we are uncertain as to why this mineralization developed in only the moderate shock level rocks, where calcium levels were equally high in the high shocked vials.

5.5 Concluding Remarks

In summary, shocked gneisses are indeed capable of not only providing a suitable endolithic environment, but are a viable habitat in hydrothermal systems, where high porosity allows for good flow-through of fluids, thus allowing for significant colonization by suspended organisms. The extensive calcium deposits and infilling of pore spaces by iron sulfides suggests that pore spaces may eventually become closed off and any

associated biology entombed within the sample. This may have positive implications for past-life detection within rocks. Extensive cratering on Mars has led to a globally distributed layer of impactites and impact-associated hydrothermal deposits (Michalski et al. 2013). If life did exist within these hydrothermal systems, it is possible that entombment of these organisms could have occurred within shocked lithologies, such as basalts. Coupled with potential later endolithic colonization after the hydrothermal phase of the crater, shocked crystalline rocks prove to be an excellent target for life detection. Further work should be completed to investigate the habitability of shocked basalts in circumneutral hydrothermal systems, where a potentially more nutrient rich shocked rock could provide a suitable microenvironment for life.

5.6 References

- Abramov, O., and Kring, D. A. 2005. Impact-induced hydrothermal activity on early Mars. *Journal of Geophysical Research* **110**:1–19.
- Allen, C. C., Gooding, J. L. and Keil, K. 1982. Hydrothermally altered impact melt rock and breccia - contributions to the soil of Mars. *Journal of Geophysical Research* **87**(NB12): 83–101.
- Ames, D. E., Watkinson, D. H. and Parish, R.R. 1998. Dating of a regional hydrothermal system induced by the 1850 Ma Sudbury impact event. *Geology* **26**: 47–450.
- Castanier, S., Le Métayer-Levrel, G., and Perthuisot, J.P. 1999. Ca-carbonates precipitation and limestone genesis – the microbiogeologist point of view. *Sedimentary Geology* **126**:9–23.
- Cockell, C. S., and Lee, P., 2002. The biology of impact craters - a review. *Biological Reviews* **77**:279–310.
- Cockell, C. S., McKay, C. P., and Omelon, C. R., 2003. Polar endoliths - an anti-correlation of climatic extremes and microbial diversity. *International Journal of Astrobiology* **1**:305–310.
- Cockell, C. S. and Osinski, G. R. 2007. Impact-induced impoverishment and transformation of a sandstone habitat for lithophytic microorganisms. *Meteoritics & Planetary Science* **42**:1985–1993.
- Ehlmann, B. L., Mustard, J. F., Murchie, S. L., Bibring, J. P., Meunier, A., Fraeman, A. A. and Langevin, Y. 2011. Subsurface water and clay mineral formation during the early history of Mars. *Nature* **479**: 53–60.

- Ehrenfreund, P., Röling, W. F. M., Thiel, C. S., et al. 2011. Astrobiology and habitability studies in preparation for future Mars missions: trends from investigating minerals, organics and biota. *International Journal of Astrobiology* **10**(3):239–253.
- Farmer, J. D. 2000. Hydrothermal systems: doorways to early biosphere evolution. *GSA Today* **10**:1–2.
- Gogarten-Boekels, M., Hilario, E. and Gogarten, J. P. 1995. The effects of heavy meteoritic bombardment on the early evolution – the emergence of the three domains of life. *Origins of Life and Evolution of the Biosphere* **25**: 251–264.
- Hallberg, K. B., Dopson, M. and Lindström, E. B. 1996. Reduced sulfur compound oxidation by *Thiobacillus caldus*. *Journal of Bacteriology* **178**(1): 6–11.
- Hensel, R., Matussek, K., Michalke, K., Tacke, L., Tindall, B. J., Kohlhoff, M., Siebers, B. and Dielenschneider, J. 1997. *Sulfophobococcus zilligii* gen. nov., spec. nov. a novel hyperthermophilic Archaeum isolated from hot alkaline springs of Iceland. *Systematic and Applied Microbiology* **20**: 102–110.
- Holm, N. G. 1992. Why are hydrothermal systems proposed as plausible environments for the origin of life? *Origins of life and evolution of the biosphere* **22**: 5–14.
- Huber, R., Kristjansson, J. K. and Stetter, K. O. 1987. *Pyrobaculum* gen. nov., a new genus of neutrophilic, rod-shaped archaeobacteria from continental solfataras growing optimally at 100°C. *Archives of Microbiology* **49**(2): 95–101.
- Lazcano, A. and Miller, S. L. 1996. The Origin and Early Evolution of Life: Prebiotic Chemistry, the Pre-RNA World, and Time. *Cell* **85**(6): 793–798.
- Lim, D. S. S. and Douglas, M. S. V. 2003. Limnological characteristics of 22 lakes and ponds in the Houghton crater region of Devon Island, Nunavut, Canadian High Arctic. *Arctic, Antarctic and Alpine Research* **35**(4):509–519.
- Maher, K. A. and Stevenson, D. J. 1988. Impact frustration of the origin of life. *Nature* **331**: 612–614.
- Marzo, G. A., Davila, A. F., Tornabene, L. L., Dohm, J. M., Fairen, A. G., Gross, C. Kneissl, T., Bishop, J. L., Roush, T. L. and McKay, C. P. 2010. Evidence for Hesperian impact-induced hydrothermalism on Mars. *Icarus* **208**:667–683.
- Michalski, J. R. and Niles, P. B. 2010. Deep crustal carbonate rocks exposed by meteor impact on Mars. *Nature Geoscience* **3**:751–755.
- Michalski, J. R., Cuadros, J., Niles, P. B., Parnell, J., Rogers, A. D. and Wright, S. P. 2013. Groundwater activity on Mars and implications for a deep biosphere. *Nature Geoscience*. *Advanced online publication*.

- Miller, S. L. and Lazcano, A. 1995. The Origin of Life – Did it Occur at High Temperatures? *Journal of Molecular Evolution* **41**:689–692.
- Mojzsis, S. J., Arrhenius, G., McKeegan, K. D., Harrison, T. M., Nutman, A. P. and Friend, C. R. L. 1996. Evidence for life on Earth before 3,800 million years ago. *Nature* **384**:55–59.
- Mustard, J. F., Murchie, S. L., Pelkey, S. M. et al. 2008. Hydrated silicate minerals on Mars observed by the Mars Reconnaissance Orbiter CRISM instrument. *Nature* **454**:305–309.
- Naumov, M. V. 2002. Impact-generated hydrothermal systems: Data from Popigai, Kara, and Puchezh-Katunki impact structures. In J. Plado & L. J. Pesonen (Eds.), *Impacts in Precambrian shields*. Berlin: Springer-Verlag. pp. 117–171.
- Naumov, M. V. 2005. Principal features of impact-generated hydrothermal circulation systems: mineralogical and geochemical evidence. *Geofluids*, **5**:165–184.
- Nesse, W. 2000. *Introduction to Mineralogy*, 1st Ed. Oxford University Press, New York. p. 206.
- Osinski, G. R., Lee, P., Parnell, J., Spray, J. G. and Baron, M. 2005. A case study of impact-induced hydrothermal activity: the Houghton impact structure, Devon Island, Canadian High Arctic. *Meteoritics & Planetary Science* **40**:1859–1877.
- Osinski, G. R., Tornabene L. L., Banerjee, N. R., Cockell, C. S., Flemming, R., Izawa, M. R. M., McCutcheon, J., Parnell, J., Pickersgill, A. E., Pontefract, A., Preston, L., Sapers, H. M. and Southam, G. 2013. Impact-generated hydrothermal systems on Earth and Mars. *Icarus* **224**:347–363.
- Osinski, G. R., Spray, J. G., and Lee, P. 2001. Impact-induced hydrothermal activity within the Houghton impact structure, arctic Canada: Generation of a transient, warm, wet oasis. *Meteoritics & Planetary Science* **36**:731–745.
- Pace, N. R. 1991. Origin of life – facing up to the physical setting. *Cell* **65**(4):531–533.
- Parnell, J., Boyce, A., Thackrey, S., Muirhead, D., Lindgren, P., Mason, C., Taylor, C., Still, J., Bowden, S., Osinski, G. R. and Lee, P. 2010. Sulfur isotope signatures for rapid colonization of an impact crater by thermophilic microbes. *Geology* **38**:271–274.
- Sæmundsson, K. and Karson, J. A. 2006. Stratigraphy and tectonics of the Húsavík – Western Tjörnes Area. *ÍSOR-2006/032*.
- Schopf, J. W. and Packer, B. M. 1987. Early Archean (3.3-billion to 3.5-billion-year-old) microfossils from Warrawoona Group, Australia. *Science* **237**:70–73.

Stainthorpe, A. C. and Williams, R. A. D. 1988. Isolation and properties of *Clostridium thermocellum* from Icelandic hot springs. *International Journal of Systematic Bacteriology* **38**(1):119–121.

Sutherland, R. A. 1998. Loss-on-ignition estimates of organic matter and relationships to organic carbon in fluvial bed sediments. *Hydrobiologia* **389**:153–167.

Chapter 6 : Discussion

6.1 Meteorite Impacts and Endolithy

Impact cratering is one of the most important geological processes in the Solar System that has profoundly affected the evolution of life on Earth and, perhaps, its origins. This work has focused on understanding the beneficial microbial effects of impact events through the study of a unique meteorite impact site – the 23 km diameter Haughton impact structure – in the Canadian High Arctic. The Haughton impact event released a shock wave which resulted in a large portion of the target rocks being heated to temperatures in excess of 2000°C (Osinski et al., 2005), cooling down gradually over time to allow the formation of a hydrothermal system, a post-impact lake, and finally dissipating entirely to leave behind the impact melt rock hills situated within barren arctic tundra that are observed today (Cockell and Lee 2002). The colonization of lithic environments has long been documented; however, these environments typically occur within rocks that have an inherent level of porosity and translucency (e.g., sandstones and evaporites), which makes them ideal for colonization. Crystalline rocks such as granites, for example, are rarely colonized, or if so are limited to the epilithic or hypolithic environment with the potential for colonization of macrofractures (Omelson 2008; Kahn et al., 2011). As such, the endolithic habitat generated within impacted gneisses is a novel occurrence, creating habitat where none existed previously. However, due to the impact cratering process, one must hypothesize that physical and chemical changes might affect how colonization occurs and by which organisms. In addition to this, it must be recognized that different substrates respond very differently to shock and thus provide varying levels of habitability.

6.1.1 *Microbial Biomass as a Function of Shock Metamorphism*

This study has shown that the relationship between biomass and shock level within these samples is sinusoidal, being a function both of porosity and translucency of the substrate, fitting a 4th order polynomial distribution. In a previous study of shocked gneisses at Haughton by Singleton et al. (2011), it was shown that there was a very high level of

variability in porosity within each given shock level, likely resulting from compositional differences among the thirteen different gneissic types from the Precambrian shield on Devon Island. As such, porosity within a sample and its resulting biomass must be discussed in terms of means. Initial colonization of the substrate is purely epilithic, if it occurs at all, and microscopic observations reveal stratification, with dead cells comprising the outermost layer, conveying protection to the active photosynthetic layer. Biomass counts increase though, by an order of magnitude when one progresses to the rocks from a range of mid-shock level gneiss (~30–40 GPa). Still, however, microbial counts are quite low and more representative of a glacial ice community (Fierer et al., 2011). It is not until pressures of ~50 GPa are reached that we see another increase – by an order of magnitude – in the biomass levels associated with these rocks. At this stage, extensive endolithic colonization is sometimes observed. On the macroscopic level, coherent bands of photosynthetic growth millimetres beneath the surface are visible. From the in situ CSLM studies conducted (see Chapter 3), it was possible to visualize this subsurface environment and see that the microbial zone can extend upwards of a centimetre into the rock (Appendix B). Statistically, the high shock samples (levels 5 and 6) maintained a higher level of biomass than the other shock levels, higher even than the shock level 7 samples. Intuitively one would expect the shock level 7 rocks to possess the most biomass, especially based on the data which shows that porosity in these rocks continues to increase until the target is completely vaporized. Though porosity is important for the occurrence of these endolithic communities, another important factor controlling growth is the connectivity of these pore spaces, both with each other and with the surface (i.e., permeability). In this instance, the pressure that these rocks were exposed to resulted in complete melting and flow of the substrate and may have effectively inhibited connections between the pores, lowering the effective permeability for microbial colonization.

Using scanning electron microscopy back-scattered electron imaging SEM-BSE in conjunction with the CSLM (confocal scanning laser microscopy) transects, we were able to correlate areas of growth with substrate type in two dimensions to ascertain whether or not some substrates would provide increased nutrients to microbial colonies over other possible surfaces. In over 42 transects studied we found that there was no such preference

and that the microbial colonies within these gneisses are following both macro- and microfractures to the interior of the rock, eventually colonizing the interiors of vesicles. This correlates with the observation that there was a notable lack of infiltration of glasses in any of the petrographic, SEM or CSLM images. Much of the glass is Si-rich and these impact formed glasses likely do not provide much in the way of nutrients to the microbial colonies.

6.1.2 *Prevalence of Bioessential Elements in Shocked Lithologies*

Due to the immense energy of an impact event it is reasonable to surmise that there may be impoverishment of the substrate. The fact that most of the glasses within the impact shocked gneisses are SiO₂-rich likely results from intense volatilization and melting that occurred as a result of this impact affecting the more labile elements in the target substrates, i.e., oxides, resulting in brecciated samples that were composed primarily of Si and O. Mean values of the data for all samples (both sedimentary and crystalline) were calculated, but it was only when plotting the means of the major oxides for the crystalline samples that a decrease in concentration with shock level was observed. The lack of any decline within the sedimentary samples is unclear, but may be due to a combination of factors: 1) The lack of a fine-scale categorization of shock level available for sedimentary rocks; 2) The fact that recrystallization occurs at pressures exceeding 35 GPa, which may limit the amount of volatilization of biologically relevant elements experienced by the substrate. What did remain clear, however, was that there was a distinct reduction in available bioessential elements such as Mg, Fe and Mn beyond a mid-shock level range (see Chapter 4). That there is an increase in elemental concentrations from the unshocked to the mid-shock levels is presumably an artefact of sampling and results from the fact that no unshocked basement is accessible in the area immediately beneath or adjacent to the crater and can only be accessed 100 kilometres away in Sverdrup Inlet, which from our geochemical results are notably different in composition from the original target rock. A further disparity is in the singular presence of rocks belonging to the shock levels 1 and 2. Within the crater these rocks are present at very low abundance and a total of 4 samples for these levels have been collected in the last decade. As previously noted, the reasons for this are heretofore unknown and the deficiency has been noted in previous studies of

the crater (e.g., Metzler et al., 1988). Combining the observed colonization of the rock with bulk geochemical data it is clear that growth within these shocked gneisses and especially the “hot spots” of growth that are observed are governed by three main factors: 1) The trade-off between the depth of PAR (photosynthetically active radiation) for a given sample vs. the ability to act as a sufficient UV shield – the depth of which seems to occur 1 to 2 mm beneath the surface, 2) the connectivity of pore spaces within the rock, and 3) the connectivity of these spaces with macro- and microfractures to the surface, allowing the percolation of pore waters, dissolved nutrients and movement of microbiota.

6.1.3 *Community Composition*

The microorganisms of the endolithic environment of the crater are selected from a globally distributed pool of microbial ecotypes, where organisms adapted to a sub-lithic lifestyle are then able to propagate, forming the community that we see today. The use of a “shotgun” approach to sequencing has allowed us to view the bacterial population, not only for an Arctic endolithic community, but for a novel impact-generated habitat, for which there is only culture-dependent isolate data (Deslippe et al., 2012; Nemergut et al., 2005). Within the shocked gneiss microbial community the Actinobacteria are the most abundant contributor, followed by the Alpha- and Gamma-proteobacteria – all of which are large contributors to soil communities and trend with work done on Arctic soil ecosystems (Deslippe et al., 2012; Nemergut et al., 2005). What was surprising was the relative lack of presence of the cyanobacteria as seen in Antarctic endolithic communities. The primary phototroph is instead a member of the Chloroflexi: *Chloroflexus sp.*, a class that is virtually absent in Antarctic rocks. Cyanobacteria do not appear in great number until the higher shock levels are attained and even then are only present in low amounts (~ 6% of sequences), which was surprising given that shocked gneisses have a significantly higher porosity than other rock types such as sandstones which generally host large cyanobacterial communities. As a whole, the communities within the shocked gneisses are dominated by heterotrophic bacteria with the producers supplying only a small percentage of the total active community, suggesting that the organisms must also rely on an exogenous form of carbon input from the environment, likely along with other nutrients such as phosphorus and nitrogen.

Overall, an increase in microbial diversity with increasing shock pressure in the gneisses was observed, resulting in the formation of distinct communities based on the level of porosity that was created and translucency within the rock. Relative species abundances remained fairly similar between populations due to the fact that they were highly uneven – thus it was only with a univariate analysis that we were able to show a distinct difference in community composition between the unshocked and shocked populations. High variability within the samples made it impossible to discern significant differences between the two shocked populations, where some samples collected from opposite regions within the crater plotted together, while samples collected near each other along the same escarpment do not. This variability is possibly the result of factors such as specific wind patterns within the crater, drainage patterns along escarpments, sun exposure, the prevalence and positioning of macrofractures within the sample, as well as any potential mineralization from ground water interactions leading to reduced access to the interior of the rock.

6.1.4 *Shocked Lithologies in Hydrothermal Systems*

Significant amounts of water interaction with the impact brecciated lithologies of the crater have occurred throughout the history of the crater, beginning with the generation of the hydrothermal system, which likely lasted on the order of tens of thousands of years (Osinski et al., 2001, 2005). Within the Haughton impact structure, calcium- and sulfate-rich hydrothermal fluids resulted in the deposition of large amounts of alteration phases in the form of calcite and selenite, a transparent form of gypsum. Large inputs of soluble iron also resulted in the formation of various sulfides such as marcasite and pyrite, recent evidence of which points to a microbial origin for the sulfur within these deposits (Parnell et al., 2010). In other craters on Earth and on Mars, phyllosilicates appear to be the more dominant form (Allen et al., 1982; Naumov et al., 2005; Osinski et al., 2013). Focusing on the type of target involved in the impact event will allow one to understand what types of products may occur as a result of extensive rock/water interaction on the surface and subsurface, and will inform whether or not such an environment will be habitable.

The exploration of the interaction of shocked gneiss in both natural and simulated hydrothermal systems revealed the efficacy of the substrate for promoting and sustaining

epilithic and endolithic growth. Within the natural environments (Seltún and Geysir in Iceland), which were quite different from each other in terms of pH and temperature, the same principles held true: shocked rocks provided the best substrate for colonization, with no significant difference in the level of colonization observed between the moderate shock levels and the higher shocked samples (see Chapter 5). Using controlled laboratory experiments, the effects of shock metamorphism and substrate size on the growth of the sulfate reducing bacterium was obvious. Moderate and highly shocked coarse-grained samples showed rapid surface colonization and reduction in turbidity, showing that epilithic/endolithic growth was selective for higher porosity samples. Using scanning electron microscopy, infilling of all pore spaces with iron sulfides and bacteria within an EPS lattice was observed, as well as weathering of the rock around these areas due to the localized production of acid as a by-product of FeS generation in these vesicular in-fills. Exposure of these shocked gneisses to this hydrothermal system did produce weathering of the substrate, where the most marked changes were seen in the moderate shocked vials (coarse and fine grained), and the highly shocked sand vials. The presence of microorganisms did appear to accelerate this process, and these vials had values that were typically 30–50% higher in dissolved cations than in the abiotic experiments. The fact that the moderately shocked vials showed consistently high levels of dissolved cations, even though the high shocked samples are largely composed of soluble glasses, can be linked to the fact that major oxides concentrations in bulk chemical analyses have been shown to decrease in concentration with increasing pressure (Chapter 2).

We have seen that shocked gneisses are not only capable of providing an excellent endolithic habitat within polar desert environments, but that they are also a viable habitat within hydrothermal systems, where residence on and within the rock is preferred even in a closed system. In a system where light is not an issue, colonization can continue until the pore spaces of the rock are completely filled, causing organisms to be preserved within them.

6.2 Meteorite Impacts and the Origins of Life

It has long been proposed that the origins of life were hot, seeded in hydrothermal vent systems deep in Earth's early oceans (e.g. Orgel 1998; Copley et al., 2007). Similarly,

molecular analyses of 16S RNA present a last universal common ancestor (LUCA) that is buried within the hyperthermophiles of the Bacteria and Archaea, branching among H_2/S° chemolithotrophs (Brack et al., 2010). There is, of course, much contention with this theory: 1) high temperatures make RNA synthesis difficult as these nucleic acids will tend to denature; 2) tree construction using alternate molecules such as RNA polymerases branch out instead within mesophilic organisms; 3) there is no obvious concentration mechanism in hydrothermal vent systems that might allow for the formation of a pre-biotic cell. So how did life occur? Life as we know it requires an energy gradient, or a $-\Delta G$, and a solvent (water). Added to this is the need for encapsulation via some type of boundary molecules, informational molecules such as RNA or PNA (the purported precursor to RNA), and catalytic molecules such as enzymes (Monnard and Deamer 2002). The formation of all of these molecules requires endergonic reactions and must somehow be derived from a chemical gradient that would force these reactions to occur (e.g. Schwartz 1995; Orgel 1998). A recent paper by Russell et al. (2013) has returned to these hydrothermal vent systems and proposed that cellular life was preceded by abiotic metabolisms derived from the dissipation of physical energy in sea floor fracturing to chemical energy through serpentinization and the formation of precipitated hydrothermal mounds. The authors argue that the release of H_2 and CH_4 could have reacted with available electron acceptors (CO_2 , NO_3 , NO_2 , Fe^{2+} , Mg^{2+}) in the acidic Hadean ocean, where the gradient in pH between the highly alkaline effluent and the acidic ocean could have driven the first primitive proton pumps across the hydrothermal mound. These initial processes could have allowed for increased complexity and the generation of pyrophosphate in ferrous hydroxide layers, which would have acted as permeable “membranes”. A similar argument for a non-biotic membrane was proposed by Cairns-Smith and Hartman (1986), who argued that a complex molecule such as RNA could not have been created *de novo* and instead proposed the idea of self-replicating clays, where negative layers are held together by cations in the intervening spaces, spaces that also contain H_2O and could eventually act as a template for more complex molecules.

The reliance on hydrothermal vent systems in the early earth to provide the starting mechanisms for the origins of life is restrictive and poses many problems. An alternative to this vein of thought can be found in the relationship between impact craters and life.

As we have discussed, impact craters have been shown to provide habitats for contemporary (and past) endolithic organisms in polar deserts; having important implications for Mars, which can be considered as an extreme version of Earth's polar regions. The largely unknown facet of impact craters, however, is their ability to support life during a generated hydrothermal stage and the potential for providing a viable chemical system for the origins of life. Impact cratering does, however, provide us with many of the physical and chemical parameters that make hydrothermal vent systems such attractive prospects for the origins of life. Impact into a terrestrial target causes massive fracturing and brecciation of the substrate as well as disruption of the deep subsurface (Cockell et al., 2012), dramatically increasing the surface area of the region. In the event that a hydrothermal system is generated, the dissolution of the fractured, shocked target will occur, resulting in the generation of primary minerals such as quartz, amphibole-group minerals, phyllosilicates and zeolites, carbonates, sulfides, sulfates, oxides and halides (Osinski et al., 2013). Secondary, or weathered, mineral assemblages can also occur in the form of Fe-sulfates, and oxyhydroxides such as goethite (Izawa et al., 2011). In the event that an impact occurs into a mafic target such as basalt, serpentinization will occur, resulting in the release of methane and hydrogen gas (Marzo et al., 2010). The crater itself, especially in an impact into a continental plate, serves as the concentrating mechanism, providing a bowl shaped depression that will tend to collect fluids and potentially serve as an evaporative pond within which life could have arisen (Cockell 2006).

During the early Hadean, the impact flux into Earth, and indeed every other terrestrial body in the solar system was much greater than today (Sleep et al., 1989), indicating that many of these "warm ponds" would have been present, thus increasing the chances for many potential origins. The spike in the cratering record between 4.0 Ga and 3.8 Ga, known as the late heavy bombardment (LHB) would have provided even more available habitat for the above scenario to occur. Some believe that the period of cratering during the LHB was so intense that it would have either precluded the existence of life prior to 3.8 Ga, or acted as a thermal bottlenecking event causing the selection of hyperthermophiles over other present life resulting in the skewed evolutionary tree that we see today (e.g. Nisbet and Sleep 2001; Kring and Cohen 2002; Brack et al., 2010). In a

study by Abramov and Mojzsis (2009), which explores the habitability of the Earth during the LHB, their modeling of the extent of hydrothermal systems revealed that hyperthermophilic regimes would only have consisted of a relatively small portion of the Earth's crust and that temperatures would have dissipated quickly enough, that life (if it did exist) should have survived the bombardment.

In the aftermath of such extensive cratering as well as the cooling and dissipation of hydrothermal systems, we would be left with significant disruption of the deep subsurface, providing refugia for microbial organisms as they do on Earth (Wanger et al., 2006), extending the depth of the biosphere (Cockell et al., 2012). On Mars, where liquid water is not stable on the surface due to low atmospheric pressure, these deep-seated niches could have provided sanctuary for any putative life long after the surface became inhospitable (Boston et al., 1992; Michalski et al., 2013). Further available habitats remain in the impact breccias which, as we saw in Chapter 5 could have been colonized during a hydrothermal period, and would have had the potential to provide refuge for any endolithic organism after the cessation of the hydrothermal stage.

Though gneisses are by no means a primary rock type on other planets, such as Mars, the understanding of the response of this target to shock and the corresponding colonization by microorganisms can be used as a template for understanding how other typically dense, non-porous crystalline targets, such as basalt, may respond and help to inform further biological investigations of impact shocked lithologies. This work has clearly shown that these impact generated habitats are long-lasting and are capable of providing refuge for microorganisms on a geologic timescale, from the post-impact environment through to the present day.

6.3 Future Work

Research on impact-generated habitats is still in its early stages of inception, with only a handful of publications depicting the relationship between shock metamorphism and the corresponding benefits to microbial endolithic colonization. In Chapter 3 we discussed whether the relationship between colonization and shock metamorphism was linear, or perhaps fit a more complex polynomial relationship. If indeed the relationship is polynomial, significant work must be completed in order to quantify the separate affects

of translucency, porosity, permeability and substrate type on growth as well as the combined effects in order to effectively model microbial growth within the target rock. Understanding the changes in permeability, especially, is a facet of these systems that has yet to be studied and may in fact be a large determinant in community development. In terms of the colonizers themselves, broad scale sequencing can identify DNA present within a community, but given the global distribution of microorganisms and the constant rain-down of material in polar environments, this genomic data may not be representative of the active community, requiring analysis utilizing real-time genomic sequencing.

Perhaps most importantly, the next steps in the understanding of the ability of impact craters to foster habitats for life and perhaps their roles in the origins of life in the solar system, is the need for biological studies of impact-shocked basalt. The prevalence of this substrate type on Mars, and that the planet possessed environmental conditions suitable for life previously, necessitates an in-depth understanding of the ability of shocked basalt to provide an efficacious habitat, as well as the inherent differences between mafic and felsic substrates, especially in terms of generated translucency for the penetration of photosynthetically active radiation. The colonization of basaltic glasses on Earth reveals that they are a viable substrate for euendolithic organisms (endoliths that burrow into the substrate) in terms of bioessential elements. Translating this idea to the realm of basaltic impact-glasses, one could surmise that similar processes could ensue. Coupled with associated impact-induced hydrothermal systems and the by-products of resulting serpentinization, impact events into basaltic craters may have provided the necessary building blocks for the origins of life and warrants significant future investigation.

6.4 Epilogue

Irrefutable evidence on how life originated is still outside of our grasp, however, there are many varied hypotheses, beginning with Oparin (1953) and the Miller-Urey experiments (1959), and continuing today with top-down approaches, striving to understand the minimal genetic requirements for a cell (see Peters and Williams 2012). There is, however, a certain appeal and symmetry to the idea that life could have originated amongst the chaos of impact bombardment, where the intense entropy of the system could

have provided the energy for the ordered complexity of life as we know it, establishing the beginnings that Darwin envisioned in his “warm little pond.” (1871).

6.5 References

Abramov, O. and Mojzsis, S. J. 2009. Microbial habitability of the Hadean Earth during the late heavy bombardment. *Nature* **459**:419–422.

Allen, C. C., Gooding, J. L. and Keil, K. 1982. Hydrothermally altered impact melt rock and breccia - contributions to the soil of Mars. *Journal of Geophysical Research* **87**(NB12):83–101.

Brack, A., Horneck, G., Cockell, C. S., Bérces, A., Belisheva, N. K., Eiroa, C., Henning, T., Herbst, T., Kaltenegger, L., Léger, A., Liseau, R., Lammer, H., Selsis, F., Beichman, C., Danchi, W., Fridlund, M., Lunine, J., Paresce, F., Penny, A., Quirrenbach, A., Röttgering, H., Schneider, J., Stam, D., Tinetti, G. and White, G. J. 2010. Origin and Evolution of Life on Terrestrial Planets. *Astrobiology* **10**:69–76.

Boston, P. J., Ivanov, M. V. and McKay, C. P. 1992. On the possibility of chemosynthetic ecosystems in subsurface habitats on Mars. *Icarus* **95**:300-308.

Cairns-Smith, A. G. and Hartman, H. 1986. Clay minerals and the origin of life. Cambridge University Press, New York.

Cockell, C. S. 2006. The origin and emergence of life under impact bombardment. *Philosophical Transactions of the Royal Society B* **361**:1845–1856.

Cockell, C. S. and Lee, P. 2002. The biology of impact craters - a review. *Biological Reviews* **77**:279–310.

Cockell C. S., McKay, C. P. and Omelon, C. 2003. Polar endoliths – an anticorrelation of climactic extremes and microbial diversity. *International Journal of Astrobiology* **1**:305–310.

Copley, S. D., Smith, E. and Morowitz, H. J. 2007. The origin of the RNA world: Co-evolution of genes and metabolism. *Bioorganic chemistry* **35**:430–443.

Cockell, C. S., Voytek, M. A., Gronstal, A. L., Finster, K., Kirshtein, J. D., Kallmeyer, J., Kelly, L. and Powars, D. S. 2012. Impact disruption and recovery of the deep subsurface biosphere. *Astrobiology* **12**:231–246.

Darwin, C. 1871. Letter to Hooker, J.D.

Deslippe, J. R., Hartmann, M., Simard, S. W., and Mohn, W. W. 2012. Long-term warming alters the composition of Arctic soil microbial communities. *FEMS Microbiology Ecology* **82**:303–315.

- Fierer, N. and Lennon, J. T. 2011. The Generation and Maintenance of Diversity in Microbial Communities. *American Journal of Botany* **98**:439–448.
- Fike D. A., Cockell C. S., Pearce D., and Lee P. 2003. Heterotrophic microbial colonization of the interior of impact-shocked rocks from Houghton impact structure, Devon Island, Nunavut, Canadian High Arctic. *International Journal of Astrobiology* **1**: 311–323.
- Izawa, M. R. M., Bannerjee, N. R., Osinski, G. R., Flemming, R. L., Parnell, J. and Cockell, C. S. 2011. Weathering of post-impact hydrothermal deposits from the Houghton Impact Structure: implications for microbial colonization and biosignature preservation. *Astrobiology* **11**(6):537–550.
- Kahn, N., Tuffin, M., Stafford, W., Cary, C., Lacap, D. C., Pointing, S. B. and Cowan, D. 2011. Hypolithic microbial communities of quartz rocks from Miers Valley, McMurdo Dry Valleys, Antarctica. *Polar Biology* **34**:1657-1668.
- Kring, D.A. and Cohen, B.A. 2002. Cataclysmic bombardment throughout the inner solar system 3.9-4.0 Ga. *Journal of Geophysical Research* **107**(E2):5009, 1–6.
- Marzo, G. A., Davila, A. F., Tornabene, L. L., Dohm, J. M., Fairén, A. G., Gross, C., Kneissl, T., Bishop, J. L., Roush, T. L. and McKay, C. P. 2010. Evidence for Hesperian impact-induced hydrothermalism on Mars. *Icarus* **208**:667–683.
- Michalski, J. R., Cuadros, J., Niles, P. B., Parnell, J., Rogers, A. D. and Wright, S. P. 2013. Groundwater activity on Mars and implications for a deep biosphere. *Nature Geoscience*. *Advanced online publication*.
- Metzler A., Ostertag R., Redeker H. J., and Stöffler, D. 1988. Composition of the crystalline basement and shock metamorphism of crystalline and sedimentary target rocks at the Houghton Impact Crater, Devon Island, Canada. *Meteoritics* **23**:197–207.
- Miller, S. L. and Urey, H. C. 1959. Organic compound synthesis on the primitive Earth. *Science* **130**:245–251.
- Monnard, P. A. and Deamer, D. W. 2002. Membrane self-assembly processes: steps toward the first cellular life. *The Anatomical Record* **268**:196–207.
- Naumov, M. V. 2005. Principal features of impact-generated hydrothermal circulation systems: mineralogical and geochemical evidence. *Geofluids* **5**:165–184.
- Nemergut, D. R., Costello, E. K., Meyer, A. F. and Pescador, M. Y. 2005. Structure and function of alpine and arctic soil communities. *Research in Microbiology* **156**:775–784.
- Nisbet, E. G. and Sleep, N. H. 2001. The habitat and nature of early life. *Nature* **409**: 1083–1091.
- Oparin, A. I. 1952. *Origin of Life*. Dover Publications, New York. pp. 196.

Orgel, L. E. 1998. The origin of life – a review of facts and speculations. *Trends in Biochemical Sciences* **23**:491–495.

Osinski, G. R., Spray, J. G., and Lee, P. 2001. Impact-induced hydrothermal activity within the Haughton impact structure, arctic Canada: Generation of a transient, warm, wet oasis. *Meteoritics & Planetary Science* **36**:731–745.

Osinski, G. R., Lee, P., Parnell, J., Spray, J. G., and Baron, M. 2005. A case study of impact-induced hydrothermal activity: the Haughton impact structure, Devon Island, Canadian High Arctic. *Meteoritics & Planetary Science* **40**:1859–1877.

Osinski, G. R., Tornabene L. L., Banerjee, N. R., Cockell, C. S., Flemming, R., Izawa, M. R. M., McCutcheon, J., Parnell, J., Pickersgill, A. E., Pontefract, A., Preston, L., Sapers, H.M. and Southam, G. 2013. Impact-generated hydrothermal systems on Earth and Mars. *Icarus* **224**: 347–363.

Parnell, J., Boyce, A., Thackrey, S., Muirhead, D., Lindgren, P., Mason, C., Taylor, C., Still, J., Bowden, S., Osinski, G. R., and Lee, P. 2010. Sulfur isotope signatures for rapid colonization of an impact crater by thermophilic microbes. *Geology* **38**:271–274.

Peters, J. W. and Williams, L. D. 2012. The origin of life: look up and look down. *Astrobiology* **12**(11):1087–1092.

Russell, M. J., Nitschke, W. and Branscomb, E. 2013. The inevitable journey to being. *Philosophical Transactions of the Royal Society B* **368**:1–20.

Schwartz, A. W. 1995. The RNA world and its origins. *Planetary and Space Science* **43**: 161–165.

Singleton, A. C., Osinski, G. R., McCausland, P. J. A., and Moser, D. E. 2011. Shock-induced changes in density and porosity in shock-metamorphosed crystalline rocks, Haughton impact structure, Canada. *Meteoritics & Planetary Science* **46**:1774–1786.

Sleep, N. H., Zahnle, K. J., Kasting, J. F. and Morowitz, H. J. 1989. Annihilation of ecosystems by large asteroid impacts on the early Earth. *Nature* **342**: 139–142.

Wanger, G., Southam, G., and Onstott, T. C. 2006. Structural and chemical characterization of a natural fracture surface from 2.8 kilometers below land surface: biofilms in the deep subsurface. *Geomicrobiology Journal* **23**:443–452.

Appendix A

A1. Shock level categories based on petrographic analysis of crystalline (gneiss) rock. Adapted from Singleton et al. (2011).

Shock Stage	Pressure Range (GPa)	Mineral Shock Effects				Rock Features
		<i>Quartz</i>	<i>K-feldspar</i>	<i>Plag-feldspar</i>	<i>Biotite</i>	
0		-	-	-	-	Unshocked
1	2-6	-	-	-	Kink Banding	Rock Fracturing begins; Shatter cones
2	<5	Fracturing	Fracturing	Fracturing	Kink Banding	Shatter Cones; Fracturing
	5-7	Planar Fracturing	Fracturing	Fracturing and Checkerboard pattern	Kink Banding	
	8-10	Fracturing	Fracturing	PDFs; Checkerboardin g	Kink Banding	
3	10-25	PDFs; Toasting	PDFs	PDFs and Checkerboardin g	-	First microscopic deformations
	10	PDFs			-	PDFs beginning to form
	12-15	Quartz to Stishovite			-	First phase transition of Quartz; PDFs established
	20	PDFs; lowered birefringence and toasting	PDFs; Lowered birefringenc e	PDFs; Checkerboardin g and lowered birefringence.	-	Toasting of Quartz and lowering of birefringence
4	25-35	Toasting up to 30GPa	PDFs	Checkerboard up to 30GPa	Loss of Pleiochroi sm	Beginning of diaplectic glass formation and loss of Shatter Cones.
	>30	Coesite; PDFs; Presence of Coesite	PDFs	PDFs	-	No more Shatter Cones; Phase transition of Quartz to Coesite
5	35	Diaplectic glass formation	Glass formation	Glass formation	-	Beginning of selective partial melting.
	35-45	Loss of extinction; Diaplectic glass; No more PDFs	Diaplectic to flowed and vesicular; Partial Melting	-	Partial Melting	
	45	Diaplectic	Vesiculated Glass	Vesiculated Glass	-	
6	45-55	Loss of Diaplectic outlines	Flowed and Frothy glass	Flowed and Frothy glass	Absent	Reduction of density. Flattened holes where amphiboles have melted.
	55-60	-	-	-	-	Rock glasses; crystallized melt rocks
	60	-	-	-	-	
7	60-80?	Complete melting of all minerals				Visible flow and Differentiation

A2. Sample coordinates shown in UTM as well as sample descriptions for all three suites of rocks utilized in this study. NAD83 is used for all samples, UTM grid 16.

Sample	UTM Coordinates		Sample Description
	Easting	Northing	
<i>Suite 1 – TOC Analysis</i>			
Carbonate			
00-012	420,920	8,371,065	Lower Mb Allen Bay limestone
01-051	440,830	8,365,813	Thumb Mt FM limestone
01-050	440,830	8,365,813	Thumb Mt FM limestone
02-136	423,560	8,368,490	Eleanor River FM limestone
02-118	423,040	8,372,550	Eleanor River FM limestone
05-010	582,940	8,374,420	Middle Mb Allen Bay FM limestone
05-044	454,652	8,355,458	Allen Bay FM limestone
JPBR	416,615	8,367,467	View Hill.
JPYB	419,413	8,375,962	Fine grey carbonate.
DVA	438,952	8,364,324	Fine, yellow-brown carbonate. Allen Bay Formation.
Sulfate			
SBF 1	428,920	8,368,430	Allen Bay formation. Sulfate clast within dolomite.
SBF 2	428,920	8,368,430	Allen Bay formation. Sulfate clast within dolomite.
Sandstone			
Sand 1	424,731	8,368,565	Anomaly Hill sandstone.
Sand 2	424,731	8,368,565	Anomaly Hill sandstone.
Sand 3	424,731	8,368,565	Anomaly Hill sandstone.
99-114	424,410	8,368,630	Blanley Bay Formation. Central uplift.
Shale			
Shale 1 TH	418,718	8,363,722	Bioturbated brown-grey carbonate.
Shale 2 TH	418,718	8,363,722	Bioturbated brown-grey carbonate.
02-047	426,540	8,361,980	Bay Fiord formation. Dolomite.
01-047	440,830	8,365,810	Bay Fiord formation. Dolomite. Outside crater.
CMR			
MBTL	420,533	8,371,064	Trinity Lake, Allen Bay formation.
MBDH	422,176	8,371,680	Drill Hill
MBSE	429,758	8,365,086	Sapphire Lake
MBAH	424,731	8,368,565	Anomaly Hill
WDH	422,176	8,371,680	Drill Hill
CMR – Clast			
GEM2B-B	418,718	8,363,722	Gemini Hill. Bioturbated brown-grey carbonate.
SBC	426,292	8,371,376	Breccia Cliff, carbonate clast.
SDS	422,176	8,371,680	Drill Hill, carbonate clast.
SMP	416,335	8,370,284	Muddy Pass, small carbonate clast.
SSAPEM	429,758	8,365,086	Sapphire Lake, small carbonate clast.
STR12B	420,533	8,371,064	Trinity Lake, small carbonate clast.
<i>Suite 2 – Sedimentary Samples</i>			
Post-Impact			
03-019	419,914	8,369,104	Haughton Formation – Dolomite, Qz, Cal
03-024	419,910	8,369,030	Haughton Formation – Greenish sand
03-052	419,293	8,368,520	Haughton Formation – Limestone
04-057	424,464	8,367,937	Haughton Formation
04-058	424,795	8,367,540	Reworked clast-rich melt rock
04-060	423,132	8,370,098	Reworked clast-rich melt rock
04-061	423,132	8,370,098	Haughton Formation
04-062	423,132	8,370,098	Reworked clast-rich melt rock
Clast-rich Melt Rock (CMR)			
99-108	433,100	8,365,530	Breccia Dike
00-023	420,560	8,370,965	Carbonate rich melt rock.
00-035	420,440	8,370,955	Carbonate rich melt rock.
00-175	418,620	8,363,695	Carbonate rich melt rock.
00-220	425,340	8,372,445	Carbonate rich melt rock.
00-249	423,060	8,371,495	Carbonate rich melt rock.
02-119	423,680	8,372,930	Carbonate rich melt rock.
04-059	423,412	8,370,967	Carbonate rich melt rock.

05-026	418,011	8,364,086	Carbonate rich melt rock.
06-109	422,477	8,372,364	Carbonate rich melt rock.
CMR Clast			
00-174b	418,560	8,363,375	Carbonate clast.
04-001	418,585	8,364,468	Sandstone clast.
04-002	418,585	8,364,468	Sandstone clast.
04-003	418,585	8,364,468	Sandstone clast.
04-004	418,585	8,364,468	Sandstone clast.
04-005	418,585	8,364,468	Sandstone clast.
04-007	418,650	8,364,255	Sulfate clast (white).
04-008	418,730	8,364,262	Sulfate clast (brecciated).
04-032	423,990	8,371,726	Sulfate clast.
04-034	423,990	8,371,726	Sulfate clast.
04-040	426,169	8,371,304	Sulfate clast.
05-024	418,011	8,364,086	Carbonate clast.
05-025	418,011	8,364,086	Carbonate clast.
05-029	418,011	8,364,086	Sulfate clast.
Low Shock Central Uplift			
99-114	424,410	8,368,630	Blanley Bay Fm. Sandstone from central uplift.
02-118	423,040	8,372,550	Eleanor River Fm.
04-041	426,169	8,371,304	Sulfate clast from parautochthonous breccias.
04-044	427,476	8,371,198	Bay Fiord Fm. Sulfate from central uplift.
04-045	427,476	8,371,198	Bay Fiord Fm. Sulfate from central uplift.
04-053	425,507	8,370,215	Bay Fiord Fm. Sulfate from central uplift.
05-004	419,815	8,371,815	Middle Mb Allen Bay.
05-005	418,902	8,371,815	Middle Mb Allen Bay.
05-007	417,277	8,372,712	Middle Mb Allen Bay.
05-008	416,329	8,373,256	Middle Mb Allen Bay.
06-001	420,422	8,371,019	Lower Mb Allen Bay Formation.
Unshocked			
01-050	440,830	8,365,813	Thumb Mountain Fm. Outside crater.
05-009	583,587	8,373,627	Middle Mb Allen Bay.
05-010	582,940	8,374,420	Middle Mb Allen Bay.
05-035	454,222	8,355,604	Bay Fiord Fm. Sulfate. Outside crater.
05-037	454,269	8,355,563	Bay Fiord Fm. Sulfate. Outside crater.
05-038	454,337	8,355,535	Bay Fiord Fm. Sulfate. Outside crater.
05-039	454,337	8,355,535	Bay Fiord Fm. Sulfate. Outside crater.
05-040	454,427	8,355,529	Bay Fiord Fm. Sulfate. Outside crater.
05-042	454,489	8,355,512	Bay Fiord Fm. Sulfate. Outside crater.
<i>Suite 3 – Crystalline Samples</i>			
Shock Level 0			
DIO8-VO-1	425,924	8,369,633	Unshocked basement gneiss.
DIO8-VO-3	425,924	8,369,633	Amphibole and feldspar rich. Lots of sulfides.
SI001-A	541,625	8,366,491	Sverdrup Inlet - Siliminite and biotite rich felsic sample.
SI001-B1	541,625	8,366,491	Sverdrup Inlet - Siliminite and biotite rich felsic sample.
HMP-00-203	514,390	8,350,575	Unshocked basement gneiss. Amphibole and feldspar rich.
HMP-00-195	514,390	8,350,575	Unshocked basement gneiss. Felsic, plagioclase.
HMP-00-196	514,390	8,350,575	Unshocked basement gneiss. Siliminite and biotite rich.
HMP-00-218	514,390	8,350,575	Unshocked basement gneiss. Felsic. Granitic composition.
HMP-00-198	514,390	8,350,575	Unshocked basement gneiss. Mafic. Amphibole with some plagioclase.
HMP-00-204	514,390	8,350,575	Unshocked basement gneiss. Felsic. Granitic composition.
HMP-00-047b	422,150	8,372,835	Allen Bay Formation, middle member. Brecciated Gneiss
HMP-00-214	514,390	8,350,575	Unshocked basement gneiss. Felsic. Amphibole, siliminite.
Shock Level 1			
DI08-7-7	429,282	8,369,910	Highly altered. Kink banding in biotite, no PDFs or toasting. Mafic.
Shock Level 2			
DI08-26-1	428,487	8,369,942	Felsic. PF formation in Quartz. Presence of sulfides and clinopyroxenes.
DI08-24-1	425,537	8,371,436	Garnet and biotite rich. Some feldspars. Kink banding and pleochroism.
Shock Level 3			
DI08-20-1	425,813	8,367,533	Garnet and biotite rich with feldspars. Kink banding in biotite.

DI08-7-2	429,282	8,369,910	Siliminite rich. Quartz with PFs and some PDFs.
BE009-A2	427,859	8,368,697	Quartz with some PDFs. Significant levels of plagioclase.
BE010-A	427,846	8,366,592	Quartz rich. Toasting with PDFs. Good grain boundaries, full extinction.
DV10	425,924	8,369,633	Quartz with some toasting and multiple PDFs.
BE009-A13	428,128	8,368,856	Quartz with siliminite, biotite, garnets and feldspars. PDFs with toasting.
BE009-A10	428,128	8,368,856	Garnet rich with biotite. PDFs, toasting and kink banding.
Shock Level 4			
HMP-99-094	428,310	8,369,740	Gneiss clast from melt rich rock.
DI08-18-1	427,787	8,368,668	Garnet rich. Biotite with pleiochromism. Bands of siliminite.
DI08-30-1	429,699	8,365,478	Mafic. Amphiboles. PDF's with toasting in quartz.
DI08-9-1	427,916	8,368,940	Mafic sample. Biotite present with pleiochromism. Quartz with PDFs.
DI08-34-11	422,354	8,370,785	Felsic. Plagioclase rich. PDF's and PF's prevalent. Good extinction.
Shock Level 5			
DI08-6-1	425,563	8,372,271	Vesiculated glass. Very altered sample.
DI08-10-2	426,292	8,371,376	Vesiculated glass. Very altered sample.
DI08-30-3	429,699	8,365,478	Siliminite rich. Quartz extinction still visible. Diaplectic glass formation.
BE005-C	427,473	8,366,944	Bruno Escarpment. Some Orthopyroxene. Largely diaplectic glass.
DI08-20-6	420,598	8,371,046	Felsic with mafic bands. Some PDF's. Vesicularized glass, some diaplectic.
DI08-21-5	420,400	8,371,139	Siliminite rich. Diaplectic glass with dark brown matrix. Some PDF's.
DI08-24-8	425,537	8,371,436	Siliminite rich. Largely diaplectic glass. Calcite deposition. Mafic banding.
AH11	424,731	8,368,565	Anomaly Hill. Diaplectic glass with some flow.
DI08-34-12	422,354	8,370,785	Glass with some flow visible. Lots of sericite.
WSR002B	429180	8366530	Biotite rich with kink banding. Ballen quartz with some diaplectic glass.
Shock Level 6			
HMP99-070B	424,560	8,367,830	Glass with some diaplectic outlines.
WSR001-A2	429,198	8,366,671	Quartz rich. Significant flow, very frothy. Presence of sulfides.
DI08-3-10	423,181	8,371,712	Mafic sample. Mainly glass. Some areas with vesicularized frothy flow.
DI08-20-7	420,598	8,371,046	Quartz and feldspathic glass. Calcite deposition.
AH6	424,731	8,368,565	Anomaly Hill. Glass with alteration. Flow of feldspars with vesicles.
BE10	428,128	8,368,856	Diaplectic glass beginning to lose outlines.
BE009-A11	428,128	8,368,856	Glass with siliminite.
DI08-35-10	428,087	8,364,588	Quartz losing diaplectic outlines. Frothy glass.
Shock Level 7			
HMP99-068A	424,690	8,368,120	Frothy glass with good flow textures.
AH003-A	424,731	8,368,565	Felsic sample with frothy flow. Some crystallization of quartz.
BE009-A14	428,128	8,368,856	Sample has large mafic bands throughout. Significant flow of melt.
DI08-24-7	425,537	8,371,436	Good flow texture, complete melting. Calcite deposition.
BE002-A	427,718	8,366,610	Frothy glass with crystallization of quartz. Calcite deposition present.

A3. The total amount of organic carbon (% TOC) in Haughton target rocks and clast-rich melt rocks. Samples are from Suite 1 collection (see Methods).

Target Rocks	Sample ID	% TOC
Carbonate	02-136	0.07
	02-118	0.12
	01-051	0.08
	01-050	0.11
	05-044	0.30
	00-012	0.14
	05-010	0.13
	JPBF	0.16
	JPYB	0.10
	DVL	0.06
Sulfate	SBF 1	0.13
	SBF 2	0.03
Sandstone	Sand 1	0.03
	Sand 2	0.06
	Sand 3	0.05
	99-114	0.06
Shale	Shale 1 TH	0.48
	Shale 2 TH	5.02
	02-047	1.11
	01-047	11.43
Clast-Rich Melt Rock		% TOC
Whole rock of clast-rich melt rock	MBDM	0.10
	MBAH	0.17
	MBTL	0.14
	MBSE	0.14
	WDM	0.14
Carbonate clast fraction of clast-rich melt rock	SMP	0.15
	SSAPEM	0.15
	SDS	0.14
	GEM2B-B	0.12
	STRI2B	0.14
	SBC	0.12

A4. Table shows XRF results depicting major oxide composition of sedimentary rocks from the Haughton Crater.

Sample	Mineral Composition (% weight)										Total	
	SiO ₂	TiO ₂	Al ₂ O ₃	Fe ₂ O ₃	MnO	MgO	CaO	Na ₂ O	K ₂ O	P ₂ O ₅		LOI
Post-Impact												
03-019	6.32	0.060	0.99	0.47	0.010	18.26	30.11	0.24	0.12	0.017	43.63	100.12
03-024	6.80	0.047	0.49	0.31	0.010	18.66	29.82	n.d.	0.07	0.010	43.87	100.09
03-052	7.33	0.109	2.28	1.00	0.083	10.15	36.25	0.24	0.43	0.340	41.64	99.87
04-057	5.71	0.056	0.91	0.40	0.010	17.36	31.82	0.03	0.25	0.025	43.58	100.16
04-058	27.58	0.254	5.53	1.79	0.030	8.19	24.78	0.49	2.22	0.048	28.78	99.75
04-060	15.23	0.136	3.29	1.28	0.024	10.87	30.43	0.36	0.61	0.056	37.60	99.95
04-061	6.81	0.068	1.66	0.55	0.012	14.04	32.23	0.26	0.22	0.025	44.10	99.99
04-062	18.31	0.158	3.85	1.37	0.029	9.34	30.53	0.09	0.68	0.049	35.79	100.23
<i>Std Dev</i>	<i>7.93</i>	<i>0.07</i>	<i>1.75</i>	<i>0.54</i>	<i>0.02</i>	<i>4.28</i>	<i>3.18</i>	<i>0.17</i>	<i>0.70</i>	<i>0.11</i>	<i>5.47</i>	
Clast-rich Melt Rock (CMR)												
99-108	0.034	0.012	0.12	0.06	0.024	1.51	52.80	0.01	n.d.	0.012	44.92	99.81
00-023	21.78	0.216	4.28	1.73	0.033	10.29	27.26	0.11	0.97	0.051	33.23	99.99
00-035	22.96	0.244	4.87	1.91	0.034	9.56	26.42	0.11	1.05	0.058	32.86	100.11
00-175	11.77	0.081	1.86	0.71	0.014	9.37	37.36	0.05	0.41	0.027	38.86	100.05
00-220	18.53	0.140	3.17	1.19	0.024	11.12	30.99	0.08	0.66	0.037	33.81	99.78
00-249	18.35	0.127	3.16	1.14	0.021	11.12	30.46	0.09	0.70	0.039	34.52	99.75
02-119	18.91	0.141	3.46	1.19	0.025	9.88	31.03	0.07	0.80	0.042	34.17	99.74
04-059	15.45	0.124	2.92	1.08	0.023	9.19	33.64	0.08	0.51	0.043	36.62	99.73
05-026	12.25	0.084	1.86	0.78	0.016	10.88	35.78	0.02	0.47	0.029	37.85	100.10
06-109	17.53	0.136	3.33	1.12	0.024	10.77	30.00	0.10	0.47	0.043	36.41	99.96
<i>Std Dev</i>	<i>6.59</i>	<i>0.07</i>	<i>1.35</i>	<i>0.52</i>	<i>0.01</i>	<i>2.85</i>	<i>7.57</i>	<i>0.04</i>	<i>0.30</i>	<i>0.01</i>	<i>3.59</i>	
CMR Clast												
00-174b	81.64	0.016	0.14	0.31	0.005	0.45	9.22	0.03	0.07	0.015	7.83	99.88
04-001	95.26	0.027	0.07	0.39	0.005	0.18	1.46	0.04	0.09	0.013	2.28	99.82
04-002	93.70	0.016	0.05	0.38	0.005	0.19	1.76	0.03	0.03	0.009	3.75	99.95
04-003	73.43	0.026	0.21	0.24	0.007	0.47	13.64	0.03	0.07	0.019	11.72	99.89
04-004	92.01	0.029	0.18	0.51	0.004	0.40	2.00	0.04	0.10	0.014	4.75	100.07
04-005	92.17	0.020	0.12	0.38	0.005	0.47	3.06	0.03	0.04	0.014	3.37	99.79
04-007	0.20	0.014	n.d.	0.04	0.003	0.02	32.00	0.03	0.01	0.010	67.35	99.69
04-008	21.29	0.012	n.d.	0.10	0.004	0.08	25.83	0.05	0.01	0.010	52.36	99.76
04-032	0.32	0.014	0.05	0.06	n.d.	0.11	31.90	0.03	0.01	0.008	67.31	99.83
04-034	0.57	0.013	0.08	0.09	0.004	0.66	32.23	0.03	0.01	0.012	66.05	99.77
04-040	0.37	0.012	0.02	0.02	0.003	0.11	31.95	0.03	0.01	0.010	67.14	99.68
05-024	2.18	0.026	0.39	0.15	0.008	3.60	50.52	0.04	0.03	0.010	43.10	100.06
05-025	2.06	0.025	0.38	0.15	0.008	3.80	50.12	0.02	0.04	0.009	43.19	99.80
05-029	75.90	0.020	0.16	0.29	0.007	1.24	11.75	0.02	0.03	0.014	10.42	99.86
<i>Std Dev</i>	<i>43.54</i>	<i>0.006</i>	<i>0.12</i>	<i>0.16</i>	<i>0.002</i>	<i>1.25</i>	<i>17.41</i>	<i>0.01</i>	<i>0.03</i>	<i>0.003</i>	<i>28.09</i>	
Low Shock Central Uplift												
05-004	0.18	0.009	0.09	0.05	0.003	21.41	31.33	n.d.	n.d.	0.006	46.87	99.94
05-005	0.77	0.009	0.17	0.04	n.d.	20.13	30.68	0.19	0.01	0.013	47.82	99.83
05-007	0.47	0.010	0.22	0.07	n.d.	21.14	30.92	0.20	0.01	0.012	46.84	99.89
05-008	0.31	0.010	0.08	0.05	0.003	21.52	31.36	n.d.	n.d.	0.006	46.58	99.91
99-114	99.39	0.025	0.07	0.25	0.005	0.03	0.08	0.03	0.04	0.011	0.17	100.11
02-118	0.64	0.017	0.22	0.18	0.012	20.39	30.84	n.d.	0.04	0.009	47.73	100.07
04-041	0.94	0.020	0.18	0.12	n.d.	0.08	31.26	0.06	0.08	0.010	66.62	99.39
04-044	5.03	0.044	0.07	0.52	0.014	5.07	30.18	0.07	0.37	0.024	57.88	99.95
04-045	1.64	0.028	0.33	0.17	0.005	0.29	31.54	0.05	0.12	0.012	65.54	99.73
04-053	1.02	0.013	0.03	0.03	0.004	0.98	31.77	0.04	0.01	0.008	65.89	99.80
06-001	64.02	0.499	16.93	4.15	0.085	2.26	4.68	4.74	1.40	0.251	0.89	99.99
<i>Std Dev</i>	<i>33.53</i>	<i>0.145</i>	<i>5.04</i>	<i>1.21</i>	<i>0.028</i>	<i>10.27</i>	<i>11.67</i>	<i>1.41</i>	<i>0.45</i>	<i>0.073</i>	<i>23.39</i>	
Unshocked												
01-050	0.52	0.013	0.31	0.27	0.009	14.65	38.23	0.17	0.05	0.018	45.91	100.15
05-009	0.04	0.008	0.13	0.09	n.d.	21.14	30.49	0.13	n.d.	0.012	47.83	99.87
05-010	0.50	0.015	0.20	0.06	0.004	20.87	31.14	n.d.	0.01	0.007	47.19	99.99
05-035	2.89	0.013	0.03	0.05	0.004	0.16	31.32	0.03	0.01	0.010	65.25	99.77
05-037	0.14	0.010	0.03	0.03	0.004	2.49	31.51	0.02	n.d.	0.009	65.55	99.79
05-038	4.79	0.044	0.78	0.19	0.005	0.96	30.38	0.05	0.47	0.015	61.96	99.66
05-039	0.35	0.009	0.03	0.05	0.003	0.12	32.27	0.06	0.01	0.011	66.90	99.82
05-040	1.64	0.020	0.21	0.45	0.018	4.57	31.24	0.04	0.04	0.013	61.72	99.96
05-042	1.13	0.017	0.13	0.12	0.006	0.87	31.71	0.08	0.02	0.012	65.71	99.81
<i>Std Dev</i>	<i>1.58</i>	<i>0.011</i>	<i>0.24</i>	<i>0.14</i>	<i>0.005</i>	<i>8.97</i>	<i>2.39</i>	<i>0.06</i>	<i>0.15</i>	<i>0.003</i>	<i>8.95</i>	

A5. Table shows XRF and ICP results depicting major oxide composition of crystalline rocks from the Haughton Crater. Note that a duplicate value is shown for shock level 5 to indicated agreement between XRF and ICP data.

Sample	Mineral Composition (% weight)											Total
	SiO ₂	TiO ₂	Al ₂ O ₃	Fe ₂ O ₃	MnO	MgO	CaO	Na ₂ O	K ₂ O	P ₂ O ₅	Cr ₂ O ₃	
Shock Level 0												
DIO8-VO-1	55.52	0.63	17.54	9.64	0.13	4.15	7.15	4.12	1.22	0.16	n.d.	100.26
DIO8-VO-3	74.90	0.03	13.17	1.79	0.02	0.08	0.23	2.52	6.84	0.01	0.010	99.60
SI001-A	82.84	0.15	10.75	1.28	0.01	0.41	0.11	0.42	2.72	0.02	0.003	98.71
SI001-B1	79.46	0.12	9.36	1.90	n.d.	0.50	0.21	0.52	5.83	0.05	n.d.	97.95
HMP-00-203	65.92	0.41	16.44	4.36	0.05	1.95	3.09	3.62	2.69	0.12	0.003	98.65
HMP-00-195	71.72	0.03	15.03	1.26	n.d.	0.05	0.49	3.05	7.93	0.06	n.d.	99.62
HMP-00-196	70.67	0.39	14.74	3.41	0.03	0.81	2.77	3.71	2.79	0.10	n.d.	99.42
HMP-00-218	74.10	0.02	13.89	0.62	n.d.	0.20	0.86	2.23	7.18	0.09	n.d.	99.19
HMP-00-198	67.30	0.46	16.18	3.88	0.04	1.43	3.52	4.42	2.03	0.16	0.002	99.42
HMP-00-204	68.22	0.34	14.06	4.20	0.06	1.89	4.59	3.64	1.40	0.22	0.005	98.63
HMP-00-047b	71.44	0.02	14.76	0.79	n.d.	0.08	0.78	2.55	8.26	0.09	n.d.	98.77
HMP-00-214	67.05	0.88	15.09	3.96	0.01	1.65	1.75	2.63	5.44	0.10	0.007	98.57
<i>Std Dev</i>	<i>7.00</i>	<i>0.28</i>	<i>2.31</i>	<i>2.49</i>	<i>0.04</i>	<i>1.21</i>	<i>2.18</i>	<i>1.28</i>	<i>2.65</i>	<i>0.06</i>	<i>0.003</i>	
Shock Level 1												
DI08-7-7	59.58	1.33	16.48	4.37	0.02	2.14	1.25	1.11	7.48	0.38	0.005	94.12
Shock Level 2												
DI08-26-1	65.53	0.40	13.16	2.64	0.02	1.53	7.24	1.75	6.24	0.09	0.010	98.61
DI08-24-1	50.61	0.64	24.59	6.15	0.11	2.15	5.24	4.09	3.14	0.07	0.010	96.80
Shock Level 3												
DI08-20-1	53.50	0.59	25.71	2.41	n.d.	1.99	0.39	0.37	8.60	0.06	0.010	93.63
DI08-7-2	61.70	0.76	18.50	5.28	0.07	1.78	3.90	1.74	3.84	0.11	0.010	97.69
BE009-A2	56.74	0.62	13.59	4.76	0.05	3.24	6.88	2.34	3.92	0.15	0.003	92.29
BE010-A	67.66	0.57	14.39	3.37	0.04	0.96	1.61	1.91	7.29	0.15	n.d.	97.95
DV10	62.51	0.52	17.67	2.99	0.02	1.35	1.99	2.20	6.34	0.07	0.039	95.70
BE009-A13	62.04	0.47	16.07	7.06	0.16	2.31	3.74	1.58	2.46	0.13	0.006	96.03
BE009-A10	64.31	0.72	13.97	8.42	0.22	2.54	2.39	1.33	2.67	0.07	0.009	96.65
<i>Std Dev</i>	<i>4.71</i>	<i>0.10</i>	<i>4.22</i>	<i>2.21</i>	<i>0.08</i>	<i>0.76</i>	<i>2.10</i>	<i>0.66</i>	<i>2.39</i>	<i>0.04</i>	<i>0.01</i>	
Shock Level 4												
HMP-99-094	79.43	0.18	9.90	0.79	0.01	0.12	0.16	0.80	7.16	0.01	0.10	98.57
DI08-18-1	48.02	0.83	27.74	4.91	0.04	2.36	0.87	0.28	6.98	0.06	0.019	92.11
DI08-30-1	47.50	2.04	14.18	17.19	0.26	6.50	7.26	1.06	2.23	0.05	0.002	98.27
DI08-9-1	72.53	0.13	12.87	1.06	n.d.	0.91	1.43	1.00	5.92	n.d.	0.002	95.85
DI08-34-11	72.84	0.11	12.93	1.15	n.d.	0.32	0.50	1.80	6.87	0.02	n.d.	96.54
<i>Std Dev</i>	<i>15.14</i>	<i>0.83</i>	<i>7.01</i>	<i>7.01</i>	<i>0.11</i>	<i>2.64</i>	<i>2.95</i>	<i>0.55</i>	<i>2.07</i>	<i>0.03</i>	<i>0.01</i>	
Shock Level 5												
DI08-6-1	73.23	0.12	13.90	1.47	0.01	0.28	1.25	2.39	5.39	0.02	n.d.	98.06
DI08-10-2	47.10	1.62	14.96	14.07	0.19	6.39	10.09	2.83	0.97	0.12	0.010	98.35
DI08-30-3	87.35	0.21	6.56	1.77	0.01	0.71	0.25	0.16	1.02	0.02	0.010	98.07
BE005-C	60.60	0.60	17.25	4.09	0.05	1.54	3.97	2.91	5.15	0.14	0.003	96.30
DI08-20-6(ICP)	79.57	0.26	9.90	1.03	n.d.	0.61	1.27	0.27	3.77	0.03	0.009	96.72
<i>DI08-20-6(XRF)</i>	<i>79.57</i>	<i>0.26</i>	<i>9.90</i>	<i>1.03</i>	<i>0.01</i>	<i>0.61</i>	<i>1.27</i>	<i>0.27</i>	<i>3.77</i>	<i>0.03</i>	<i>0.01</i>	<i>99.81</i>
DI08-21-5	65.11	0.26	11.04	4.09	0.02	1.93	6.43	0.18	2.29	0.02	0.023	91.39
DI08-24-8	81.42	0.19	8.24	0.72	n.d.	0.78	1.83	0.32	2.17	0.02	n.d.	95.69
AH11	83.99	0.11	7.58	0.93	n.d.	0.71	1.48	0.13	2.01	0.01	0.003	96.95
DI08-34-12	70.58	0.17	11.42	1.08	n.d.	1.25	2.01	0.76	6.92	0.02	n.d.	94.21
WSR002B	62.52	0.86	14.64	6.31	0.14	3.33	2.90	1.35	3.85	0.08	0.006	95.72
<i>Std Dev</i>	<i>12.35</i>	<i>0.48</i>	<i>3.56</i>	<i>4.13</i>	<i>0.07</i>	<i>1.85</i>	<i>3.00</i>	<i>1.16</i>	<i>2.00</i>	<i>0.05</i>	<i>0.01</i>	
Shock Level 6												
HMP99-070B	69.07	0.65	7.44	2.34	0.01	1.43	3.20	0.47	3.98	0.29	0.010	88.89
WSR001-A2	52.14	0.46	9.43	2.57	0.01	1.29	10.23	0.24	4.03	0.04	0.004	80.44
DI08-3-10	70.27	0.58	12.52	2.82	0.02	1.99	3.79	2.18	2.61	0.05	0.007	96.84
DI08-20-7	73.90	0.16	11.53	1.65	0.02	0.74	3.40	2.44	2.12	0.02	n.d.	95.98
AH6	61.61	0.17	12.89	0.78	n.d.	0.94	5.53	1.02	8.14	0.05	n.d.	91.13
BE10	66.78	0.12	10.98	0.88	n.d.	0.99	5.69	1.59	5.57	0.02	n.d.	92.62
BE009-A11	79.28	0.33	9.74	3.14	0.01	1.29	1.10	0.40	1.25	0.01	0.003	96.55
DI08-35-10	72.63	0.16	12.28	0.98	n.d.	0.37	1.04	2.10	6.45	0.02	n.d.	96.03
<i>Std Dev</i>	<i>8.31</i>	<i>0.21</i>	<i>1.87</i>	<i>0.94</i>	<i>0.01</i>	<i>0.49</i>	<i>2.97</i>	<i>0.89</i>	<i>2.33</i>	<i>0.09</i>	<i>0.00</i>	
Shock Level 7												
HMP99-068A	66.36	0.39	13.79	4.00	0.01	1.61	1.44	0.69	7.59	0.11	0.010	96.00
AH003-A	76.29	0.17	11.14	0.58	n.d.	0.18	0.87	1.42	6.53	0.02	n.d.	97.20
BE009-A14	79.99	0.18	7.25	0.65	n.d.	1.07	1.63	0.36	2.52	0.01	0.002	93.66
DI08-24-7	71.82	0.27	11.34	1.41	n.d.	0.87	3.03	1.53	5.09	0.05	n.d.	95.41
BE002-A	61.71	0.01	0.08	n.d.	n.d.	0.21	20.94	n.d.	0.03	n.d.	n.d.	82.98
<i>Std Dev</i>	<i>7.37</i>	<i>0.14</i>	<i>5.37</i>	<i>1.58</i>	<i>0.00</i>	<i>0.61</i>	<i>8.62</i>	<i>0.66</i>	<i>3.07</i>	<i>0.04</i>	<i>0.00</i>	

A6. Table shows ICP results depicting trace element composition of crystalline rocks from the Haughton Crater. Values beneath element symbols indicate detection limits.

Sample ²	Mineral Composition (% weight)											
	Cu 5ppm	Ba 5ppm	Zn 5ppm	Ni 20ppm	Co 20ppm	Sr 2ppm	Zr 5ppm	Ce 30ppm	Y 3ppm	Sc 1ppm	TotC %	TotS %
Shock Level 0												
SI001-A	n.d.	660	28	n.d.	31	29	74	n.d.	7	5	0.16	n.d.
SI001-B1	58	766	28	n.d.	29	121	297	33	n.d.	n.d.	0.31	n.d.
HMP-00-203	31	533	81	24	n.d.	509	153	54	11	11	0.04	0.07
HMP-00-195	48	175	6	n.d.	n.d.	55	7	n.d.	5	n.d.	0.04	n.d.
HMP-00-196	9	1315	40	n.d.	n.d.	308	198	81	4	3	0.04	n.d.
HMP-00-218	6	1103	n.d.	n.d.	n.d.	168	39	n.d.	n.d.	n.d.	0.08	n.d.
HMP-00-19	10	529	76	n.d.	n.d.	419	142	47	9	4	0.04	n.d.
HMP-00-20	7	389	48	n.d.	n.d.	743	98	85	10	6	0.22	n.d.
HMP-00-047b	7	429	n.d.	n.d.	n.d.	104	58	00	n.d.	n.d.	0.11	n.d.
HMP-00-214	11	898	53	22	n.d.	166	805	574	14	4	0.06	n.d.
<i>Std Dev</i>	20	347	29	10	13	231	233	174	5	4	0.09	0.02
Shock Level 1												
DI08-7-7	15	5006	136	n.d.	n.d.	997	932	956	20	4	0.11	0.04
Shock Level 3												
DV10	n.d.	1450	17	33	n.d.	557	406	38	7	10	0.12	0.10
BE009-A13	n.d.	804	65	n.d.	n.d.	469	177	94	23	18	0.21	0.04
BE009-A2	n.d.	1486	32	n.d.	27	579	366	130	38	15	1.21	0.30
BE010-A	n.d.	2346	30	n.d.	26	516	404	273	23	8	0.09	0.02
BE009-A10	42	634	81	21	36	282	272	196	66	27	0.12	0.35
<i>Std Dev</i>	17	1613	44	14	17	236	263	341	20	8	0.44	0.15
Shock Level 4												
DI08-18-1	n.d.	666	14	39	23	397	275	174	31	23	0.07	0.18
DI08-30-1	10	79	175	n.d.	48	325	54	n.d.	25	46	0.06	0.14
DI08-9-1	n.d.	1842	8	n.d.	n.d.	312	189	55	8	2	0.36	n.d.
DI08-34-11	n.d.	1820	n.d.	n.d.	24	224	272	85	17	3	0.03	0.13
<i>Std Dev</i>	5	876	84	20	20	71	104	73	10	21	0.15	0.08
Shock Level 5												
BE005-C	13	1748	47	n.d.	33	732	458	111	31	13	0.09	0.09
DI08-20-6	n.d.	859	12	98	28	26	168	97	7	4	0.26	n.d.
DI08-21-5	80	641	101	88	25	61	279	103	18	6	1.60	0.19
DI08-24-8	n.d.	870	18	n.d.	28	1600	141	38	n.d.	2	0.34	0.06
AH11	n.d.	771	n.d.	20	28	91	102	00	5	2	0.54	0.03
DI08-34-12	n.d.	884	5	n.d.	24	283	193	106	30	4	0.42	0.05
WSR002B	15	793	80	n.d.	n.d.	694	248	140	32	13	0.25	0.03
<i>Std Dev</i>	29	367	40	44	11	568	118	48	14	5	0.51	0.06
Shock Level 6												
BE009-A11	n.d.	510	23	n.d.	n.d.	82	235	78	21	13	0.34	0.08
WSR001-A2	7	1388	17	n.d.	25	371	445	152	22	9	0.08	5.09
DI08-3-10	7	591	60	n.d.	32	184	165	237	8	3	0.43	0.05
DI08-20-7	n.d.	427	10	n.d.	23	149	289	128	38	6	0.45	n.d.
AH6	n.d.	3588	7	n.d.	n.d.	462	147	261	5	n.d.	1.33	0.08
BE10	n.d.	893	9	n.d.	21	1297	170	92	31	4	1.05	0.03
DI08-35-10	n.d.	580	7	n.d.	27	270	205	192	44	4	0.15	0.02
<i>Std Dev</i>	3	1128	19	0	13	416	104	70	15	4	0.47	1.91
Shock Level 7												
AH003-A	n.d.	1066	6	n.d.	27	386	221	78	4	2	0.10	n.d.
BE009-A14	n.d.	985	5	n.d.	26	377	298	37	n.d.	2	0.11	0.41
DI08-24-7	n.d.	1105	6	n.d.	n.d.	1418	149	109	32	6	0.31	0.19
BE002-A	n.d.	147	n.d.	n.d.	n.d.	302	16	00	n.d.	n.d.	4.60	0.05
<i>Std Dev</i>	<i>n.a.</i>	521	3	<i>n.a.</i>	15	533	120	48	15	3	2.22	0.18

² Note that no trace element data was available for shock level 2.

A7. Calculated Z-values for select major oxide data for the crystalline samples using a non-parametric Mann-Whitney U-test. Z-values above 1.96 show significance at $p < 0.01$ (where p denotes probability), and values between 1.65 and 1.96 indicate significance at $p < 0.05$. An α of 0.05 was used, where α is the likelihood of error.

Shock Level Comparison	Major Oxide					
	Al ₂ O ₃	Fe ₂ O ₃	MnO	MgO	Na ₂ O	CaO
0 vs. 3	2.79	1.69	1.65	2.11	2.45	2.45
3 vs. 4	0.57	1.06	0.97	0.89	1.71	1.21
4 vs. 5	0.86	0.00	0.12	0.12	0.49	1.22
5 vs. 6	0.71	0.62	0.36	0.09	0.71	0.80
6 vs. 7	0.59	1.32	1.39	1.02	1.02	0.88
0 vs. 7	0.21	1.69	2.27	0.11	2.53	2.64
0 vs. 3	2.03	2.35	2.35	2.35	2.03	0.41

Appendix B

B1. Site locations for samples used in bulk cell counts and CSLM counts.

Sample	UTM Coordinates			Sample Description
	Easting	Northing	Grid	
Shock Level 0				
SI001-A-1	541,625	8,366,491	16	Sverdrup Inlet - Siliminite and biotite rich felsic sample.
HMP-00-195	514,390	8,350,575	16	Unshocked basement gneiss. Felsic, plagioclase.
HMP-00-214	514,390	8,350,575	16	Unshocked basement gneiss. Felsic. Amphibole, siliminite.
Shock Level 1				
DI08-7-7	429,282	8,369,910	16	Highly altered. Kink banding in biotite, no PDFs or toasting. Mafic.
Shock Level 2				
DI08-26-1	428,487	8,369,942	16	Felsic. PF formation in Quartz. Presence of sulfides and clinopyroxenes.
DI08-24-1	425,537	8,371,436	16	Garnet and biotite rich. Some feldspars. Kink banding and pleiochromism.
Shock Level 3				
BE009-A2	427,859	8,368,697	16	Quartz with some PDFs. Significant levels of plagioclase.
BE010-A	427,846	8,366,592	16	Quartz rich. Toasting with PDFs. Good grain boundaries, full extinction.
BE009-A13	428,128	8,368,856	16	Quartz with siliminite, biotite, garnets and feldspars. PDFs with toasting.
BE009-A10	428,128	8,368,856	16	Garnet rich with biotite. PDFs, toasting and kink banding.
Shock Level 4				
BE009-A12	428,128	8,368,856	16	Gneiss clast from melt rich rock.
DI08-30-1	429,699	8,365,478	16	Mafic. Amphiboles. PDF's with toasting in quartz.
DI08-9-1	427,916	8,368,940	16	Mafic sample. Biotite present with pleiochromism. Quartz with PDFs.
DI08-34-11	422,354	8,370,785	16	Felsic. Plagioclase rich. PDF's and PF's prevalent. Good extinction.
Shock Level 5				
BE005-C	427,473	8,366,944	16	Bruno Escarpment. Some Orthopyroxene. Largely diaplectic glass.
DI08-21-5	420,400	8,371,139	16	Siliminite rich. Diaplectic glass with dark brown matrix. Some PDF's.
DI08-24-8	425,537	8,371,436	16	Siliminite rich. Largely diaplectic glass. Calcite deposition. Mafic banding.
BE005-A	427,473	8,366,944	16	Anomaly Hill. Diaplectic glass with some flow.
BE008A1	427,859	8,368,697	16	Biotite rich with kink banding. Ballen quartz with some diaplectic glass.
Shock Level 6				
BE009A1	428,128	8,368,856	16	Glass with some diaplectic outlines.
AH003A1	424,731	8,368,565	16	Mafic sample. Mainly glass. Some areas with vesicularized frothy flow.
DI08-20-7	420,598	8,371,046	16	Quartz and feldspathic glass. Calcite deposition.
BE009-A11	428,128	8,368,856	16	Glass with siliminite.
BV001A5	428,559	8,366,622	16	Quartz losing diaplectic outlines. Frothy glass.
Shock Level 7				
AH003-A	424,731	8,368,565	16	Felsic sample with frothy flow. Some crystallization of quartz.
BE009-A14	428,128	8,368,856	16	Sample has large mafic bands throughout. Significant flow of melt.
DI08-24-7	425,537	8,371,436	16	Good flow texture, complete melting. Calcite deposition.
BE002-A	427,718	8,366,610	16	Frothy glass with crystallization of quartz. Calcite deposition present.

B2. Bulk cell count raw data using Zeiss Z1 compound microscope in bright field. Each sample represents cell counts per 1g of rock.

Sample	# cells/g	Sample	# cells/g
Shock Level 0		Shock Level 6	
HMP00214	2.00E+06	BV001-A5	1.200E+08
SIOO1A1	8.466E+07	BE009A1	2.520E+08
HMP00195	1.320E+08	DI08-20-7	6.200E+08
<i>StD</i>	<i>5.84E+07</i>	AH003A1	5.106E+08
Shock Level 1		BE009A11	3.333E+08
DI08-7-7	1.390E+08	<i>StD</i>	<i>1.67E+08</i>
Shock Level 2		Shock Level 7	
DI08-26-1	2.090E+08	BE002A	2.637E+08
Shock Level 3		BE009A14	3.783E+08
BE009A2	2.100E+08	AH003A	5.301E+08
BE010A	1.956E+08	DI08-24-7	1.682E+08
BE009A13	2.310E+08	<i>StD</i>	<i>1.05E+08</i>
BE009A10	2.000E+08		
<i>StD</i>	<i>1.58E+07</i>		
Shock Level 4			
BE009A12	1.830E+08		
DI08-34-11	4.310E+08		
DI08-30-1	1.490E+08		
DI08-09-1	1.330E+08		
<i>StD</i>	<i>2.55E+07</i>		
Shock Level 5			
DI08-21-5	4.720E+08		
DI08-24-8	2.940E+08		
BE005A	1.564E+08		
BE005C	3.647E+08		
BE008A1	1.885E+08		
<i>StD</i>	<i>1.29E+08</i>		

B3. *In situ* cell counts (live and dead) per 150,000 μm^2 area bin using the CSLM. Ex. Depth point 0 represents a bin from 0 to 500 μm . Theoretical confocal depth is taken to be 1.9 μm .

Shock Level 0					
	SI001A Transect			SI001A1 Transect	
	<i>1</i>	<i>2</i>	<i>3</i>	<i>1</i>	<i>2</i>
Depth					
0	21	4	36	1	1
500	0	0	0	0	0
1000	6	1	0	0	0
1500	3	0	0	0	0
2000	1	1	3	0	0
2500	2	0	3	0	0
3000	4	0	0	0	0
3500	1	0	0	0	0
4000	6	0	0	0	0
4500	7	1	0	0	0
5000	10	2	0	0	0
5500	6	0	13	1	0
6000	2	0		0	3
Total	69	9	55	2	4

Shock Level 1				Shock Level 2		
	DI08-7-7 Transect			DI08-26-1 Transect		
	<i>1</i>	<i>2</i>	<i>3</i>	<i>1</i>	<i>2</i>	<i>3</i>
Depth						
0	30	58	40	29	103	57
500	21	33	136	74	51	48
1000	43	6	21	11	56	70
1500	39	20	22	84	71	40
2000	8	29	4	45	25	40
2500	76	1	20	61	33	24
3000	7	20	51	201	47	54
3500	1	6	119	82	2	158
4000	0	0	115	7	2	33
4500	14	8	—	0	5	—
5000	31	0	—	1	49	—
5500	35	17	—	0	20	—
6000	11	39	—	0	82	—
Total	316	237	528	595	546	524

Shock Level 3						
	BE009A10			DI08-34-8		
	Transect			Transect		
	<i>1</i>	<i>2</i>	<i>3</i>	<i>1</i>	<i>2</i>	<i>3</i>
Depth						
0	37	117	266	22	40	108
500	7	161	237	1	20	5
1000	6	11	87	3	3	1
1500	23	11	0	0	0	2
2000	17	30	58	0	0	2
2500	8	19	9	0	0	0
3000	97	3	44	8	0	1
3500	190	2	235	7	0	0
4000	25	25	55	0	0	0
4500	28	147	1	1	0	0
5000	128	70	74	2	5	0
5500	—	99	8	0	12	0
6000	—	143	9	0	0	0
Total	566	838	1083	44	80	119

Shock Level 4						
	BE009A13			DI08-09-1		
	Transect			Transect		
	<i>1</i>	<i>2</i>	<i>3</i>	<i>1</i>	<i>2</i>	<i>3</i>
Depth						
0	34	53	5	6	1	98
500	0	8	5	2	0	53
1000	0	4	1	1	16	9
1500	0	0	0	8	6	20
2000	0	1	0	20	4	29
2500	0	1	0	3	3	1
3000	0	0	1	0	72	20
3500	0	0	0	7	5	6
4000	2	12	1	69	6	0
4500	0	5	1	48	3	8
5000	2	9	1	8	4	5
5500	0	0	0	1	8	29
6000	3	8	1	9	8	39
Total	41	101	16	182	136	317

Shock Level 5						
	6AH			BE005C		
	Transect			Transect		
	<i>1</i>	<i>2</i>	<i>3</i>	<i>1</i>	<i>2</i>	<i>3</i>
Depth						
0	56	18	23	76	41	69
500	31	38	16	36	2	3
1000	35	86	33	30	4	15
1500	5	47	98	5	2	4
2000	52	15	68	13	3	102
2500	29	12	23	16	58	16
3000	164	67	34	21	1	70
3500	227	7	13	10	1	4
4000	125	105	27	6	2	—
4500	90	33	27	3	4	—
5000	13	43	9	69	26	—
5500	59	12	14	—	82	—
6000	154	33	35	—	8	—
Total	1040	516	420	285	234	283

Shock Level 6						
	BE009A11			DI08-20-7		
	Transect			Transect		
	<i>1</i>	<i>2</i>	<i>3</i>	<i>1</i>	<i>2</i>	<i>3</i>
Depth						
0	34	43	3	240	474	154
500	5	0	4	53	503	134
1000	17	2	2	72	147	100
1500	7	15	2	163	427	111
2000	11	7	0	353	166	520
2500	8	1	0	434	541	79
3000	34	29	64	85	154	39
3500	8	1	70	164	50	293
4000	3	5	98	364	33	442
4500	6	2	17	1119	218	—
5000	9	10	27	136	163	—
5500	20	6	4	418	223	—
6000	2	16	4	337	153	—
Total	164	137	295	3938	3252	1872

Shock Level 7					
	DI08-24-7		BE009A14		
	Transect		Transect		
	<i>1</i>	<i>2</i>	<i>1</i>	<i>2</i>	<i>3</i>
Depth					
0	192	168	94	41	32
500	488	450	0	2	14
1000	69	241	0	12	3
1500	70	36	0	0	14
2000	13	13	5	10	0
2500	4	18	1	15	1
3000	10	21	13	0	6
3500	17	48	4	8	6
4000	1	381	9	0	0
4500	0	109	2	25	4
5000	0	44	17	5	0
5500	59	105	1	0	0
6000	61	117	0	0	0
Total	984	1751	146	118	80

Appendix C

C1. BG-11 Media

Chemical	g/L of solution
NaNO ₃	1.5
K ₂ PHO ₄	0.0305
CaCl ₂ •2H ₂ O	0.036
Citric Acid	0.006
EDTA	0.001
Na ₂ CO ₃	0.02
MgSO ₄ •7H ₂ O	0.075*
Fe-Am-Citrate	0.006*
A5 Metal Mix	1mL*
Agar	20

Instructions: In one litre of distilled water mix together above ingredients and autoclave. The MgSO₄•7H₂O and Fe-Am-Citrate should be filter sterilized and added after autoclaving.

C2. A5 Metal Mix

Chemical	g/L of solution
H ₃ BO ₃	2.86
MnCl ₂	1.81
ZnSO ₄ •7H ₂ O	0.222
Na ₂ MoO ₄ •2H ₂ O	0.390
CuSO ₄ •5H ₂ O	0.079
Co(NO ₃) ₂ •6H ₂ O	0.0494

Dissolve above ingredients in 1L of distilled water and filter sterilize.

C3. Raw 16S rDNA data for the Bacterial classes for unshocked gneisses

Class Name	Unshocked					
	HMP00198	SI001A	HMP00195	SI001B2	SI001D2	HMP00214
Actinobacteria (class)	41	12	462	1237	1885	4193
Acidobacteria (class)	18	0	3	0	3	0
Alphaproteobacteria	238	14	74	1677	2013	147
Gammaproteobacteria	2144	0	242	39	571	2550
Chloroflexi (class)	0	0	242	0	24	88
Cytophagia	0	0	13	81	15	0
Sphingobacteria	0	0	0	0	8	0
Caldilineae	0	0	0	0	0	1
Deltaproteobacteria	0	0	0	0	0	0
Anaerolineae	0	0	0	0	0	0
Deinococci	2	0	89	0	0	0
Planctomycetacia	0	0	1	10	0	0
Cyanobacteria (class)	0	16	31	2	54	0
Betaproteobacteria	12	0	0	1978	7	3
Clostridia	0	3	0	0	15	360
Bacilli	4	1	1	45	23	184
Bacteroidia	0	0	0	0	0	81
Verrucomicrobiae	0	0	0	0	0	0
OP10 (class)	0	0	0	0	0	0
BRC1 (class)	0	0	0	0	0	0
Gemmatimonadetes (class)	0	0	3	0	0	0
Flavobacteria	0	0	0	0	0	0
TM7 (class)	0	0	0	0	0	1
Aquificae (class)	0	0	0	0	0	0
Dictyoglomia	0	0	0	0	0	0
Thermotogae (class)	0	0	0	0	0	0
Oscillatoriales	0	0	0	0	0	0
Ignavibacteria	0	0	0	0	0	0
Nitrospira (class)	0	0	0	0	0	1
Spirochaetia	0	0	0	0	0	0
Erysipelotrichi	0	0	0	0	0	57
Ktedonobacteria	0	0	0	0	0	0
Chroococcales	0	0	0	4	0	0
Fusobacteria (class)	0	0	0	0	1	38
Synergistia	0	0	0	0	0	0
Dehalococcoidetes	0	0	0	0	0	0
Caldisericia	0	0	0	0	0	0
Solibacteres	0	0	0	0	0	0
Gloeobacteria	0	1	0	9	1	0
Pleurocapsales	0	0	11	0	0	0
Thermodesulfobacteria (class)	0	0	0	0	0	0
Thermolithobacteria	0	0	0	0	0	0
Opitutae	0	0	0	0	0	0
Holophagae	0	0	0	0	0	0
Deferribacteres (class)	0	0	0	0	0	0
Elusimicrobia (class)	0	0	0	0	0	0
Fibrobacteres (class)	0	0	0	0	0	0
Epsilonproteobacteria	0	0	0	0	0	0
Mollicutes	0	0	0	0	0	0
Stigonematales	0	0	0	0	0	0
Lentisphaerae (class)	0	0	0	0	0	0
Chlamydiia	0	0	0	0	0	0

C5. Raw 16S rDNA data for the Bacterial classes for highly shocked (6-7) gneisses.

Class Name	Highly Shocked							
	AH6	BE009 A11	BV001- A5	AH003 A1	BE009 A11	WSR001 A2	DI08- 20-7	AH00 3A
Actinobacteria (class)	5192	1131	3534	1753	1119	338	1541	1154
Acidobacteria (class)	123	2	5	32	4	0	0	23
Alphaproteobacteria	226	173	478	281	205	0	20	200
Gammaproteobacteria	2	5	49	9	8	577	16	16
Chloroflexi (class)	373	156	1454	261	337	0	347	502
Cytophagia	9	26	22	7	19	0	0	11
Sphingobacteria	32	47	41	6	37	0	0	11
Caldilineae	126	175	48	8	12	0	2	9
Deltaproteobacteria	5	1	53	5	6	0	5	5
Anaerolineae	353	54	0	0	0	0	0	0
Deinococci	0	26	21	28	48	0	0	12
Planctomycetacia	37	6	7	0	4	0	0	3
Cyanobacteria (class)	56	223	354	2	276	0	2	22
Betaproteobacteria	15	8	10	5	5	1359	4	20
Clostridia	2	1	7	4	5	2	10	0
Bacilli	5	0	4	11	1	103	6	32
Bacteroidia	2	0	0	7	0	0	0	2
Verrucomicrobiae	34	0	0	0	0	0	0	0
OP10 (class)	13	0	0	0	0	0	0	0
BRC1 (class)	4	0	0	0	0	0	0	0
Gemmatimonadetes (class)	28	0	31	6	11	0	0	7
Flavobacteria	23	0	14	14	0	0	8	25
TM7 (class)	13	0	31	3	0	0	2	4
Aquificae (class)	0	0	0	0	0	0	0	0
Dictyoglomia	0	0	0	0	0	0	0	0
Thermotogae (class)	0	0	0	0	0	0	0	0
Oscillatoriales	0	0	233	0	4	0	0	0
Ignavibacteria	0	0	0	0	0	0	0	0
Nitrospira (class)	0	0	54	15	8	0	10	8
Spirochaetia	0	0	0	0	0	0	0	0
Erysipelotrichi	0	0	0	0	0	0	0	0
Ktedonobacteria	0	0	0	0	0	0	0	0
Chroococcales	0	0	301	29	3	0	0	162
Fusobacteria (class)	0	0	0	0	0	0	0	0
Synergistia	0	0	0	0	0	0	0	0
Dehalococcoidetes	0	0	2	0	0	0	2	2
Caldisericia	0	0	0	0	0	0	0	0
Solibacteres	0	0	0	0	0	0	0	0
Gloeobacteria	0	0	42	0	1	0	0	0
Pleurocapsales	0	0	0	0	2	0	0	2
Thermodesulfobacteria (class)	0	0	0	0	0	0	0	0
Thermolithobacteria	0	0	0	0	0	0	0	0
Opitutae	0	0	0	0	0	0	0	0
Holophagae	0	0	1	0	3	0	0	0
Deferribacteres (class)	0	0	0	0	0	0	0	0
Elusimicrobia (class)	0	0	0	0	0	0	0	0
Fibrobacteres (class)	0	0	0	0	0	0	0	0
Epsilonproteobacteria	0	0	0	0	0	0	0	0
Mollicutes	0	0	0	0	0	0	0	0
Stigonematales	0	0	0	0	0	0	0	0
Lentisphaerae (class)	0	0	0	0	0	0	0	0
Chlamydiia	0	0	2	0	0	0	0	0

C6. Raw DNA data for Eukaryal (16S) and fungal (18S) classes for two samples; where AH003A represents a highly shocked rock, and BE009A13, a moderate shock level.

Class Name	Samples	
	AH003A	BE009A13
		Eukarya
Phaeophyceae (class)	12	0
Xanthophyceae (class)	4	0
Ulvophyceae	5	0
Trebouxiophyceae	54	113
Chlorophyceae	31	0
Klebsormidiophyceae	5	0
		Fungi
Microsporidetes	168	—
Eurotiomycetes	510	—
Monoblepharidomycetes	3	—
Chytridiomycetes	2	—
Entomophthoromycota (class)	8	—
Agaricomycetes	14	—
Leotiomycetes	29	—
Fungi (class)	1	—
Dothideomycetes	3	—
Sordariomycetes	2	—
Saccharomycetes	12	—
Exobasidiomycetes	1	—
Sordariomycetes	4	—

Appendix D

D1. Modified Barr's Medium for sulfate reducing bacteria.

Chemical	g/L of solution
MgSO ₄ •7H ₂ O	2.0
K ₂ PHO ₄	0.5
Sodium Citrate	5.0
CaSO ₄	1.0
NH ₄ Cl	1.0
Sodium Lactate	3.5
Yeast Extract	1.0
Fe(NH ₄) ₂ (SO ₄) ₂	5%*
Resazurin	1 mg

Mix above components, accepting the ferric ammonium sulfate, pH adjust to 7.5 and filter sterilize. Filter sterilize a 5% Fe(NH₄)₂(SO₄)₂ solution and add 0.1mL to 0.5mL to the medium prior to inoculation. To make anoxic, right before use mix 0.75 g/L each of Na-thioglycollate and Ascorbic acid in 100 mL of water. pH adjust to 7.5 using NaOH or KOH and filter sterilize. Mix 1.2 mL for every 12 mL of media. Resazurin is used as a redox indicator and will start blue, but then grade to red or pink when environment is reduced. If redox potential goes even lower, mixture will become clear.

D2. Houghton Minimal Media Recipe.

Chemical	g/L of solution
MgSO ₄ •7H ₂ O	0.018
K ₂ PHO ₄	0.05
CaSO ₄	0.0262
NH ₄ Cl	0.1
Sodium Lactate	0.35
Yeast Extract	0.1
Fe(NH ₄) ₂ (SO ₄) ₂	0.5%
Trace metal mix*	10μL
Resazurin	1 mg

*Trace Metal Mix

Chemical	g/100 mL of solution
ZnSO ₄	0.002
CuCl ₂	0.004
Na ₂ CO ₃	0.00245

Follow procedures for Modified Barr's Medium (D1). pH adjust to 6.0.

D3. ICP-AES/IC and ICP-MS data for Houghton hydrothermal experiment.

Aluminum – Limit 0.30 µg/L							
Sample	Substrate	Week 1	Week 2	Week 3	Week 4	Week 5	Week 6
1	0 Coarse	1.7	0.98	2.14	0.61	0.38	0.69
2	0 Fine	5.81	5.33	3.75	1.3	2.48	1.8
3	3/4 Coarse	0.37	ND	1.01	ND	ND	0.18
4	3/4 Fine	1.19	ND	1.74	ND	ND	0.41
5	7 Coarse	2.38	1.08	1.76	0.34	0.43	0.59
6	7 Fine	1.92	2.09	4.34	0.37	0.28	0.45
7	0 Coarse	0.34	0.74	2.55	0.32	0.6	2.54
8	0 Fine	2.15	0.96	2.53	2.14	4.59	5.57
9	3/4 Coarse	0.42	0.16	1.35	ND	ND	0.15
10	3/4 Fine	0.54	1.56	2.59	0.83	0.78	0.81
11	7 Coarse	0.53	0.59	1.97	1.22	2.84	1.87
12	7 Fine	0.61	0.29	2.77	1.04	1.47	1.31
13	Media	0.29	ND	0.58	ND	0.12	ND
14	3/4-4cb				ND		
15	3/4-4fb				0.74		

Barium - Limit 0.02ug/mL							
Sample	Substrate	Week 1	Week 2	Week 3	Week 4	Week 5	Week 6
1	0 Coarse	0.04	0.05	0.07	0.86	0.07	0.05
2	0 Fine	0.05	0.06	0.04	0.82	0.04	0.04
3	3/4 Coarse	0.09	0.33	0.1	2.74	0.08	0.1
4	3/4 Fine	0.11	0.21	0.07	0.07	0.08	0.09
5	7 Coarse	0.12	0.11	0.1	2.71	0.08	1.32
6	7 Fine	0.09	0.09	0.29	1.08	0.04	0.05
7	0 Coarse	0.02	0.02	0.05	2.55	0.03	0.04
8	0 Fine	0.06	0.06	0.04	0.04	0.07	0.06
9	3/4 Coarse	0.04	0.06	0.09	0.07	0.08	0.09
10	3/4 Fine	0.08	0.22	0.11	0.06	0.07	0.06
11	7 Coarse	0.12	0.07	0.05	0.06	0.07	0.06
12	7 Fine	0.13	0.1	0.07	0.05	0.05	0.06
13	Media	0.01	0.01	ND	ND	0.02	ND
14	3/4-4cb				3.21		
15	3/4-4fb				2.77		

Copper - Limit 0.004 ug/mL							
Sample	Substrate	Week 1	Week 2	Week 3	Week 4	Week 5	Week 6
1	0 Coarse	0.02	0.004	0.003	0.014	ND	ND
2	0 Fine	0.057	0.006	0.006	0.023	0.004	0.012
3	3/4 Coarse	0.021	0.097	0.008	0.007	0.045	ND
4	3/4 Fine	0.003	0.038	ND	0.013	0.089	0.008
5	7 Coarse	0.032	0.089	ND	0.007	0.089	0.004
6	7 Fine	0.007	0.079	0.011	0.008	0.106	0.017
7	0 Coarse	0.001	0.065	0.109	0.043	0.108	0.041
8	0 Fine	0.002	0.126	0.004	0.02	0.092	0.027
9	3/4 Coarse	0.007	0.058	ND	ND	0.131	0.017
10	3/4 Fine	0.003	0.047	0.006	0.008	0.103	0.022
11	7 Coarse	0.022	0.013	0.002	ND	0.118	0.003
12	7 Fine	0.006	0.012	0.012	0.01	0.024	0.023
13	Media	0.008	0.131	0.054	0.047	0.030	0.024
14	3/4-4cb				0.001		
15	3/4-4fb				0.001		

Calcium - Limit 1.00 ug/mL							
Sample	Substrate	Week 1	Week 2	Week 3	Week 4	Week 5	Week 6
1	0 Coarse	5.53	5.97	5.71	5.57	5.37	5.76
2	0 Fine	8.73	7.86	5.7	5.04	4.5	5.83
3	3/4 Coarse	15.6	16.48	16.48	11.17	10.28	8.87
4	3/4 Fine	13.84	16.68	19.95	8.58	9.78	11.42
5	7 Coarse	27.17	26.04	19.79	13.65	12.11	13.2
6	7 Fine	17.08	18.5	31.86	11.81	14.44	13.51
7	0 Coarse	4.75	4.51	5.46	5.27	4.75	5.72
8	0 Fine	6.57	9.2	8.17	6.58	6.6	6.3
9	3/4 Coarse	11.93	12.44	9.57	8.37	7.8	9.13
10	3/4 Fine	21.58	16.39	18.14	9.51	13.6	11.24
11	7 Coarse	16.69	12.84	11.72	9.46	12.07	11.86
12	7 Fine	22.94	19.74	18.38	12.93	14.6	13.39
13	Media	4.7	5.21	3.45	3.98	5.03	3.56
14	3/4-4cb				26.05		
15	3/4-4fb				25.16		

Potassium - Limit 1.00 ug/mL							
Sample	Substrate	Week 1	Week 2	Week 3	Week 4	Week 5	Week 6
1	0 Coarse	65.35	36.23	35.24	29.13	25.82	25.04
2	0 Fine	73.15	69.23	34.97	28.02	25.41	26.53
3	3/4 Coarse	108.34	76.48	52.26	40.87	35.1	32.71
4	3/4 Fine	85.29	84.48	48.68	43.22	34.88	33.88
5	7 Coarse	94.4	57.95	55.75	38.7	35.54	32.58
6	7 Fine	97.84	84.92	48.8	41.2	33.09	31.26
7	0 Coarse	42.65	34.47	30.15	27.27	24.06	23.93
8	0 Fine	50.53	36.29	28.98	25.04	24.5	24.23
9	3/4 Coarse	84.02	63.6	58.62	40.83	43.63	30.93
10	3/4 Fine	87.28	63.8	60.54	47.69	43.18	36.75
11	7 Coarse	71.99	52.39	62.15	51.31	42.9	36.31
12	7 Fine	71.34	54.39	51.44	40.26	39.81	33.32
13	Media	20.27	25.95	18.79	20.36	25.58	16.97
14	3/4-4cb				112.32		
15	3/4-4fb				111.79		

Magnesium - Limit 0.5 ug/mL							
Sample	Substrate	Week 1	Week 2	Week 3	Week 4	Week 5	Week 6
1	0 Coarse	15.8	9.8	8.62	6.53	5.89	5.07
2	0 Fine	18.5	16.54	8.04	5.67	5.28	5.09
3	3/4 Coarse	26.66	18.48	12.67	9.66	8.13	7.47
4	3/4 Fine	26.3	20	13.57	8.93	7.84	7.58
5	7 Coarse	28.26	15.97	14.86	10.09	9.1	8.23
6	7 Fine	30.39	21.28	16.94	9.16	7.15	6.16
7	0 Coarse	3	3.7	4.45	4.05	4.43	4.69
8	0 Fine	4.48	4.46	4.66	4.54	5.37	4.94
9	3/4 Coarse	13.29	11.79	11.96	8.12	7.87	6.32
10	3/4 Fine	12.11	10.17	12.05	8.95	8.21	6.39
11	7 Coarse	8.77	8.08	8.83	7.97	7.37	5.8
12	7 Fine	9.03	8.01	9.48	6.73	6.66	5.55
13	Media	3.43	3.9	3.2	3.23	4.18	1.59
14	3/4-4cb				31.92		
15	3/4-4fb				30.54		

Iron - Limit 0.5 ug/mL							
Sample	Substrate	Week 1	Week 2	Week 3	Week 4	Week 5	Week 6
1	0 Coarse	18.18	13.17	6.83	6.39	9.21	6.13
2	0 Fine	17.74	17.15	2.88	1.49	5	4.02
3	3/4 Coarse	8.14	36.81	14.06	3.57	4.14	1.9
4	3/4 Fine	2.84	15.81	2.55	0.81	0.7	0.77
5	7 Coarse	9.27	11.68	2.76	1.09	1.6	1.32
6	7 Fine	3.58	3.74	6.23	0.73	0.84	1.36
7	0 Coarse	7.21	9.22	12.06	10.12	12.16	14.28
8	0 Fine	30.56	21.56	18.62	14.11	18.63	17.02
9	3/4 Coarse	7.94	10.55	17.51	12.22	15.1	13.22
10	3/4 Fine	11.39	13.87	18.81	15.25	17.5	15.04
11	7 Coarse	8.14	8.82	11.47	10.27	10.3	9.48
12	7 Fine	15.43	12.33	14.04	12.86	11.91	14.37
13	Media	9.09	11.46	9.98	10.07	9.65	8.29
14	3/4-4cb				8.77		
15	3/4-4fb				9.27		

Sulphate - Limit 0.05 ug/mL							
Sample	Substrate	Week 1	Week 2	Week 3	Week 4	Week 5	Week 6
1	0 Coarse	ND	ND	ND	ND	172.2	21.4
2	0 Fine	ND	ND	ND	ND	204.5	89.9
3	3/4 Coarse	ND	ND	ND	ND	85.4	110
4	3/4 Fine	ND	ND	ND	ND	108.4	85.6
5	7 Coarse	ND	ND	ND	ND	95.5	98.4
6	7 Fine	ND	ND	ND	ND	5.4	71.9
7	0 Coarse	55.6	60.1	66	156	166.7	160.8
8	0 Fine	146	122.5	89.8	187	185.5	142.5
9	3/4 Coarse	109	90.9	80.3	180	168.5	162.3
10	3/4 Fine	170	127.8	113.6	186	189.1	197.9
11	7 Coarse	138	101.9	115.8	106	177.7	97.6
12	7 Fine	185	135	153.1	150	167.3	132.6
13	Media	48.6	63.2	74.2	113	167.6	154
14	3/4-4cb				90.7		
15	3/4-4fb				71.4		

Chloride - Limit 0.05 ug/mL							
Sample	Substrate	Week 1	Week 2	Week 3	Week 4	Week 5	Week 6
1	0 Coarse	61.4	93	64.1	78.4	69.2	78.2
2	0 Fine	64.3	77.8	63.5	71.9	69.9	80.1
3	3/4 Coarse	65.6	77.4	64.5	89.6	62	77.8
4	3/4 Fine	61.3	76.1	63.9	69.8	75.3	79.7
5	7 Coarse	63.5	80.6	65.2	89.4	ND	86
6	7 Fine	67.2	84.1	66.9	66.2	77.4	80.9
7	0 Coarse	75.3	70.5	62.9	92.9	80.2	84.4
8	0 Fine	76.8	75.4	65	74	80.7	82.6
9	3/4 Coarse	76.1	74.1	69	74.9	79.9	81.3
10	3/4 Fine	75.7	75.2	67.6	72.4	78	82.2
11	7 Coarse	80.9	76.2	70.5	75.9	77.8	79.9
12	7 Fine	71.6	71.9	70.8	74.7	78.9	80.4
13	Media	59.8	65.3	61.5	73.1	89.4	94.4
14	3/4-4cb				156		
15	3/4-4fb				152		

pH*							
Sample	Substrate	Week 1	Week 2	Week 3	Week 4	Week 5	Week 6
1	0 Coarse	7.28	6.73	6.63	6.33	6.3	6.35
2	0 Fine	6.97	6.98	6.56	6.5	6.07	6.25
3	3/4 Coarse	6.95	6.95	6.64	6.55	6.32	6.34
4	3/4 Fine	6.93	6.98	6.65	6.46	6.67	6.59
5	7 Coarse	7.09	7.01	6.62	6.62	6.6	6.72
6	7 Fine	7.04	7.11	6.59	6.6	6.65	6.65
7	0 Coarse	5.58	5.84	5.94	5.9	5.8	5.55
8	0 Fine	5.41	5.43	6.02	6	5.87	5.63
9	3/4 Coarse	5.64	5.91	6.14	6.2	6.3	6.38
10	3/4 Fine	5.46	5.82	6.27	6.29	6.35	6.34
11	7 Coarse	5.53	5.9	6.33	6.33	6.4	6.38
12	7 Fine	5.52	5.98	6.29	6.4	6.62	6.4
13	Media	5.98	5.99	6.01	6.08	6.1	6.3
14	3/4-4cb				6.78		
15	3/4-4fb				6.81		

* Week 1 and 2 pH readings were taken several hours after sampling and are not representative.

Curriculum Vitae

Name: Alexandra Pontefract

Post-secondary Education and Degrees: McMaster University
Hamilton, Ontario, Canada
2002-2006 H.B.Sc.

McMaster University
Hamilton, Ontario, Canada
2006-2008 M.Sc.

Honours and Awards: Natural Sciences and Research Council
PGS-D Scholarship
2010-2013

Canadian Astrobiology Training Program
Doctoral Fellowship
2010-2013

Canadian Astrobiology Training Program
Post-Doctoral Fellowship
2013-2015

Related Work Experience Teaching Assistant
McMaster University
2005-2009

Teaching Assistant
University of Western Ontario
2009-2013

Publications:

Pontefract, A., Osinski, G. R., Lindgren, P., Parnell, J., Cockell, C. S. and Southam G. 2012. The effects of meteorite impacts on the availability of bioessential elements for endolithic organisms. *Meteoritics & Planetary Science* **47**(10): 1681-1691.

Osinski, G. R., Tornabene L. L., Banerjee, N. R., Cockell, C. S., Flemming, R., Izawa, M. R. M., McCutcheon, J., Parnell, J., Pickersgill, A. E., **Pontefract, A.**, Preston, L., Sapers, H. M. and Southam, G. 2013. Impact-generated hydrothermal systems on Earth and Mars. *Icarus* **224**: 347–363.